

Pathogenetic, Prognostic, and Therapeutic Role of Fucosylation in Intrahepatic Cholangiocarcinoma



Dissertation
zur Erlangung des Doktorgrades
der Biomedizinischen Wissenschaften
(Dr. rer. physiol.)

der
Fakultät für Medizin
der Universität Regensburg

vorgelegt von
Cindy Eva Ament
aus
Weiden

im Jahr
2023

Pathogenetic, Prognostic, and Therapeutic Role of Fucosylation in Intrahepatic Cholangiocarcinoma



Dissertation
zur Erlangung des Doktorgrades
der Biomedizinischen Wissenschaften
(Dr. rer. physiol.)

der
Fakultät für Medizin
der Universität Regensburg

vorgelegt von
Cindy Eva Ament
aus
Weiden

im Jahr
2023

Dekan: Prof. Dr. Dirk Hellwig

Betreuer/in: Prof. Dr. Diego F. Calvisi

Tag der mündlichen Prüfung:

For the largest degree, this work was conducted by myself, the author. If not otherwise specified, all experiments in this work were carried out exclusively by myself. For the in vivo experiments (Cam assay), I was trained by Dr. Sara Steinmann and received partial help handling the eggs. In addition, I did the statistical analysis of all experiments. Survival correlation analyses were performed by Prof. Giovanni Mario Pes (Professor of Statistics at the University of Sassari, Sassari, Italy).

Parts of this dissertation have already been published in a peer-reviewed journal (Impact Factor 2023: 17.425):

Cindy E. Ament, Sara Steinmann, Katja Evert, Giovanni M. Pes, Silvia Ribback, Isabella Gigante, Elena Pizzuto, Jesus M. Banales, Pedro M. Rodrigues, Paula Olaizola, Haichuan Wang, Gianluigi Giannelli, Xin Chen, Matthias Evert, Diego F. Calvisi. *Aberrant fucosylation sustains the NOTCH and EGFR/NF- κ B pathways and has a prognostic value in human intrahepatic cholangiocarcinoma*. *Hepatology* 2023 (accepted for publication).

Table of Contents

Zusammenfassung	1
Summary	5
1. Introduction.....	5
1.1 Cholangiocarcinoma - Classification and Epidemiology	5
1.2 Intrahepatic Cholangiocarcinoma	6
1.3 Risk Factors	8
1.4 Symptoms	10
1.5 Diagnosis.....	10
1.6 Treatment.....	11
1.7 The Fucosylation Pathway	12
1.8 iCCA and the Notch Pathway	14
1.9 The Notch Pathway and Fucosylation	15
1.10 NF- κ B in Cancer	17
2. Material and Methods	22
2.1 Material.....	22
Table 1. Consumables	22
Table 2. Media, Buffers, and Reagents	24
Table 3. Kits Used During this Project.....	27
Table 4. Antibodies for Immunohistochemistry and Western Blotting	28
Table 5. TaqMan Gene Expression Probes	31

Table 6. Clinicopathological Features of iCCA Patients	32
Table 7. Software for Data Analysis and Illustration.....	33
iCCA Cell Lines and Patient Material	34
2.2 Methods.....	35
2.2.1 Cell Culture.....	35
2.2.2 Human Tissue Specimens.....	35
2.2.3 siRNA Silencing.....	36
2.2.4 Inhibition with 6-Alkynylfucose	37
2.2.5 Protein Extraction and Quantification.....	37
2.2.6 LDS-PAGE Gel Electrophoresis	38
2.2.7 Lectin Blotting	40
2.2.8 RNA Isolation	42
2.2.9 Reverse Transcription Polymerase Chain Reaction (rt-PCR).....	42
2.2.10 Quantitative Real-Time RT-PCR (qRT-PCR)	43
2.2.11 Immunohistochemistry and Assessment of Proliferation, Apoptosis and NOTCH1 index	43
2.2.12 Real-time Cell Analysis (RTCA) and Assessment of Proliferation <i>In Vitro</i>	45
2.2.13 Analysis of Cell Motility.....	46
2.2.14 Nuclear and Cytoplasmic Extraction	46
2.2.15 NF- κ B p65 Transcription Factor Assay.....	47

2.2.16 Co-Immunoprecipitation	47
2.2.17 Flow Dual Luciferase Assay and Notch1 Pathway Reporter Kit	48
2.2.18 Flow Cytometry for Apoptosis	48
2.2.19 Human Cancer-Associated Fibroblasts (hCAFs) Isolation	49
2.2.20 Chick Chorioallantoic Membrane (CAM) Assay	50
2.2.21 CRISPR knockout of <i>SLC35C1</i> and <i>FX</i>	51
2.2.22 Statistical Analysis	52
3. Results.....	53
3.1 Evaluation of Overall Fucosylation Levels in Human iCCA	53
3.1.1 Aberrant Protein Fucosylation in Human iCCA.	53
3.1.2 Fucosylation Levels Increased in Human iCCA Cell Lines Compared to NHC.....	54
3.1.3 Aberrant Fucosylation Levels Are Upregulated in Human iCCA Tissue Lysates and Correlate with Overall Patient Survival	56
3.2 Major Players of Fucosylation and their Role in Human iCCA.....	57
3.2.1 Elevated Levels of Significant Players of Fucosylation in Human iCCA...58	
3.2.2 <i>SLC35C1</i> or <i>FX</i> Knockdown and 6AF Treatment Reduces Protein Fucosylation Levels, Notch Receptor Expression, and Notch Signal Transduction in Human iCCA Cell Lines	61
3.3 Increased NOTCH Activation due to Aberrant FRINGE Levels in Human iCCA	66

3.6 Fucosylation Influences the NF- κ B Pathway in Human iCCA Cells.....	68
3.7 EGFR as a Possible Link between NF- κ B and Fucosylation in Human iCCA Cell Lines	71
3.8 6-Alkynylfucose Inhibits Cell Proliferation and Migration of iCCA Cell Lines ...	73
3.9 Suppression of Fucosylation Reduces iCCA Growth <i>In Vivo</i>	76
3.10 Aberrant Fucosylation in Mouse iCCA Lesions	81
3.11 Impaired Colony Formation due to CRISPR Gene Knockout in Murine and Human iCCA Cells	83
3.12 Increased Fucosylation in Cancer-Associated Fibroblasts (CAF).....	84
3.13 Fucosylation Regulates Pro-Inflammatory Signals in Human iCCA	87
3.14 No Evidence of Further Signaling Pathways Affected by Fucose in Human iCCA.....	89
4. Discussion	91
References	94
List of Abbreviations	104
List of Figures	106
List of Tables	109
Supplementary Material.....	110
Acknowledgements	115
Selbstständigkeitserklärung.....	116

Zusammenfassung

Das intrahepatische Cholangiokarzinom (iCCA) ist eine der tödlichsten Formen des primären Leberkrebses. Die Inzidenz des iCCA nimmt weltweit zu und es gibt nur begrenzte therapeutische Möglichkeiten. Daher sind innovative Therapien unerlässlich, um diese aggressive Erkrankung zu bekämpfen. Eine abnormale Glykosylierung, eine posttranskriptionelle Modifikation von Proteinen, gilt als eines der charakteristischen Merkmale von Krebs. In dieser Studie habe ich die Rolle der Fucosylierung bei der Cholangiokarzinogenese umfassend untersucht. Dabei konnte ich nachweisen, dass die globale Fucosylierung und die Komponenten des Fucosylierungsweges in menschlichen iCCA-Proben, im Vergleich zu nicht-tumorösem Lebergewebe und normalen Cholangiozyten ubiquitär hochreguliert sind. Zudem wurde auch in murinen iCCA Modellen ein Pro-Fucosylierungs Phänotyp der Leberläsionen beobachtet. Darüber hinaus korreliert der Fucosylierungsgrad signifikant mit einer schlechten Prognose der Patienten. Eine Hemmung der Protein Fucosylierung durch Zufuhr von 6-Alkynylfucose (6AF) bewirkte eine dosisabhängige Verringerung der Proliferation und Migration von iCCA-Zelllinien. Die Zugabe von Fucose zum Zellmedium hob diese Effekte auf. Auf molekularer Ebene führte die Verabreichung von 6AF sowie ein Knockdown der GDP-L-Fucose-Synthetase (*FX*) und des GDP-Fucose-Transmembran-Transporters (*SLC35C1*), beides zentrale Akteure der zellulären Fucosylierung, zu einer Verminderung der NOTCH-Aktivität, der NOTCH1/Jagged1-Interaktion, der NOTCH-Rezeptor Level und der damit verbundenen Expression der Zielgene in iCCA-Zelllinien. In denselben Zellen sanken die EGFR-, NF- κ B p65- und Bcl-xL-Proteinlevel, während I κ B α (ein wichtiger zellulärer NF- κ B-Inhibitor) nach *FX/SLC35C1*-Knockdown oder 6AF Zugabe anstieg. Im

Chorioallantoismembran (CAM) Assay verringerte die Behandlung mit 6AF das Wachstum von iCCA-Zellen erheblich. Zusammenfassend zeigen die Ergebnisse dieser Arbeit, dass iCCA beim Menschen (und bei der Maus) durch eine erhöhte globale Fucosylierung gekennzeichnet ist, die zu einer verstärkten NOTCH- und EGFR/NF- κ B-Aktivierung sowie zu erhöhtem Zellwachstum und erhöhter Migration führt. Daher könnte eine abweichende Fucosylierung zur Pathogenese von iCCA beim Menschen beitragen und ein potenzielles neues therapeutisches Ziel bei dieser tödlichen Neoplasie darstellen.

Summary

Intrahepatic cholangiocarcinoma (iCCA) is one of the most lethal forms of primary liver cancer. The incidence of iCCA is growing worldwide, and limited therapeutic options exist for this aggressive tumor. Therefore, innovative therapies are imperative to make this disease curable. Aberrant glycosylation, a post-transcriptional modification of proteins, is considered one of the hallmarks of cancer. In this study, I thoroughly investigated the role of fucosylation in cholangiocarcinogenesis. Through the present investigation, I revealed that global fucosylation and members of the fucosylation pathway are ubiquitously upregulated in human iCCA specimens compared to non-tumorous surrounding liver tissues and normal biliary cells. Similarly, a pro-fucosylation phenotype was also observed in liver lesions developed in mouse models of iCCA. Moreover, total fucosylation levels significantly correlate with poor patient prognoses. In addition, fucosylation inhibition by 6-alkynylfucose (6AF) administration decreased the proliferation and migration of iCCA cells in a dose-dependent manner. The addition of fucose to the cell culture medium annulled these effects. Furthermore, iCCA cell lines showed decreased NOTCH activity, NOTCH1/Jagged1 interactions, NOTCH receptors, and NOTCH target gene levels after incubation with 6AF or silencing of GDP-L-fucose synthetase (*FX*) and GDP-fucose transmembrane transporter (*SLC35C1*), both key players in cellular fucosylation. In the same cells, EGFR, NF- κ B p65, and Bcl-xL protein levels decreased, whereas I κ B α (a critical cellular NF- κ B inhibitor) increased after *FX/SLC35C1* knockdown or 6AF administration. Notably, 6AF treatment profoundly suppressed the growth of iCCA cells in the chick chorioallantoic membrane (CAM) assay. In summary, the results from this thesis indicate that human (and mouse) iCCA is characterized by elevated levels of global fucosylation, leading

to augmented NOTCH and EGFR/NF- κ B activation and increased cell growth and migration. Hence, aberrant fucosylation may contribute to human iCCA pathogenesis and represent a potential novel therapeutic target in this deadly neoplasm.

1. Introduction

1.1 Cholangiocarcinoma - Classification and Epidemiology

Primary liver cancer is the second most common cause of cancer mortality globally, with increasing incidence and few therapeutic options (Bridgewater et al., 2014). The most prevalent liver tumor types are hepatocellular carcinoma (HCC) and intrahepatic cholangiocarcinoma (iCCA). The global incidence and mortality of iCCA constantly increased over the last two decades, making it a major health concern worldwide (Khan et al., 2008; Moeini et al., 2016). The highest incidence occurs in Asia, but the number of deaths due to cholangiocarcinoma is also significantly growing in Western Europe and the United States of America. The tumor manifests predominantly in the elderly, between 60 and 70 years on average (Banales et al., 2020).

Cholangiocarcinoma (CCA) can occur at any point of the biliary tree. In terms of the anatomical site of origin, cholangiocarcinoma is classified as intrahepatic (iCCA), perihilar (pCCA), and distal (dCCA). In particular, pCCA is the most frequent type. Each subtype presents its own risk factors, pathobiology, clinical presentation, management, and prognosis. Moreover, mounting evidence indicates that CCA can originate from various cell types, namely hepatic progenitor cells (HPC), intrahepatic biliary epithelial cells (cholangiocytes), or even mature hepatocytes (Moeini et al., 2016).

A common source for tumor onset and growth is the chronic inflammation of the biliary epithelium and/or the bile stasis. The risk of CCA is increased by severe alcohol consumption, smoking, or chronic viral infections like Hepatitis B and C. The importance of metabolic syndrome and nonalcoholic fatty liver disease (NAFLD), which have been rising in Western society in the last decade, are additional risk factors for

CCA. The asymptomatic tumor growth during the early stages makes the diagnosis difficult (Banales et al., 2020; Braconi et al., 2019; Rizvi and Gores, 2013). Because early symptoms are highly unspecific, CCA is often diagnosed in advanced stages or incidentally. Symptoms of biliary obstruction such as jaundice, asthenia, abdominal pain, nausea, or anorexia are typically associated with extrahepatic CCA or only occur at the late stage of the disease. iCCA tumors display less specific signs, such as weight loss and general fatigue (Doherty et al., 2017).

This type of malignancy has deadly and aggressive behavior. The only potentially curative treatment is surgical resection of the tumor, which is limited to the early stages of CCA. When the cancer is inoperable, the only available treatment is conventional chemotherapy, combining gemcitabine with platin-derived drugs. However, the benefits for CCA patients in terms of overall survival are limited (Wang et al., 2018). After surgery, the tumor also has a high recurrence rate (50 to 60 %) and an extremely low five-year survival rate (Wirasorn et al., 2013; Blechacz et al., 2011).

1.2 Intrahepatic Cholangiocarcinoma

iCCAs can be classified macroscopically into three types: mass-forming, periductal infiltrating, and intraductal growing (Figure 1). Mass-forming lesions form in hepatic parenchyma, periductal tumors infiltrate and grow along duct walls and intraductal masses grow into duct lumens.

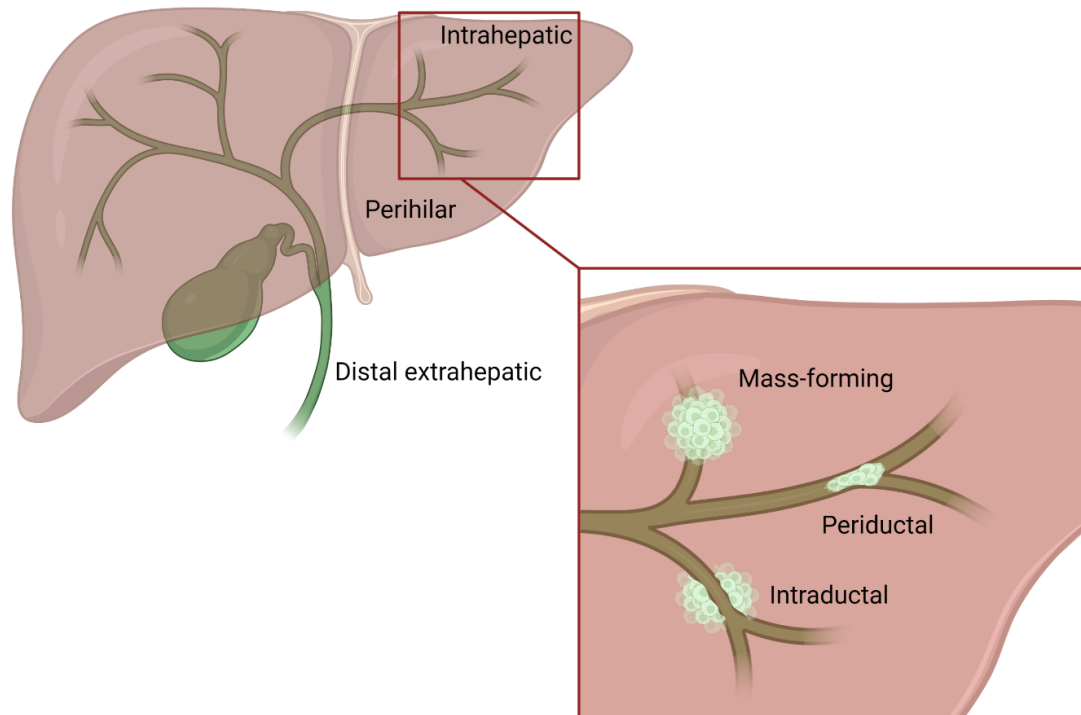


Figure 1. Intrahepatic cholangiocarcinoma classification. Cholangiocarcinoma can be distinguished based on the localization in the biliary tree. iCCA occurs in the liver in small and/or large peripheral bile ducts, whereas extrahepatic CCA is divided in perihilar cholangiocarcinoma or distal cholangiocarcinoma. iCCA can manifest as a mass-forming, a periductal-infiltrating or as an intraductal-growing tumor.

Histologically, iCCA can be divided into two distinct major subtypes. Depending on the level and size of the affected duct, the WHO classified iCCAs into small and large duct types. The small duct type represents up to 84% of iCCA and occurs as perihilar, ductular, and cholangiolar iCCA. It is characterized by weak mucin production, and it is often associated with chronic liver diseases like hepatitis B or C, alcoholic hepatitis, and non-alcoholic steatohepatitis. The large duct type can form as a bile duct or perihilar type and originates from large intrahepatic bile ducts. It is characterized by high mucin production from columnar cells and shows a strong invasive behavior. The large duct type displays chronic liver lesions caused by hepatolithiasis, primary sclerosing cholangitis, or parasitic infection of the bile ducts.

1.3 Risk Factors

The occurrence of iCCA shows a solid demographic correlation. This coincidence can be explained by the concentration of risk factors in the respective regions. One risk factor, chemical exposure, is particularly evident in the Japanese. Dichloromethane (DCM) is a carcinogenic substance mainly used in Japanese printing plants. Thus, increased cases of iCCA occur, especially among this population group (Kumagai et al. 2013). Liver flukes represent another prominent risk factor for iCCA. The *Clonorchis Sinensis* and *Opisthorchis Viverrini* parasites induce bile duct inflammation, likely leading to iCCA as a late consequence. The WHO classified them as group 1 carcinogens. Liver flukes occur mainly in East Asia and countries like Thailand and account for an increased incidence of iCCA cases in this area (Shaib et al. 2005; Dodson et al. 2013). Biliary tract diseases are among the most well-known and prevalent risk factors. One of these diseases is primary sclerosing cholangitis (PSC). PSC is a rare liver disease caused by the liver immune system and occurs in the intrahepatic bile ducts (Lewis 2017). PSC patients have a 5-10% increased risk of iCCA throughout their lives, and half of these cases are identified in the first two years after PSC diagnosis (Razumilava und Gores 2014).

Viral hepatitis B and C and liver cirrhosis are also recognized risk factors for iCCA, which are geographically different. Indeed, in Western countries, the hepatitis C virus is a risk factor for iCCA, whereas HBV plays a more critical role in Asia (El-Serag et al. 2009; Lee et al. 2008). Cirrhosis is another significant risk factor, which can contribute as an independent cause and as an associated disease to HBV and HCV chronic infections, severe alcohol consumption, and hemochromatosis (Khan et al. 2019; Palmer und Patel 2012). CCA is associated with metabolic and endocrine disorders,

such as type II diabetes, obesity, non-alcoholic fatty liver disease (NAFLD), and non-alcoholic steatohepatitis (NASH) (Khan et al. 2019, Li et al. 2015, Petrick et al. 2017). These diseases favor cholangiocellular malignancies by affecting insulin, leptin, and cytokine levels, thereby influencing proliferation and inflammation (Khan et al. 2019, Petrick et al. 2017). There are positive associations between alcohol consumption and smoking, although the etiological impact remains controversial (Khan et al. 2019; Palmer und Patel 2012). It has also been hypothesized that a number of genetic polymorphisms may favor CCA development, which are related to multidrug resistance, xenobiotic detoxification enzymes, DNA repair, the immune system, and folate metabolism have also been hypothesized to favor CCA development (Khan et al. 2019).

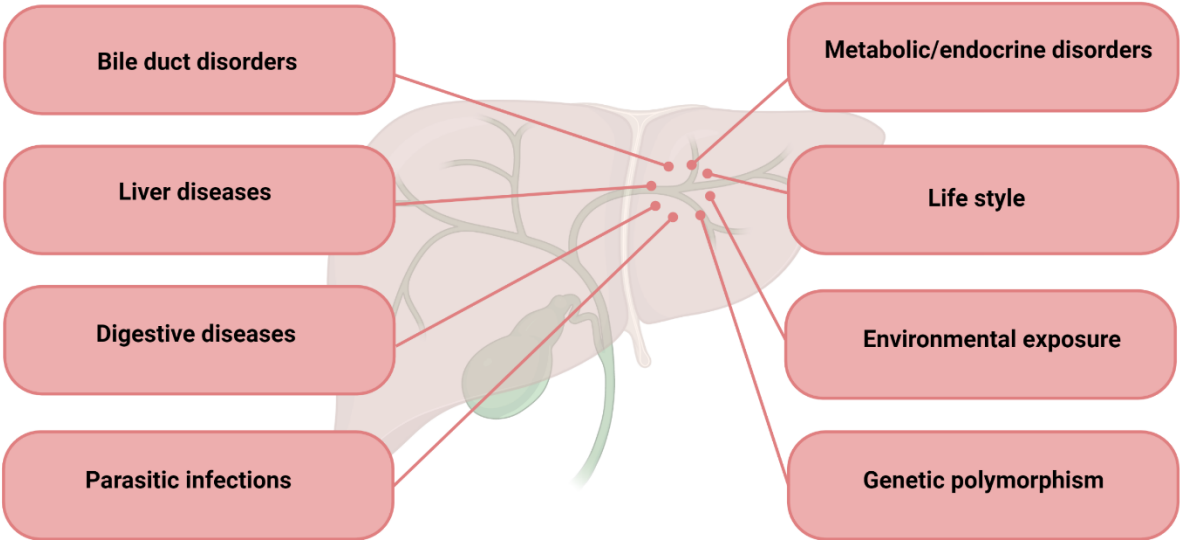


Figure 2. Risk factors for intrahepatic cholangiocarcinoma. Shown is a collection of known risk factors for CCA. (Khan et al. 2019)

1.4 Symptoms

The diagnosis of iCCA remains extremely problematic to this day. Most patients show only non-specific symptoms or remain asymptomatic. About 10% to 15% of patients are primarily diagnosed with jaundice and subsequently found to have a mass in the liver (Shimada et al. 2007). A diagnosis is often made incidentally or by finding diverse metastases for the remaining patients. Therefore, most tumors are generally found at advanced stages, surgical resection is usually no longer possible, and the prognosis of the patients is extremely poor. In addition to jaundice, pale stools can also serve as an indication of intrahepatic biliary disease. The increased conjugated bilirubin causes unbound bilirubin not to reach the duodenum, and thus the stool slowly loses its color. However, patients often present with non-specific symptoms such as fatigue, exhaustion, sweating, nausea, and weight loss (Forner et al. 2019).

1.5 Diagnosis

As described above, iCCA often shows only unspecific symptoms, which makes an early diagnosis of iCCA very unlikely. In addition, most cases of iCCA even occur without any present risk factor requiring regular examination of the patient (Banales et al. 2016). Differential diagnosis with HCC is critical to treat iCCA. MRI investigation can help to clarify this issue if the distribution of the contrast medium is correctly evaluated, but imaging procedures are still rather problematic (Banales et al. 2016). After HCC is excluded, a biopsy might be necessary (Bridgewater et al. 2014). To date, there are hardly any representative and specific markers for the immunohistological differentiation of HCC and iCCA. A combination of CK7⁺, CK19⁺, CK20⁺, and Hep-Par1 can distinguish iCCA from HCC (Rullier et al. 2000; Lau et al. 2002). Magnetic

resonance cholangiopancreatography, in combination with MRI, can provide information about the size and location of the tumor (Banales et al. 2016). However, to make a definite diagnosis, endoscopic retrograde cholangiopancreatography must be performed along with several other procedures. Consequently, iCCA is often misdiagnosed for HCC, and diagnosis is corrected after surgical removal of the tumor and a final classification as iCCA (EASL Clinical Practice Guidelines: management of cholestatic liver diseases 2009; Navaneethan et al. 2015). In general, the available methods for diagnosis lead to relatively moderate success. As a result, about 40% of patients undergo surgery without a clear diagnosis, and after 10% of the surgeries, no cancer can be diagnosed (Nuzzo et al. 2012).

1.6 Treatment

Complete surgical resection of the tumor and the surrounding tissue is still the only potentially promising therapy for iCCA. However, even though this treatment has the best chance of success, only 20% of the presenting patients are eligible for surgery due to the late diagnosis and advanced tumor stage. Even if the tumor is resectable and successfully removed, the 5-year survival rate remains low, ranging from 22% to 45% (Bartolini et al. 2020). A Kaplan-Meier analysis ($p = 0.53$) from the National Cancer Database showed that liver transplantation results in approximately the same patient overall survival (OS) (36.1%) when compared to liver resection (34.7%) (Kim et al. 2022). However, the success of liver transplantation depends mainly on how early the tumor was detected. In very early iCCA with a single tumor ≤ 2 cm in size, the 5-year OS was 65%, whereas that of advanced iCCA was 45%. The difference is even more dramatic in the case of tumor recurrence. The latter occurred in 13% of the early

group and in 54.5% of the late group, which was also the main reason for the later death of the patients (Sapichin et al. 2016). Although most iCCA cases are highly susceptible to chemoresistance, this step is often the last chance to gain some time for patients with inoperable or recurrent tumors. The National Comprehensive Cancer Network guidelines recommend gemcitabine/cisplatin therapy as the first-line treatment (Benson et al. 2009). In summary, the therapeutic options for iCCA patients are limited. Only very early tumors and highly selected patients may benefit, and the primary endpoint remains the 5-year patient survival (Krenzien et al. 2022).

1.7 The Fucosylation Pathway

Fucosylation, a post-translational modification of proteins, is one of the most important tools for cell diversity and various structures (Kizuka et al., 2017). The impact of carbohydrate residues on cell signals and their significance in biomedical research are widely known, and glycan structures are extensively used as biomarkers for many types of cancer. Cellular fucosylation depends on a family of fucosyltransferases, GDP-fucose, as a donor substrate of fucosyltransferases and a GDP-fucose transporter (Furukawa and Fukuda, 2016). The fucosylation pathway comprises GDP-fucose synthesis in the cytosol and the GDP-fucose transport to the Golgi Apparatus (Golgi) or the Endoplasmic Reticulum (ER), where the fucose is transferred to an acceptor substrate. GDP-fucose is also synthesized by the *de novo* or salvage pathway via the engagement of GDP-L-fucose synthase (TSTA3), GDP-mannose 4,6-dehydratase (GMDS), L-fucose kinase (FUK) and fucose-1-phosphate guanylyltransferase (FPGT) (Ma et al. 2006; Becker and Lowe, 2003). GDP-fucose is shuttled into the Golgi lumen by a transporter called SLC35C1. In the Golgi or the ER,

a fucose residue of GDP-fucose is shifted by fucosyltransferases (FUTs) to the sugar units of glycoconjugates or directly to the serine/threonine residues on proteins. FUTs catalyze the generation of α -1,2 (by FUT1 and 2), α -1,3 (by FUT3-7 and 9-11), α -1,4 (by FUT3 and 5), and α -1,6 (by FUT8) glycosidic bonds or protein O-fucosylation (by POFUT1-2) (Ma et al., 2006; Miyoshi et al., 2012; Mollicone et al., 2009).

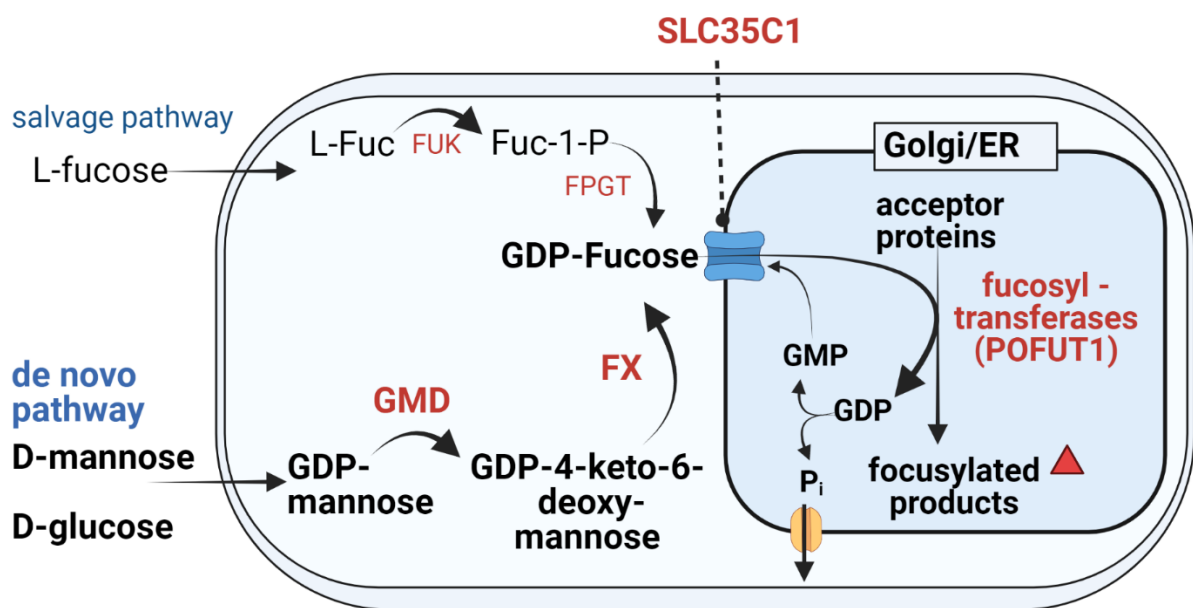


Figure 3. Overview of the Fucosylation Pathway. The salvage and the de novo pathway both feed the GDP-fucose level. The enzymes L-fucose kinase (FUK), fucose-1-phosphate guanylyltransferase (FPGT), GDP-mannose 4,6-dehydratase (GMD) and GDP-L-fucose synthase (FX) catalyze the reaction of L-fucose, D-mannose and D-glucose into the fucose donor (GDP-fucose). The fucose transporter (SLC35C1) delivers the fucose donor to the Golgi apparatus (Golgi) or endoplasmic reticulum (ER). Fucosyltransferases transfer a fucose residue to acceptor proteins.

Recently, fucosylation gained more and more attention as a possible innovative therapeutic approach against many diseases (Moriwaki et al., 2007). Indeed, fucosylation regulates various proteins with potential oncogenic activity. For example, Epidermal Growth Factor (EGF) repeats, evolutionarily conserved motifs found in secreted proteins and the extracellular domain of transmembrane proteins, are targets of post-translational modifications via glycosylation with O-glycans by an enzyme called POFUT1, initiated by O-fucose, O-glucose, or O-GlcNAc (Matsuura et al., 2008; Moloney et al., 2000a). Members of the Fringe family, such as manic fringe (MFNG), radical fringe (RFNG), and lunatic fringe (LFNG), further increase the diversity by extending the O-fucose modification with sugar nucleotides (Moloney et al., 2000b). The antagonist of POFUT1 is the lysosomal exoenzyme α -L-fucosidase-1 (FUCA1), which removes fucose residues from glycans and is downregulated in aggressive and metastatic human tumors and is a negative growth regulator downstream of the P53 tumor suppressor (Vecchio et al., 2017).

1.8 iCCA and the Notch Pathway

The Notch signaling pathway is responsible for morphogenesis and cell fate decisions in the liver, as well as proliferation and apoptosis during liver development and regeneration (Geisler and Strazzabosco, 2015). After the discovery that a mutation of the Notch ligand Jagged1 leads to the so-called Alagille syndrome (AGS) characterized by a paucity of the intrahepatic bile ducts, it was also evident that Notch plays a vital role in the differentiation of the biliary tree (EASL Clinical Practice Guidelines: management of cholestatic liver diseases, 2009; Li et al., 1997). Moreover, Notch regulates the differentiation of hepatoblasts to duct plate cells, which form the

branches of the bile duct. In a pathological event such as a liver injury or a chronic disease, a hepatocyte can even convert into a biliary progenitor cell, serving as a rescue mechanism (Zong et al., 2009; Geisler and Strazzabosco, 2015). Thus, the Notch signaling cascade is a key regulator of normal cholangiocyte differentiation. Therefore, it is not surprising that *Notch* is highly overexpressed in iCCA (Xue et al., 2015).

1.9 The Notch Pathway and Fucosylation

Fucosylation-modulated proteins with potential oncogenic features include the Notch receptors. The extracellular domain of the Notch receptor (NECD) contains up to 36 EGF-like repeats that are targets of posttranslational modifications by O-glycan glycosylation (Andersson and Lendahl, 2014; Bray, 2016; Fortini, 2009; Fryer et al., 2002; Ranganathan et al., 2011) The transfer of O-fucose to these EGF repeats by POFUT1 with an O-fucose sequence is known to be an essential feature of Notch signaling (Shi and Stanley, 2003). During normal bile tract development, the Notch cascade plays a pivotal role in biliary cell coordination, tubule formation (Zong et al., 2009), and liver homeostasis (Bray, 2016). In mammals, the Notch canonical pathway is activated by direct cell-cell interaction through four receptors (Notch1, Notch2, Notch3, and Notch4) and mainly two types of ligands, Serrate/Jagged (Jagged1 and Jagged2) and Delta-like (DLL1, DLL3, and DLL4). Receptor ligand binding triggers the cleavage of the NECD (D'Souza et al., 2008; Katsube and Sakamoto, 2005). This conformational change unleashes the Notch intracellular domain (NICD), which subsequently translocates into the nucleus. Once in the nuclear compartment, NICD induces the expression of Notch target genes, like *SRY-Box Transcription Factor 9*

(*SOX9*) and *hairy and enhancer of split-1 (HES1)* (Bray, 2016; Cigliano et al., 2017), in association with mastermind-like (MAML1, MAML2, or MAML3) and recombinant signal-binding protein for immunoglobulin kappa J region (RBPJ) coactivators. However, without EGF repeat fucosylation in the NECD domain of the receptor, the Notch receptor-ligand binding is disturbed, and the related signaling is suppressed (Furukawa and Fukuda, 2016; D'Souza et al., 2008). Therefore, a possible approach to targeting Notch activity and iCCA progression is to interfere with its sensitivity to specific ligands by fucosylation inhibition. A strategy could be to either inhibit the formation of GDP-Fucose, which serves as the substrate donor for fucosyltransferases, or later, the transport of GDP-Fucose into the Golgi. In the present work, I hypothesized that inhibition and interference with the cellular O-fucosylation process of the Notch receptor might be an innovative therapeutic option for iCCA. A recent study showed that fucose derivatives serve as substrates for their corresponding GDP-fucose analogs within cells by manipulating the fucose salvage pathway. Some of these analogs likely evoke feedback inhibition of the *de novo* biosynthesis of GDP-fucose, reducing cellular fucosylation and resulting in altered behavior of proteins (Kizuka et al., 2017).

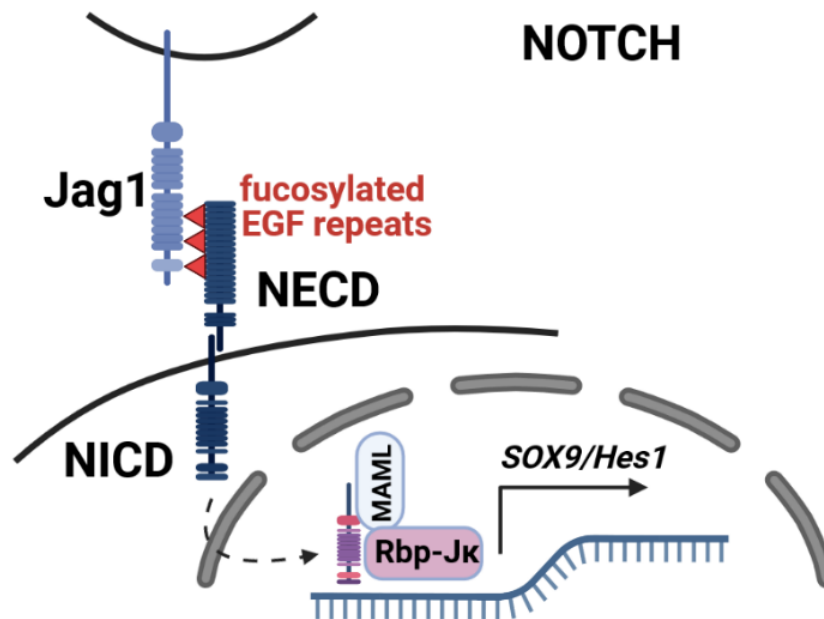


Figure 4. The Notch pathway. Signal transduction is induced by cell-cell contact. The Notch ligand Jagged1 (Jag1) binds to the Notch extracellular domain (NECD) of the Notch receptor, leading to the cleavage of the Notch intracellular domain (NICD) and its translocation to the nucleus. In the nucleus NICD induces the expression of Notch target genes, like SRY-Box Transcription Factor 9 (SOX9) and hairy and enhancer of split-1 (HES1) in association with mastermind-like (MAML1, MAML2, or MAML3) and recombinant signal-binding protein for immunoglobulin kappa J region (RBPJ) coactivators.

1.10 NF- κ B in Cancer

NF- κ B signifies a cluster of inducible transcription factors, pivotal regulators of the immune response (Pahl and Baeuerle, 1997). In 1986 NF- κ B was initially reported as a transcription factor binding a specific DNA region, the immunoglobulin chain enhancer, in mature mouse B lymphocytes (Sen and Baltimore, 1986). Later, NF- κ B was detected in many other cell types, like cells of the vascular wall and in numerous immunologically competent cells. In general, it is found in all mammal cells. The NF-

κ B family includes NF- κ B1 (p50), NF- κ B2 (p52), RelA (p65), RelB and c-Rel, and the κ B enhancer which exist as various hetero- or homo-dimers. (Liu et al., 2017) It also exists as a preformed enzyme in the cell and is directly activated after specific receptor binding. A distinction is made between the two forms of NF- κ B. An inactive form, bound to I κ B proteins in the cytoplasm (Baeuerle and Baltimore, 1988) and an active form in the cell nucleus. Furthermore, NF- κ B is constitutively activated in antibody-producing B cells, activated T cells, and macrophages (Sen and Baltimore, 1986). Various genes are regulated by NF- κ B, encoding, for instance, chemokines, cytokines, immunomodulators, cell surface receptors, and adhesion molecules (Ghosh and Karin, 2002; Pahl, 1999). Upon activation through the canonical pathway, I κ B α is phosphorylated at the N-terminal serines, which leads to its ubiquitin-dependent degradation in the proteasome. This ultimately results in the nuclear translocation of predominantly the p50/p65 and p50/c-Rel dimers (Hayden and Ghosh, 2008).

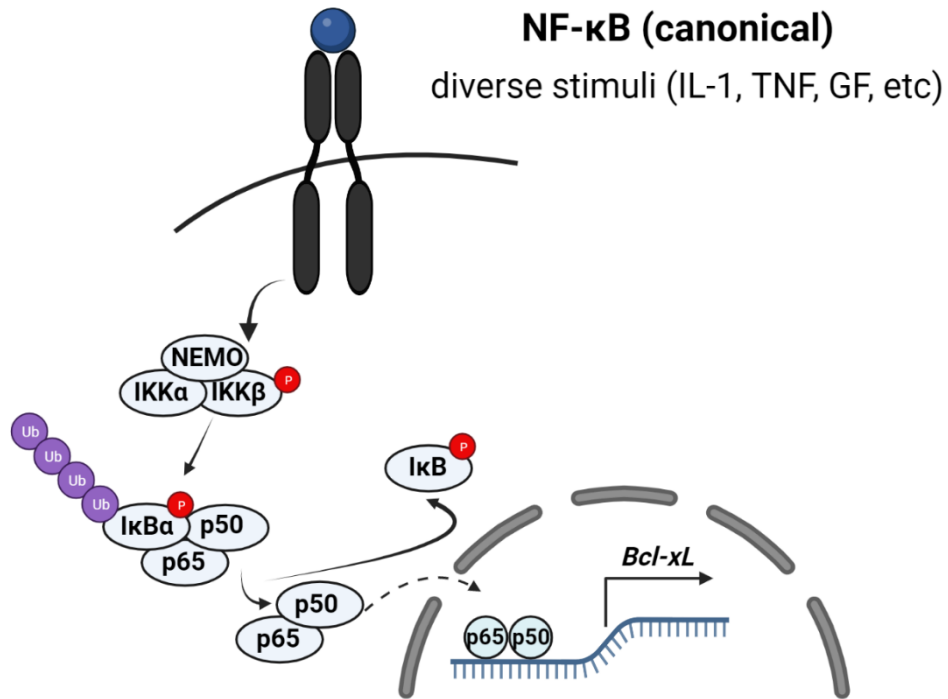
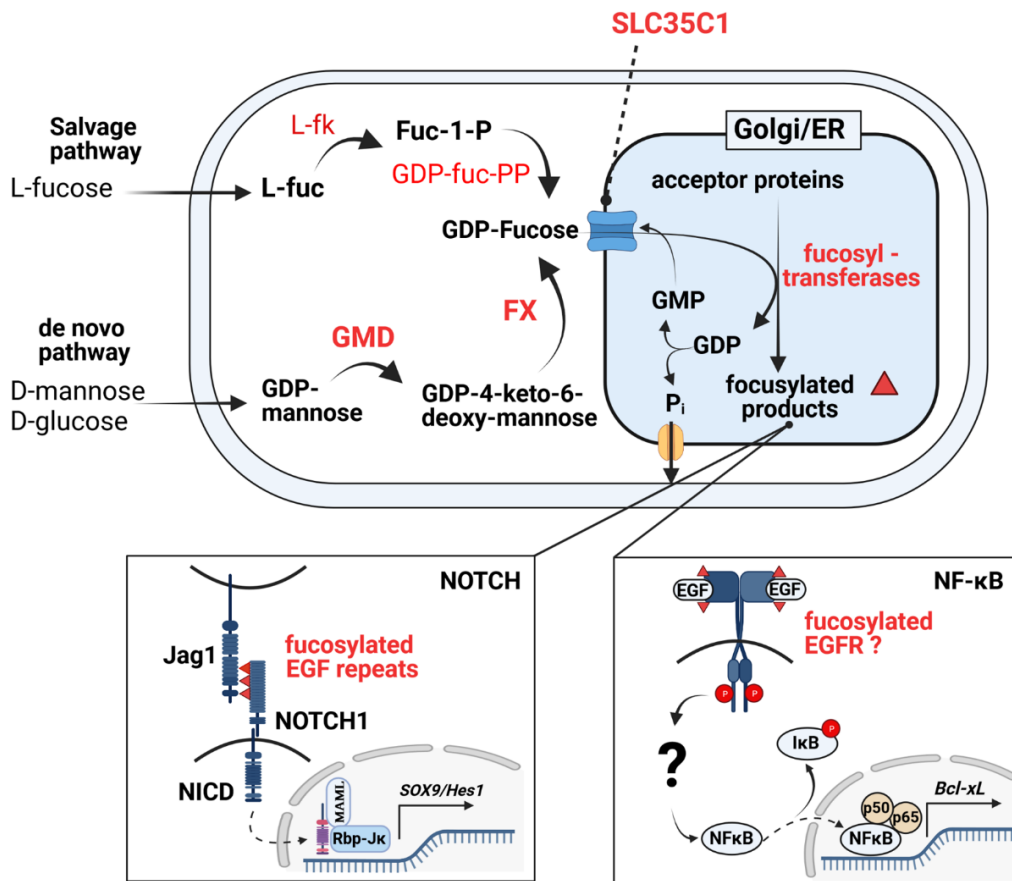


Figure 5. The NF- κ B pathway. IKK α , IKK β and the NF κ B essential modulator (NEMO) form the multi-subunit I κ B kinase (IKK) complex, which induce the proteasomal degradation of I κ B α upon receptor-ligand binding. Subsequently, the dimer of p50 and p65 can translocate into the nucleus and induce the target gene expression (*Bcl-xL*).

The role of NF- κ B in cancer is controversial, as this signaling pathway can act as a tumor activator or suppressor. However, the main function of NF- κ B is to suppress apoptosis. The typical activation of NF- κ B transcription factors by proinflammatory cytokines has been elucidated. Similarly, growth factors promoting NF- κ B activation have been identified, although the mechanisms mediating this event are still not fully understood. In 1998 and 2000, two papers demonstrated that EGF induces the NF- κ B activation by degradation of the inhibitory molecule I κ B α (Sun and Carpenter, 1998; Biswas et al., 2000). However, only recently the functional link between EGFR and NF-

κ B has been partly unraveled. Briefly, EGFR activation triggers the PKC ϵ monoubiquitination, recruiting the IKK complex to the plasma domain. PKC ϵ then activates NF- κ B through IKKb phosphorylation (Yang et al., 2012). EGFR must be fucosylated in its ligand-binding domain to bind the ligand and initiate the signaling cascade. Nevertheless, the relationship between fucosylated EGFR and the NF- κ B pathway remains poorly understood.



Intrahepatic cholangiocarcinoma development and progression

Figure 6. The interplay between Fucose and human iCCA relevant pathways and its possible targets to interfere in this relationship. The fucosylation pathway serves to maintain the GDP fucose level, which functions as a fucose donor in the Golgi or ER. Proteins fucosylated by fucosyltransferases include, for example, the Notch Receptor. The extracellular domain of Notch (NICD) must be fucosylated at EGF repeats in order to bind its ligand (Jag1) and subsequently start signal transduction via its intracellular domain (NECD). Another pathway that is important in the development of cancer is the NFκB pathway. A possible involvement of fucose occurs here via the EGF receptor, which must also be fucosylated in its ligand binding region. However, the exact relationships are still unclear.

2. Material and Methods

2.1 Material

Table 1. Consumables

<i>Product</i>	<i>Company</i>
<i>BOLT Bistris Plus 4-12% 15well #NW04125BOX</i>	<i>Life Technologies GmbH</i>
<i>iBlot™ 2 Transfer Stacks, nitrocellulose, mini #IB23002X3</i>	<i>Life Technologies GmbH</i>
<i>iBLOT NC Gel Transfer Stacks regular 10x #IB23001X3</i>	<i>Life Technologies GmbH</i>
<i>X10 iBlot&reg.; 2 TransferStacks, nitrocellulose #15296526</i>	<i>Fisher Scientific</i>
<i>Cell Counting Slides for TC10™/TC20™ Cell Counter #1450016</i>	<i>BioRad Laboratories GmbH</i>
<i>E-Plate 16 PET 1 VE=6 Platten #2801185</i>	<i>Agilent Technologies, Inc.</i>
<i>Cell Culture Cryogenic Tubes 1ml, Innengewinde #377224PK</i>	<i>Thermo Fisher Scientific Biosciences GmbH</i>
<i>Collection Tubes 2ml #740600</i>	<i>Macherey & Nagel</i>
<i>Protein LoBind Tubes, Protein LoBind, 1.5 mL #0030108116</i>	<i>Eppendorf Vertrieb Deutschland GmbH</i>
<i>Protein LoBind Tubes, Protein LoBind, 2 mL #0030108132</i>	<i>Eppendorf Vertrieb Deutschland GmbH</i>

<i>Protein LoBind Tubes, Protein LoBind, 5 mL #0030108302</i>	<i>Eppendorf Vertrieb Deutschland GmbH</i>
<i>PCR Softtubes, Flachdeckel #711080</i>	<i>Biozym Vertriebs GmbH</i>
<i>RÖHRCHEN, 50 ML, PP, 30/115 MM, STERIL, 20 ST./BTL. #227261</i>	<i>Greiner Bio-one GmbH</i>
<i>RÖHRCHEN, 15 ML, PP, 17/120 MM, #188271</i>	<i>Greiner Bio-one GmbH</i>
<i>PIPETTE, 5 ML, GRADUIERUNG 1/10 ML, STERIL #606180</i>	<i>Greiner Bio-one GmbH</i>
<i>PIPETTE, 10 ML, GRADUIERUNG 1/10 ML, STERIL #607180</i>	<i>Greiner Bio-one GmbH</i>
<i>PIPETTE, 25 ML, GRADUIERUNG 1/10 ML, STERIL #760180</i>	<i>Greiner Bio-one GmbH</i>
<i>PIPETTE, 50 ML, GRADUIERUNG 1/10 ML, STERIL #768180</i>	<i>Greiner Bio-one GmbH</i>
<i>10µl TipOne Filterspitzen (steril) #S1121-2710</i>	<i>Starlab GmbH</i>
<i>20µl TipOne Filterspitzen (steril) #S1120-1710</i>	<i>Starlab GmbH</i>
<i>200µl TipOne Filterspitzen (steril) #S1120-8710</i>	<i>Starlab GmbH</i>
<i>1000µl TipOne Filterspitzen (steril) #S1126-7710</i>	<i>Starlab GmbH</i>
<i>Combitips advanced 0,1 ml #5431808</i>	<i>OMNILAB- LABORZENTRUM GmbH & Co. KG</i>

<i>Combitips advanced 0,2 ml #5431809</i>	<i>OMNILAB- LABORZENTRUM GmbH & Co. KG</i>
<i>Combitips advanced 0,5 ml #5431810</i>	<i>OMNILAB- LABORZENTRUM GmbH & Co. KG</i>
<i>Combitips advanced 1,0 ml #5431811</i>	<i>OMNILAB- LABORZENTRUM GmbH & Co. KG</i>
<i>Combitips advanced 5,0 ml #5431813</i>	<i>OMNILAB- LABORZENTRUM GmbH & Co. KG</i>
<i>ZELLKULTUR MICROPLATTE, 96 WELL #655083</i>	<i>Greiner Bio-one GmbH</i>
<i>ZELLKULTUR MICROPLATTE, 96 WELL #655180</i>	<i>Greiner Bio-one GmbH</i>
<i>ZELLKULTURFLASCHE, 250 ML, 75CM² #658175</i>	<i>Greiner Bio-one GmbH</i>
<i>ZELLKULTURFLASCHE, 550 ML, 175 CM² #660175</i>	<i>Greiner Bio-one GmbH</i>

Table 2. Media, Buffers, and Reagents

<i>Product name</i>	<i>Company</i>
<i>Pierce™ Bovine Serum Albumin Standard Ampules, 2 mg/mL #23209</i>	<i>Thermo Fisher Scientific Biosciences GmbH</i>

Antigen Unmasking pH6.0 (CIT) #H-3300	Biozol Diagnostica Vertrieb GmbH
Antigen Unmasking pH high (Tris) #H-3301	Biozol Diagnostica Vertrieb GmbH
BOLT SAMPLE Reducing Agent, 10ml #B0009	Life Technologies GmbH
BOLT LDS Sample BUFFER(4x) #B0007	Life Technologies GmbH
Clarity Max Western ECL Substrate #1705062	BioRad Laboratories GmbH
DAKO Antibody Diluent #S202230-2	Agilent Technologies Sales & Service GmbH
DAKO Waschpuffer 10x #S3006852	Agilent Technologies Sales & Service GmbH
DMSO #25-950-CQC	VWR International GmbH
DMEM / F12, w/o L-Glutamine, w/o HEPES #AC-LM-0018	Anprotec
DPBS w/o Ca, w/o Mg #AC-BS-0002	Anprotec
7-AAD Viability Solution 2 ml #00-6993-50	<i>Thermo Fisher Scientific Biosciences GmbH</i>
FetalBovine Serum (Qualified) #AC-SM-0143	Anprotec
HALT-Protease & Phosphatase Inhibitor Cocktail (100x) #78444	Life Technologies GmbH
HEPES Buffer 1 M #AC-DS-0007	Anprotec

<i>Lipofectamine® RNAiMAX Transfection Reagent #13778150</i>	<i>Life Technologies GmbH</i>
<i>Lipofectamine™ 2000 Transfection Reagent #11668019</i>	<i>Life Technologies GmbH</i>
Loading Dye 6x DNA Gele #1660101	Bio-Rad Laboratories GmbH
L-Glutamin, 200mM #AC-AS-0001	Anprotec
Millipore water	Milli-Q® UF Plus Ultrapure Water System
Novex™ 20X Bolt™ MES SDS Running Buffer #13246499	ThermoFisher Scientific
Nuclease free Water 10x50ml #AM9937	Life Technologies GmbH
<i>NuPAGE™ Sample Reducing Agent (10X) #NP0009</i>	Thermo Fisher Scientific GmbH
<i>Opti-MEM® I Reduced Serum Medium #31985-062</i>	<i>Life Technologies GmbH</i>
Penicillin / Streptomycin #AC-AB-0024	Anprotec
Pierce™ Peroxidase-Suppressor #35000	Life Technologies GmbH
Pierce Protein-Free T20 (TBS) Blocking Buffer #37571	Life Technologies GmbH
Ponceau S (C.I. 27195), 25 g #5938.1	<i>ROTH</i>
<i>RPMI 1640, w/o L-Glutamine #AC-LM-0060</i>	Anprotec
Sodium Pyruvate #AC-DS-0023	Anprotec

SignalStain® Boost IHC Detection Reagent (HRP, Mouse) # 8125S	Cell Signaling Technology Europe, B.V.
<i>SignalStain® Boost IHC Detection Reagent (HRP, Rabbit) #8114</i>	<i>Cell Signaling Technology Europe, B.V.</i>
TaqMan Fast Advanced Master Mix #4444963	Thermo Fisher Scientific Biosciences GmbH
T-Per Tissue Protein Extraction Reagent 500ml #78510	Life Technologies GmbH
Tris Buffered Saline with Tween® 20 #9997S	Cell Signaling Technology Europe, B.V.
Trypan blue solution #T8154-20ml	Sigma-Aldrich GmbH
<i>Trypsin EDTA #AC-EZ-0020</i>	<i>Anprotec</i>
Xylene	VWR International GmbH

Table 3. Kits Used During this Project

<i>Product</i>	<i>Company</i>
Notch1 Pathway Reporter Kit (Human) #BPS-79503	<i>Biomol GmbH</i>
<i>Dual Luciferase (Firefly-Renilla) Assay System #BPS-60683-2</i>	<i>Biomol GmbH</i>
<i>NF-kB p65 Transcription Factor Assay Kit #ab133112</i>	<i>Abcam plc</i>
<i>Nuclear Extract Kit #40010</i>	<i>Active Motif</i>

<i>Human Phosphorylation Pathway Profiling Array (55 targets) #SARB0063</i>	<i>Biomol GmbH</i>
<i>TaqMan™ Advanced miRNA cDNA Synthesis Kit #A28007</i>	<i>Thermo Fisher Scientific Biosciences GmbH</i>
<i>ImmPACT® NovaRED™ Substrate Kit, Peroxidase (HRP) #SK-4805</i>	<i>Vector Laboratories, Inc.</i>
<i>Annexin V eFluor™ 450 (eBioscience™ Annexin V Apoptosis Detection Kit eFluor™ 450)</i>	<i>Invitrogen® (ThermoFisher Scientific)</i>
<i>eBioscience™ Annexin V Apoptosis Detection Kit eFluor™ 450</i>	<i>Invitrogen® (ThermoFisher Scientific)</i>

Table 4. Antibodies for Immunohistochemistry and Western Blotting

Product name	Company
Notch1 #3608S	Cell Signaling Technology
Notch2 #5732	Cell Signaling Technology
SOX9 #82630S	Abcam
NF-κB p65 #8242S	Cell Signaling Technology
Bcl-xL #2764S	Cell Signaling Technology.

IκBα #4814	Cell Signaling Technology
p4E-BP1 #2855	Cell Signaling Technology
GSK-3β #9315S	Cell Signaling Technology
LC3 A/B #4108S	Cell Signaling Technology
AKT #4691S	Cell Signaling Technology
p-AKT #4060S	Cell Signaling Technology
ERK ½ #ab214036	Abcam
p-ERK ½ #4370S	Cell Signaling Technology
cleaved Caspase-3 #9661	Cell Signaling Technology
p-S6 Ribosomal Protein #5364	Cell Signaling Technology
p-STAT3 #9145	Cell Signaling Technology
p-38 MAPK #4631S	Cell Signaling Technology
Ra1A #OSR00268W	ThermoScientific
YAP/TAZ #8418	Cell Signaling Technology
Jagged1 AC #70109	Cell Signaling Technology
AAL #B-1395	Vectorlabs
LCA #B-1045	Vectorlabs

UEA #B-1065	Vectorlabs
CK19 #ab133496	Abcam
POFUT1 #14929-1-ap	ProteinTech Group
FUCA1 #16420-1-AP	ProteinTech Group
SLC35C1 #PA5-42475	ThermoScientific
TSTA3 #15335-1-AP	ProteinTech Group
GMDS #15442-1-AP	ProteinTech Group
LFNG #LS-B9718	LSBio
MFNG #LS-B9726	LSBio
RFNG #PA5-52844	ThermoScientific
iNOS #PA3-030A	ThermoScientific
NQO1 #sc-376023	SantaCruz
NRF2 #ab137550	Abcam
CD133 #ab27092	Abcam
CXCR4 #11073-i-AP	ProteinTech Group
CD44 #37259S	Cell Signaling Technology
EGFR #4267	Cell Signaling Technology

p-EGFR #3777	Cell Signaling Technology
GAPDH #ab9485	Abcam
β -ACTIN #ab20272	Abcam

Table 5. TaqMan Gene Expression Probes

Gene name	ID
SLC35C1	Hs01018029_m1
FX	Hs00163023_m1
Notch1	Hs01062014_m1
Notch2	hs01050702_M1
Sox9	Hs00165814_m1
Hes1	Hs00172878_M1
CD44	Hs01075862_m1
CXCR4	Hs00237052-m1
Bcl-xL	Hs00236329_m1

Table 6. Clinicopathological Features of iCCA Patients

Variables	
No. of patients	37
Male	27
Female	10
Age (years)	
<60	14
≥60	27
Etiology	
HBV	9
HCV	6
Hepatolithiasis	5
NA	17
Liver cirrhosis	
Yes	11
No	26
Tumor differentiation	
Well	19
Moderately	9
Poorly	9
Tumor size (cm)	
<5	30
>5	7
Tumor number	
Single	30
Multiple	7
Prognosis	
Better (≥ 3 years)	12
Poorer (< 3 years)	25
Lymph node metastasis	
Yes	13
No	24
Lung metastasis	
Yes	7
No	30

Abbreviations: NA, not available.

Table 7. Software for Data Analysis and Illustration

Software name	Company
Attune NxT Flow Cytometer Software	Invitrogen® (ThermoFisher Scientific)
CFX Maestro™ Software	Bio-Rad Laboratories, Inc.
Excel Office 365	Microsoft Corp.
FlowJo™ (v.10.6.2)	Becton Dickinson GmbH
<i>Biorender</i>	<i>BioRender</i>
GraphPad Prism 8.0	GraphPad Software
Image Lab™ Software (v.6.0.1)	Bio-Rad Laboratories, Inc.
NIS-Elements D	Nikon Instruments Europe BV
Omega software	BMG LABTECH GmbH
Origin Home-Use 2020 (Origin)	OriginLab Corp.
PowerPoint Office 365	Microsoft Corp.
RTCA 2.1.0	ACEA Biosciences, Inc.

iCCA Cell Lines and Patient Material

The two human iCCA cell lines, HUCCT1 and K KU-M213, were used for *in vitro* experiments. The cell lines have been tested mycoplasma free before usage.

Table 6 summarizes the clinicopathological features of iCCA patients for the tissue used in this work. The local Ethical Committee of the Medical Universities of Greifswald (approval code: BB 67/10; June 3, 2010) and Regensburg (approval code: 17-1015-101; July 4, 2018) provided the Institutional Review Board approval in compliance with the Helsinki Declaration. In addition, all individuals provided informed consent in written form.

2.2 Methods

2.2.1 Cell Culture

HUCCT1 and KKU-M213 are human intrahepatic cholangiocarcinoma (iCCA) cell lines derived from patient specimens. These cells are a suitable model for research on cholangiocarcinoma and were used for the present study. The cells were cultivated in 175 mL flasks at a density of 6.0×10^6 cells per ml in either Dulbecco's modified eagle's medium (DMEM, High Glucose, Anprotec, Bruckberg, Germany) or Gibco Roswell Park Memorial Institute (RPMI, Anprotec) 1640 Medium (500mL), which were enriched with antibiotics (1%), HEPES buffer (1%), L- glutamine (1%), and sodium-pyruvate (1%) as well as FCS (10%). 10 mL 2x trypsin solution in DPBS was added to each flask after the removal of the old medium to detach the cells from the bottom. After 5-15 min incubation at 37°C, the Trypsin reaction was stopped with a medium containing FCS. After centrifugation and aspiration of supernatant, the pellet was resuspended in 10 mL fresh medium. For further experiments, 300 – 500.00 cells were seeded into 6-well plates. The total volume per well was 2mL, and fresh medium was added to the appropriate volume of cell suspension. The flasks and the plates were stored in the incubator with 5% CO₂ and 37°C. Cells were incubated at 37°C and 5.0% v/v CO₂ if not further specified. Cells were sown, treated, and harvested in a vertical laminar flow hood (Heraeus Group, Hanau, Germany).

2.2.2 Human Tissue Specimens

Fresh and formalin-fixed, paraffin-embedded human iCCA and matching non-tumorous surrounding liver tissues from surgical resections were collected at the

Universities of Greifswald (Greifswald, Germany) and Regensburg (Regensburg, Germany). Table 6 summarizes the clinicopathological features of iCCA patients. The local Ethical Committees of the Medical Universities of Greifswald (approval code: BB 67/10; June 3, 2010) and Regensburg (approval code: 17-1015-101; July 4, 2018) provided the Institutional Review Board approval in compliance with the Helsinki Declaration. All individuals provided informed written consent.

2.2.3 siRNA Silencing

HUCCT1 and KKU213 cell lines were treated with specific small interference RNAs (siRNAs; Thermo Fisher Scientific, Waltham, MA, United States) together with Lipofectamine™ RNAiMAX (Thermo Fisher Scientific). First, the cells were seeded in 6-well plates, as described above. Subsequently, the cells were transfected with siRNA against *SLC35C1* (s30784, Thermo Fisher Scientific), *TSTA3* (s14466, Thermo Fisher Scientific), *NOTCH1* (108982, Thermo Fisher Scientific), *EGFR* (1956, SiTOOLS Biotech GmbH), or scramble siRNA (as a negative control; 4392420, Thermo Fisher Scientific) following the manufacturer's instructions. In addition, fucosylation was inhibited in the iCCA cell lines with the L-Fucose analog 6-Alkynylfucose (6AF; 23007-v 0.5mg; Pepta Nova, Sandhausen, Germany). Finally, the cells were either taken after 72 hours for RNA and protein isolation to perform further experiments or used for growth and migration analyses.

For each well, the following Eppendorf tubes were prepared:

Lipofectamine Mix: 100µl Opti-MEM + 5µl RNAiMax

Control: 100µl Opti-MEM

Scramble: 100µl Opti-MEM + 10µl Scramble siRNA

2.2.4 Inhibition with 6-Alkynylfucose

The L-fucose analog 6-Alkynylfucose (6AF; Table 3) was used to inhibit the fucosylation in the intrahepatic cholangiocarcinoma cell lines. Specifically, the cells were seeded in 6-well plates, 300.000 – 500.000 cells per well, and after 24h incubation time for the attachment of the cells, they were treated with various concentrations of 6AF. The calculation for the highest concentration of inhibitor in 2 ml media was done as follows:

$$c_i \text{ (stock)} = 10\text{mM}$$

$$c_x = 0,02\text{mM}$$

$$V_x = 2\text{ml}$$

$$V_i = 2\text{ml} * 10\text{mM} = 0,004 \text{ ml}$$

The cells were either taken after 72 hours for RNA and protein isolation to perform further experiments or used for migration analysis.

2.2.5 Protein Extraction and Quantification

The cells were detached from the plate using a cell scraper, and the suspension was collected separately in 1.5 ml tubes. Next, the cell suspension was centrifuged, and the supernatant was discarded. Cells were lysed with 50-100 µl T-PER™ Tissue Protein Extraction Reagent (78510, Thermo Fisher Scientific) containing Halt™

Protease and Phosphatase Inhibitor Cocktail (87786, Thermo Fisher Scientific). The cell suspensions were incubated on ice for 30 min and were vortexed every 10 min. Afterward, the tubes were centrifuged at the highest speed for 30 min at 4°C. The supernatant was collected. A Bradford assay in a 96-well microplate was performed to quantify the amount of extracted proteins using the Bio-Rad Protein Assay Dye Reagent Concentrate (5000006, Bio-Rad, Hercules, California, United States). Bovine serum albumin (BSA) (23209, Thermo Fisher Scientific) was used as a standard.

2.2.6 LDS-PAGE Gel Electrophoresis

The extracted proteins from normal human cholangiocytes (NHC), iCCA, or human tissues were separated by Gel Electrophoresis using Bolt™ 4-12% Bis-Tris Plus 1.0 mm x 15 polyacrylamide gradient gels (NP0326BOX, Thermo Fisher Scientific). Ten µg of extracted proteins were added to the Bolt™ Sample Reducing Agent (B0009, Thermo Fisher Scientific) and Bolt™ LDS Sample Buffer (B0007, Thermo Fisher Scientific) in 1.5 ml Eppendorf tubes. The solutions were filled with nuclease-free water to a final 12 µl. The complete loading samples were heated before electrophoresis for 10 min at 71°C. Gels were loaded with 10µl of the protein loading solution. The proteins were electrophorized (120 V, 500 mA, 1 h) using 1X Novex™ NuPAGE™ MES SDS Running Buffer (NP0002, Thermo Fisher Scientific) and Novex™ SeeBlue™ Plus2 Prestained Standard (LC5925, Thermo Fisher Scientific). After electrophoresis, the gels were incubated in ethanol (20% v/v, RT, 150 rpm, 5 min), and the electrophorized proteins were blotted onto nitrocellulose membranes in a semi-dry transfer using the iBlot™ 2 transfer device (IB21001, Thermo Fisher Scientific) and the iBlot™ 2 NC Regular Stacks (IB23001, Thermo Fisher Scientific) by application of the pre-set

template P0. After blotting, the membranes were stained with Ponceau Red S solution (6226-79-5, Sigma-Aldrich, St. Louis, Missouri, United States) for loading control. Tris Buffered Saline with Tween® 20 (28360, Thermo Fisher Scientific) was used to wash out the Ponceau Red S solution. Subsequently, the membranes were incubated with Pierce™ Protein-Free T20 Blocking Buffer (37571, Thermo Fisher Scientific) on an Orbital Shaker (150 rpm, 1 h, RT). Target protein retrieval was performed by incubating the membranes with primary antibodies against NOTCH1 (3608, Cell Signaling, Danvers, Massachusetts, United States), NOTCH2 (5732S, Cell Signaling), SOX9 (82630, Cell Signaling), NF-κB p65 (8242S, Cell Signaling), Bcl-xL (2762, Cell Signaling), IκBα (9242, Cell Signaling), p4E-BP1 (9644S, Cell Signaling), GSK-3β (9332, Cell Signaling), LC3 A/B (4108S, Cell Signaling), AKT (4691S, Cell Signaling), pAKT (4060S, Cell Signaling), ERK 1/2 (9102, Cell Signaling), pERK 1/2 (4370, Cell Signaling), cleaved Caspase-3 (9661, Cell Signaling), p-S6 Ribosomal Protein (4856S, Cell Signaling), p-STAT3 (9145, Cell Signaling), p-38 MAPK (4631S, Cell Signaling), RALA (OSR00268W, Thermo Fisher Scientific), YAP/TAZ (8418, Cell Signaling), CXCR4 (11073-2-AP, Proteintech, Rosemont, IL, USA), iNOS (PA3-030A, Thermo Fisher Scientific), Jagged1 AC (sc-390177, Santa Cruz, Dallas, Texas) in Pierce™ Protein-Free T20 Blocking Buffer (1:1000) under shaking (4°C, 150 rpm, ON). After rinsing the membranes with TBST, they were incubated with horseradish peroxidase-conjugated anti-rabbit (Abbkine, A21010) or anti-mouse secondary antibodies (A21020, Abbkine, Wuhan, China) in a blocking buffer (1:20,000 150 rpm, 1 h, RT). After three washing steps followed (150 rpm, 15 min, RT), the membranes were scanned with the ChemiDoc™ MP Imaging System (Bio-Rad) after the addition of the Clarity Max™ Western ECL Substrate (1705062, Thermo Fisher Scientific). To detect fucose residues on the blotted membranes, the biotinylated lectins AAL (1:50, B1395-

1, Vector Laboratories, Newark, CA, United States), LCA (1:50, B1045-5, Vector Laboratories), and UEA-I (1:100, B-1065-2, Vector Laboratories) were used and added to the membrane after 30 min incubation with Pierce™ Protein-Free T20 Blocking Buffer (37571, Thermo Fisher Scientific) at RT. As a secondary antibody, the HRP-conjugated Streptavidin was used (1:5000; 4800-30-06; R&D System, Minneapolis, MN, United States). Subsequently, the membranes were scanned with the ChemiDoc™ MP Imaging System.

Table 8. Three steps for membrane blotting.

Transfer step	U/V	Time in minutes
Step 1	20	1
Step 2	23	4
Step 3	25	2

2.2.7 Lectin Blotting

To detect fucose residues on the blotted membranes, the biotinylated lectins AAL, UEA-I, and LCA (1:50 for AAL and LCA and 1:100 for UEA-I; Table 9) were used and added to the membrane after the incubation in blocking buffer (150 rpm, 30 min, room temperature). These lectins bind to different structures containing fucose or mannose and are suitable for providing an overview of the fucosylation levels of total protein lysates. These biotinylated antibodies could be either detected with an avidin-biotin-

based peroxidase system (VECTASTAIN® Elite ABC Kit; Vector Laboratories), which was added after washing the membrane (150 rpm, 30 min, room temperature). As a substrate for the horseradish peroxidase, the ImmPACT® NovaRED® Substrate (Vector Laboratories) was added and distributed uniformly on the membrane surface. The membranes were scanned immediately with the colorimetric program of the ChemiDoc™ MP Imaging System. Alternatively, I used the HRP-linked secondary antibody (1:5000) instead of the ABC System and detected the protein bands with the ECL substrate. The advantage of the latter method is a chemiluminescent image, which has a stronger signal and can be quantified more accurately.

Table 9. Lectins for lectin blotting and their target structure.

Antibody	Target structure	Label	Catalog number
LCA, biotinylated	α -linked mannose	Vector Laboratories	B1045-5
UEA, biotinylated	α -linked fucose residues on glycoprotein	Vector Laboratories	B-1065-2
AAL, biotinylated	Fucose linked α (1,6) N-acetylglucosamine	Vector Laboratories	B1395-1
Strep-HRP	Biotin	TACS	4800-30-06

2.2.8 RNA Isolation

The RNA was isolated with the NucleoSpin RNA Plus Kit (740984.50, Macherey-Nagel, Düren, Germany) according to the manufacturer's protocol. Then, the eluted RNA was measured with the NanoDrop™ 2000/2000c Spectrophotometer (ND-2000, Thermo Fisher Scientific).

2.2.9 Reverse Transcription Polymerase Chain Reaction (rt-PCR)

T100™ Thermal Cycler (1861096, Bio-Rad) and the High-Capacity cDNA Reverse Transcription Kit (4368814, Thermo Fisher Scientific). A complete rt-PCR master mix (10µl prepared with the reverse transcription kit was added to solutions of total RNA (1.0 µg, 10 µl) in PCR cups. The solution was kept on ice for the time of the preparation. A standard protocol for reverse transcription was applied (Table 10). After the Reverse Transcription run, the cDNA was stored at -20°C. After the PCR run, the cDNA was diluted to 20ng/µl with Nuclease-free water. The cDNA was stored at -20°C.

Table 10. Protocol for reverse transcription.

Step	t / min	T / °C
Step 1	10	25°C
Step 2	120	37°C
Step 3	5	85°C
Step 4	(hold)	4°C

2.2.10 Quantitative Real-Time RT-PCR (qRT-PCR)

qRT-PCR was performed using a CFX96™ Real-Time System (Bio-Rad) and the TaqMan™ Fast Advanced Master Mix (11380912, Thermo Fisher Scientific). The cDNA (2.0 µg · µL⁻¹, 1.0 µL) was added to the qPCR Master Mix (9µl) containing the TaqMan™ Fast Advanced Master Mix, a VIC labeled human primer for the housekeeper gene *Actin B* (Hs99999903, Thermo Fisher Scientific) and a FAM labeled human primer for the genes of interest *TSTA3* (FX, Hs00163023_m1, Thermo Fisher Scientific), *SLC35C1* (Hs01018029_m1, Thermo Fisher Scientific), *CD44* (Hs01075864_m1, Thermo Fisher Scientific), and *CXCR4* (Hs00607978_s1, Thermo Fisher Scientific). Each sample was analyzed in triplicate. The microplate was sealed using a PX1™ PCR Plate Sealer (1814000, Bio-Rad), and a standard qRT-PCR was conducted. The results were evaluated using the $\Delta\Delta C_t$ method, comparing treated cells versus untreated cells (control). The mean value of C_t and the standard error of the mean (SEM) were calculated for each sample using Microsoft Excel (Holzapfel and Wickert, 2007; Rao et al., 2013).

2.2.11 Immunohistochemistry and Assessment of Proliferation, Apoptosis, and NOTCH1 Index

For immunohistochemical analysis, tissue samples from patients affected by iCCA were analyzed. Two µm tissue sections from formalin-fixed, paraffin-embedded tissues were used. Tissue slides were deparaffinized (70°C, 30-40 min), soaked in xylene (3x 15 min), and incubated with isopropanol (from 100% to 70%, 5 min). To unmask the epitope, the slides were boiled in a citric acid-based solution (1x) pH 6.0, or, in the

case of the anti-SLC35C1 antibody, in Tris-EDTA buffer pH 9 (110°C, 8 min). After cooling, the slides were washed with Millipore water and Dako Wash Buffer (1x in Millipore water). The Pierce™ Peroxidase Suppressor (PI35000, Thermo Fisher Scientific) was employed for 15min to block the endogenous peroxidase. Next, the slides were rewashed before the primary antibodies AAL (B-1395-1, Vector Laboratories), LCA (B1045-5, Vector Laboratories), UEA-I (B-1065-2, Vector Laboratories), CK19 (61010, Progen, Heidelberg, Germany), POFUT1 (149329-1-ap, Proteintech), FUCA1 (Ab230324, Abcam, Cambridge, United Kingdom), SLC35C1 (HPA064001, Sigma-Aldrich), TSTA3 (15335-1-ap, Proteintech), GMDS (15442-1-ap, Proteintech), NOTCH1 (LS-C114369-100, Lifespan BioSciences, Seattle, WA, United States), CXCR4 (11073-2-AP, Proteintech), LFNG (LS-B9718, LifeSpan BioSciences), MFNG (LS-B9726, LifeSpan BioSciences), and RFNG (PA5-52844, Thermo Fisher Scientific) in REAL™ Antibody Diluent (8112, Cell Signaling) were applied to the sections. After the incubation with the primary antibody overnight at room temperature, the slides were washed (2x, Dako Wash Buffer). For the biotinylated lectins, the avidin-biotin-based peroxidase system VECTASTAIN® Elite ABC Kit (PK-6100, Vector Laboratories) was applied as a secondary antibody (150 µl, 1h, room temperature). The remaining slides were either incubated with SignalStain® Boost IHC Detection Reagent HRP-linked against rabbit (8114, Cell Signaling) or mouse (8115, Cell Signaling). Subsequently, the sections were washed (2x, Dako Wash Buffer), and finally, the ImmPACT® NovaRED™ Substrate (SK-4805, Vector Laboratories) was applied (15 min, RT). Slides were counterstained in hemalum solution (15 s). The staining's specificity was determined by omitting the primary antibody. The proliferation index was determined in the CAM lesions to assess proliferation by counting Ki67-positive cells on at least 1000 tumor cells per sample. The Apoptosis index was

evaluated in the same mouse samples by counting Cleaved-Caspase 3 (dilution 1:50; 9661, Cell Signaling Technology) positive cells on at least 1000 tumor cells per sample. Finally, the NOTCH1 index was determined by counting NOTCH1 (dilution 1:500; LS-C114369-100, LifeSpan BioSciences) positive cells in the nucleus on at least 1000 tumor cells per sample. Only cells stained in dark brown or black were considered "positive" when evaluating the Ki-67 and NOTCH1 indices.

2.2.12 Real-time Cell Analysis (RTCA) and Assessment of Proliferation *in Vitro*

Real-time cell analysis (RTCA) experiments based on impedance measurement were performed using an xCELLigence® RTCA DP instrument and the RTCA 2.1.0 software from ACEA Bioscience, Inc. For RTCA experiments, 10,000 HUCCT1 and KKH213 cells were sown in E-Plates 16 PET in a 150 μ L medium. The monitoring of the dynamic cell proliferation in one-hour intervals was started two hours after plating and was paused after 24 hours for cell treatment. Medium without cells and inhibitor served for blank measurement. The software automatically subtracted the blank values. After 24 hours of cell growth, 50 μ L of medium supplemented with different concentrations (2.5X) of 6AF, LFUC, or medium with pure DMSO was added. Each treatment was at least measured in triplicates. The concentration of the DMSO control was calculated based on the highest DMSO content of media after drug supplementation. Dynamic cell proliferation monitoring was conducted at 15 minutes intervals. Cell index values were manually normalized to the time of inhibitor addition. Each treatment was performed in triplicates, and each experiment was performed at least 3 times. Cell proliferation was assessed in the iCCA cell lines and the CAF at the 48-hour time point

using the BrdU Cell Proliferation Assay Kit (Cell Signaling Technology), following the manufacturer's instructions. All experiments were repeated three times in triplicate.

2.2.13 Analysis of Cell Motility

HUCCT1 and K KU213 cells were seeded into sterile six-well plates (Sarstedt AG & Co. KG) with a density of 300.000 cells in 2 mL medium. The respective medium was supplied with different concentrations of 6AF/L-Fucose or DMSO as control. The concentration of the DMSO control was calculated based on the highest DMSO content after drug supplementation. After the cells reached 100% confluency, a uniform scratch was made to the cell layer using a pipette tip. The wells were washed with PBS, and 4 ml of fresh medium containing drug or DMSO was added. The plate was covered with HoloLids (PHI AB, Lund, Sweden) and stored in an incubator. The cells were monitored using the incubator tolerant phase imaging microscope HoloMonitor® (PHI AB). Using the general capture application, the wounds were captured with the lime-lapse microscope every 2 hours for 24 hours. The wound area for each time point was measured using the ImageJ software (Schneider et al., 2012), and each experiment was performed at least 3 times.

2.2.14 Nuclear and Cytoplasmic Extraction

For the stepwise separation and preparation of cytoplasmic and nuclear fractions from HUCCT1, RBE, and K KU213 cells, the Thermo Scientific™ NE-PER™ Nuclear and Cytoplasmic Extraction Reagents (78835, Thermo Fisher Scientific) were used. After

cells were treated for 72h with 6AF 20 μ M or 40 μ M or DMSO as a control, they were harvested using a cell scraper and collected in tubes. For nuclear protein extraction, procedures were conducted following the manufacturer's instructions.

2.2.15 NF- κ B p65 Transcription Factor Assay

For the detection of specific transcription factor DNA binding activity in nuclear extracts, the NF- κ B p65 Transcription Factor Assay Kit was used (ab133112, Abcam). After the cytoplasmic extraction of HUCCT1, RBE, and K KU213 cell proteins, the NF- κ B p65 transcription factor binding activity was assessed following the manufacturer's instructions. Dual Luciferase Assay and Notch1 Pathway Reporter Kit

2.2.16 Co-Immunoprecipitation

K KU213 and HUCCT1 cells were washed three times with cold PBS (phosphate-buffered saline) and lysed with the T-PER™ Tissue Protein Extraction Reagent (78510, Thermo Fisher Scientific) containing the Halt™ Protease and Phosphatase Inhibitor Cocktail (87786, ThermoFisher) for 30 minutes on ice. After centrifugation for 30 minutes at max speed (14,000 rpm, in a microcentrifuge), the supernatant was collected, and protein concentration was determined with Bradford assay (Bio-Rad) using bovine serum albumin as a standard. Immunoprecipitations were performed in 500 μ L of RIPA buffer using 1,5 mg of protein lysate. For each protein lysate, 30 μ L of the Jagged1 antibody conjugated to agarose beads antibody (sc-390199, Santa Cruz) were added, and the lysates were incubated overnight at 4°C on a rotating platform.

The samples were washed three times with a lysis buffer, resuspended in 19,5 µl lysis buffer, 3 µl Bolt™ Sample Reducing Agent (10x), and 7,5µl Bolt™ LDS Sample Buffer (4x), and boiled for 10 minutes at 95°C. Samples were separated and blotted as described above.

2.2.17 Flow Dual Luciferase Assay and Notch1 Pathway Reporter Kit

The Notch Activity was analyzed using the human Notch1 Pathway Reporter Kit (79503, BPS Bioscience, San Diego, CA, United States). About 5000 cells per well of HUCCT1 and K KU213 cell lines were seeded in a 96-well format in 100µl of BPS medium I (79259, BPS Bioscience). The next day, the cells were transfected with the supplied DNA mixtures in Opti-MEM I medium (31985062, ThermoFisher Scientific). After 24h of incubation, the medium was changed to a fresh medium. After another 24 hours, the dual luciferase assay was performed. Dual luciferase (LUC) assay extracts were prepared using the Dual-Luciferase Reporter Assay System kit (E1910, Promega, Madison, WI, United States) according to the manufacturer's instructions. All samples were analyzed in triplicates.

2.2.18 Flow Cytometry for Apoptosis

Flow cytometric measurements were run on an Attune Nxt Acoustic Focusing Cytometer combined with the Attune Nxt Auto Sampler and the Attune Nxt Flow Cytometer Software (Invitrogen, ThermoFisher Scientific). HUCCT1 and K KU213 cells were harvested after 72h incubation with different concentrations of 6AF (DMSO Ctr, 20µM, 40µM). After rinsing the wells with PBS, the cells were incubated with Trypsin-

EDTA (3X in PBS 500 µl) until the cells were detached. The suspension was collected in the appropriate falcons. The falcons were filled up with PBS to a final volume of 14 mL, and the cell suspensions were centrifuged for five minutes at 4°C and 300 g. The supernatant was discarded. The cell pellets were suspended in binding buffer (1X, 800µl) using the Annexin V Apoptosis Detection Kit (88-8007-72, Thermo Fisher Scientific). The suspensions were transferred into 5 mL flow cytometry tubes, taking 100 µL of each sample for cell pooling. The pooled mixture was shared out between three control samples (Annexin V, 7-AAD, unstained). Samples and the Annexin V control were centrifuged for five minutes at 4°C and 300 g, while the 7-AAD control was incubated at 70°C and 400 rpm for 10 minutes. The supernatant was removed. If not further specified, all steps were performed on ice. Next, the pellets of all samples and the Annexin V control were resuspended in 100 µl binding buffer and were stained with 5µl eFluor™ 450-labeled Annexin V solution from the detection kit. The tubes were incubated in the dark and at room temperature for 45 minutes. The 7-AAD control and the unstained sample were stored on ice. Next, 100 µl binding buffer and 5 µl 7-AAD Viability Staining solution were added to all samples, apart from the Annexin V control and the unstained sample and incubated for 60 seconds on ice. All cell suspensions were further diluted with 50 µl binding buffer. The final flow cytometry apoptosis measurement was performed using the lab internal measurement protocol.

2.2.19 Human Cancer-Associated Fibroblasts (hCAFs) Isolation

Human iCCA tissues used for hCAFs isolation were collected and used following the approval by the Ethical Committees from the Azienda Ospedaliero Universitaria Consorziale Policlinico di Bari (Bari, Italy; protocol number: 254; date of release:

February 2012) and the local hospitals collaborating with the Donostia University University Hospital (San Sebastian, Spain). As previously described [Mancarella et al. 2022], upon receipt, biopsies of intrahepatic cholangiocarcinoma immediately after surgery were appropriately shredded into small pieces (1–2 mm) and stored in MACS tissue storage solution (Miltenyi Biotec, Bergisch Gladbach, Germany). Then, we performed enzymatic and mechanical digestion on iCCA tissue specimens in HBSS solution with 50-200 U/mL collagenase Type IV (Thermo Fisher Scientific, Waltham, MA, USA), 3 mM CaCl₂, and Antibiotic–Antimycotic (Thermo Fisher Scientific, Milan, Italy) at 37 °C under gentle rotation for 2 h or more as needed. The resulting cells were harvested, washed three times with HBSS by centrifugation, resuspended in IMDM with 20% FBS, and centrifuged at 500× g for 10 min. After this step, the resultant cell pellet is represented by cancer-associated fibroblasts (CAFs). CAFs were cultured in complete minimum essential medium (IMDM), a modified Dulbecco's modified Eagle medium (DMEM) with 20% fetal bovine serum (FBS, Thermo Fisher Scientific, Waltham, MA, USA), and Antibiotic–Antimycotic. CAFs isolated from multiple patients were treated in a serum-free medium with vehicle or different concentrations (5-10-20-40 μM) of L-Fucose/6-AF.

2.2.20 Chick Chorioallantoic Membrane (CAM) Assay

Chicken CAM assay fertilized, specific pathogen-free (SPF) chicken eggs (VALO Biomedica, Osterholz-Scharmbeck, Germany) were maintained at 37 °C and 80% constant humidity. On day 8, a window of 1.5–2.0 cm diameter was cut in the shell at the more rounded pole of the egg and sealed with tape (Durapore silk tape, 3M). The next day, 1.0×10^6 human tumor cells per pellet were embedded in growth factor

reduced Matrigel (Corning, Wiesbaden, Germany) serving as matrix and were transplanted onto the CAM. The window was sealed again, and the eggs were incubated for five days. Tumor growth was monitored over time using a light microscope ($\times 10$, SU 1071 Traveler). Tumors were sampled with the surrounding CAM on day 5, fixed in 4% formaldehyde, paraffin-embedded, and cut into 3–5 μm sections for immunohistochemical evaluation.

2.2.21 CRISPR Knockout of *SLC35C1* and *FX*

To delete *SLC35C1* and *FX* in mouse HCC4 cells and human HUCCT1 cells, I constructed pX330 plasmids expressing Cas9 and single-guide RNAs (sgRNAs). Also, I constructed lentiCRISPRv2 plasmids expressing mouse Cas9 and sgRNAs (Figure 28A). Mouse EGFP (YP_009062989.1), pX330-U6-Chimeric_BB-CBh-hSpCas9 (pX330), and lentiCRISPRv2-puro were obtained from Addgene (Addgene plasmid #42230, #98290). pX330 and lentiCRISPRv2-puro were digested with BbsI and BsmBI, respectively, and ligated with annealed oligos. Twenty-nucleotide sequences followed by the PAM sequence were used as seed sequences for sgRNA. An extra G is added for sgRNAs lacking a 5' G for U6 transcriptional initiation. I performed the lentiviral transduction with HEK293T cells (American Type Culture Collection, Manassas, VA, USA), which were seeded into 6-wells. When cells reached 50% confluence, 2 μg objective plasmid and 2 μg lentivirus mix (pVSVg, AddGene 8454 and psPAX2, AddGene 12260) were co-transfected into HEK293T cells by 8 μl Lipofectamine 2000 reagents (Invitrogen) with 500 μl Opti-MEM medium. After 24h, the medium was replaced with fresh DMEM containing 30% fetal bovine serum. After incubation for additional 24-48 hours at 37°C, the viral supernatant was harvested and

filtered through a 0.45-mm filter (Millipore, Bedford, MA, USA). Subsequently, HCC4-4 cells were infected with lentivirus plasmid at the volume ratio 1:1. Seventy-two hours post-infection, cells were treated with 2µg/ml puromycin to select cells containing sgSLC35C1(mouse)-pLentiCRISPRv.2 and sgFX(mouse)-pLentiCRISPRv.2. or sgSLC35C1(human)-pLentiCRISPRv.2 and sgFX(human)-pLentiCRISPRv.2.

2.2.22 Statistical Analysis

Data were analyzed using the Prism 9.0 software (GraphPad, San Diego, CA) and presented as Means ± SD. P values < 0.05 were considered statistically significant.

Additional materials and methods are available in the Supporting document.

3. Results

3.1 Evaluation of Overall Fucosylation Levels in Human iCCA

Alteration in protein glycosylation is now regarded as a critical feature of tumorigenesis in many cancer types (Jia et al., 2018; Keeley et al., 2019). Recently, published data have clearly established that glycan structures found on glycoproteins are essential attributes for many biological processes. Among the various forms of carbohydrate modifications, fucosylation is known to be one of the most important. Lectins are small proteins and glycoproteins that can bind selectively to carbohydrates and are used to quantify protein glycosylation. They do not derive from the immune system, but recognize target structures similar to an antibody-antigen binding (Matsumura et al. 2007). The three lectins used in this project are: *Aleuria aurantia lectin* (AAL), which recognizes core fucose; *Ulex europaeus agglutinin I* (UEA-I), detecting α -linked fucose; and *Lens Culinaris Agglutinin* (LCA), to evaluate α -linked mannose and additional sugars (Lis-Kuberka et al., 2015).

3.1.1 Aberrant Protein Fucosylation in Human iCCA

For an overview of the fucosylation status in iCCA, first, I evaluated the tissue distribution of UEA-I, AAL, and LCA in a vast iCCA collection (n=186) by immunohistochemistry (Figure 7). Increased immunoreactivity for UEA-I, AAL, and LCA lectins was detected ubiquitously in iCCA lesions compared to the matching non-neoplastic liver tissues. Furthermore, normal biliary epithelial cells exhibited faint or absent immunoreactivity for the same lectins. These findings illustrate that iCCA

displays elevated fucose levels when compared with respective non-tumorous surrounding tissues.

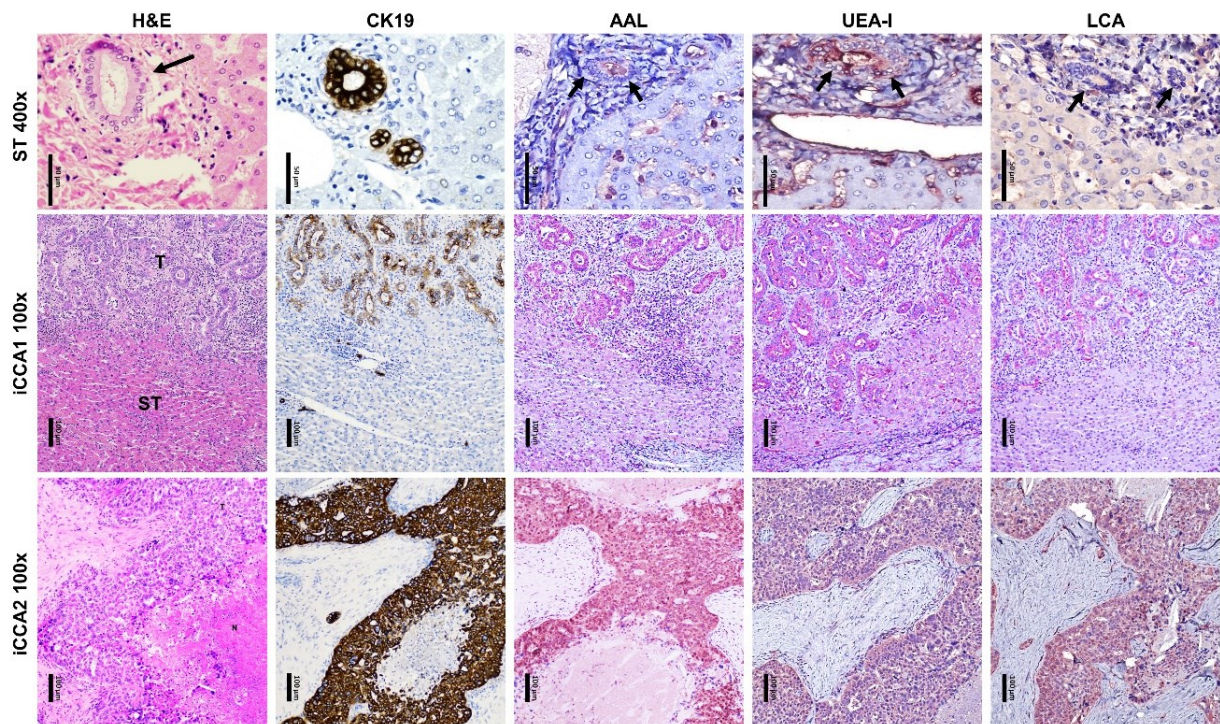


Figure 7. Representative immunohistochemical patterns of AAL, UEA-I, and LCA lectins in human intrahepatic cholangiocarcinoma (iCCA). Immunohistochemical staining of AAL, UEA-I, and LCA in one non-tumorous surrounding tissue (ST) and two human iCCA samples (iCCA1 and iCCA2; the tumor part is indicated with T) specimens. Note that the staining pattern for the three lectins is significantly stronger in the tumor compartment when compared with ST and normal biliary cells (indicated by arrows). CK19 was used as a biliary marker. Abbreviation: H&E, hematoxylin and eosin staining. Magnification: 400x in ST; 100x in iCCA1 and iCCA2. Scale bar: 50 μ m in 400x; 100 μ m in 100x. (Ament et al., 2023)

3.1.2 Fucosylation Levels Increased in Human iCCA Cell Lines Compared to NHC

Cholangiocytes are epithelial cells that line the intra- and extrahepatic ducts of the biliary tree. Intrahepatic cholangiocytes are derived from progenitor cells around the

ductal plate in the peri-portal areas. These cells can differentiate into either hepatocytes or cholangiocytes. Four human iCCA cell lines (RBE, HUCCT1, KKU156, and KKU213) and four normal human cholangiocyte (NHC) cell lines (NHC2, NHC3, NHC-SS, and C324) were used to detect possible differences in fucosylation.

Notably, a significantly increased immunoreactivity for the three lectins was detected in human iCCA cell lines compared to primary cultures of NHC (Figure 8A), suggesting the preservation of the observed fucosylation patterns in normal and neoplastic *in vitro* models.

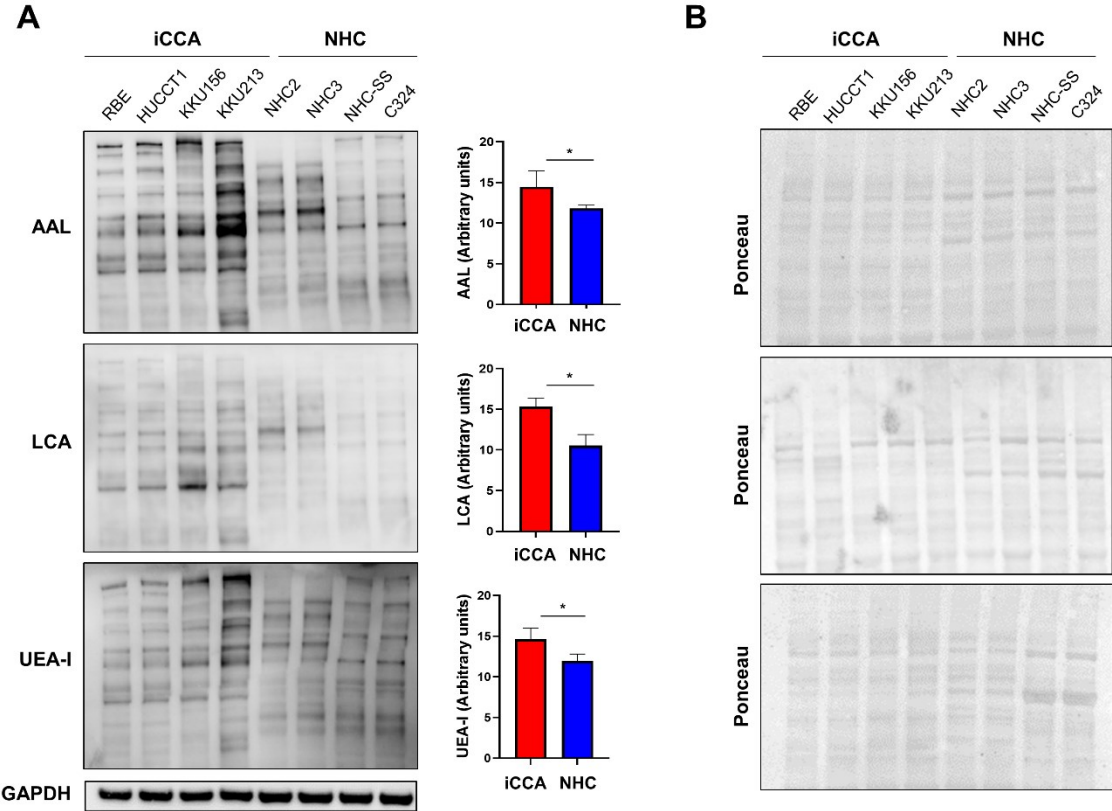


Figure 8. Levels of global fucosylation in human intrahepatic cholangiocarcinoma (iCCA) and normal human cholangiocyte (NHC) cell lines, as assessed by Western blot analysis. **(A)** The left panels show representative Western blot results of the AAL, LCA, and UEA-I lectins, while the band intensity quantification for iCCA and CC cells is depicted in the right panels. GAPDH was used as a loading

control. Student's t-test: * at least $p < 0.05$. **(B)** Reversible Ponceau Red staining of the membranes probed for AAL, LCA, and UEA-I lectins shown in (A), demonstrating equal loading in the various lanes. (Ament et al., 2023)

3.1.3 Aberrant Fucosylation Levels Increased in Human iCCA Tissue Lysates Correlate with Overall Patient Survival

I further determined by Western blot analysis the fucosylation levels in a collection of human iCCA specimens (n=37) for which the clinicopathological data were available. Notably, the quantified fucosylation levels after incubation with AAL, LCA, and UEA-I were significantly higher in tumor lesions compared to the corresponding non-neoplastic liver tissues (Figure 9A-C). Furthermore, when assessing the prognostic relevance of the three lectins, increased (α -1,2) linked fucose levels detected with UEA-I were associated with worse overall survival of patients with iCCA ($p < 0.0001$; Figure 9C, Supplementary Material). Also, patients showcasing increased cellular fucosylation detected by AAL displayed a trend toward shorter survival ($p = 0.076$; Figure 9A), and a cut-off corresponding to the third percentile showed significantly shorter survival in high-expressing fucose patients detected with AAL ($p < 0.005$; Figure 9A, Supplementary Material). In contrast, fucosylation levels detected with LCA did not separate iCCA patients based on survival length (Figure 9B). Concerning the other clinicopathological data, fucosylation levels revealed by UEA-I positively correlated with lymph node metastasis ($p = 0.002$; Supplementary Material)

Overall, these findings underline that increased fucosylation is a hallmark of human iCCA development and progression.

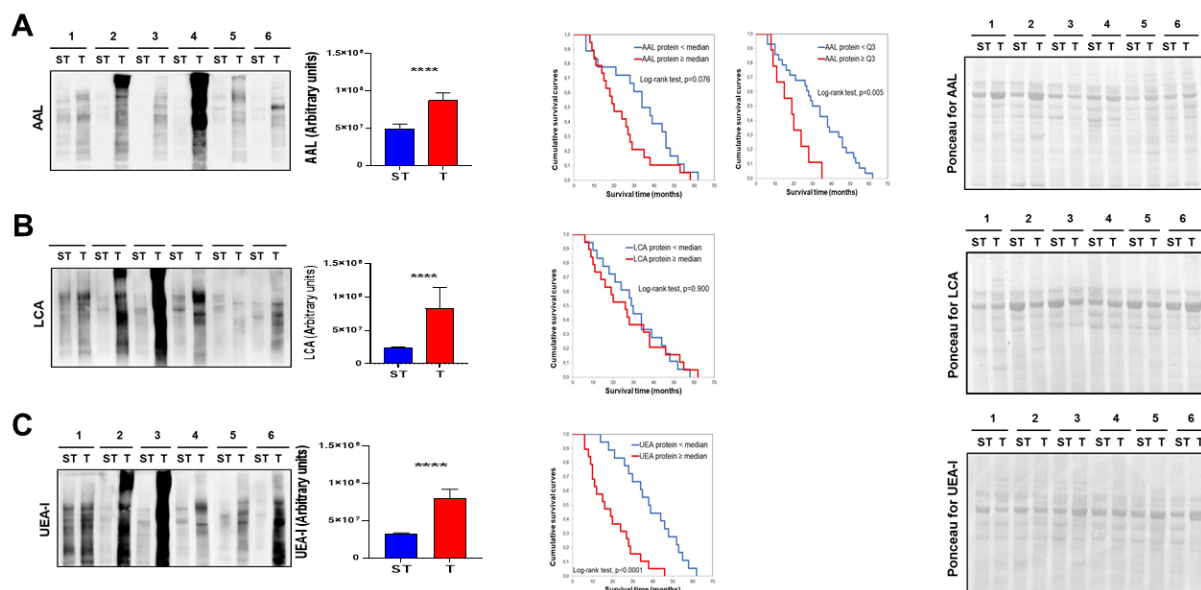


Figure 9. Levels of global fucosylation in human intrahepatic cholangiocarcinoma (iCCA) specimens. The first panels show representative Western blot results of the AAL (A), LCA (B), and UEA-I (C) lectins in the iCCA collection (n=37). Specifically, six tumors (T) and corresponding non-tumorous surrounding tissues (ST) are shown. The second panels from the left show the quantification of the protein band intensities in the whole iCCA collection. The third panels display the Kaplan-Meier curve showing that UEA-I levels significantly correlate with patients' survival in this disease. Finally, the last panels show the ponceau red stainings. (Figure modified from Ament et al., 2023)

3.2 Major Players of Fucosylation and Their Role in Human iCCA

Cellular fucosylation depends on multiple steps along the fucosylation pathway. In the de novo pathway, GDP-mannose is transferred into GDP-fucose, catalyzed by two enzymes, GMD and FX, which is followed by the transport of GDP-fucose by the SLC35C1 transporter into the lumen of the Golgi apparatus, or the endoplasmic reticulum. There, GDP fucose can be used by fucosyltransferases, like POFUT1, as a

fucose donor for protein fucosylation. The antagonist of POFUT1 is the lysosomal exoenzyme FUCA1, which removes fucose residues from glycans.

3.2.1 Elevated Levels of Significant Players of Fucosylation in Human iCCA

To gain further insights into the fucosylation status in iCCA, first, I interrogated the TCGA database containing 9 normal livers and 36 cholangiocarcinomas (CCA) samples (30 iCCA, 4 perihilar CCA, and 2 undefined CCA). Based on the UALCAN analysis (<http://ualcan.path.uab.edu/index.html>; last accessed September 28, 2022), CCA samples display a significant upregulation of *POFUT1*, *GMDS*, *SLC35C1*, *FX*, and downregulation of *FUCA1*, respectively, compared with normal surrounding liver tissues (Figure 10).

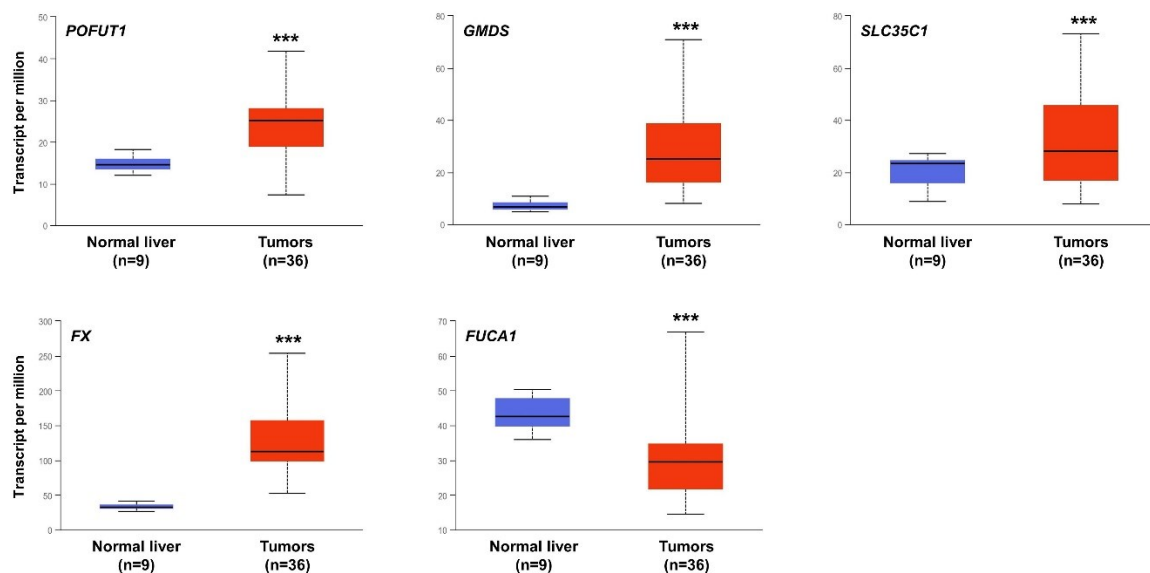


Figure 10. Levels of the main fucosylation positive regulators and the fucosylation inhibitor FUCA1 in human intrahepatic cholangiocarcinoma (iCCA) specimens. mRNA data extracted from the UALCAN

database (UALCAN, <http://ualcan.path.uab.edu>, last accessed September 28, 2022) for *POFUT1*, *GMDS*, *SLC35C1*, *FX*, and *FUCA1* genes are shown. (Ament et al., 2023)

Next, I investigated the same targets by immunohistochemistry (Figure 11). Normal cholangiocytes indicated by the black arrow showed weak or absent immunolabeling for *POFUT1*, *GMDS*, *SLC35C1*, and *FX*, but strong reactivity for *FUCA1*. iCCA specimens displayed stronger immunoreactivity for the major players of fucosylation compared to the non-tumorous surrounding tissues and biliary epithelial cells (140/186, 77.4%; 149/186, 80.1%; 154/186, 82.8%; 165/186, 88.7%; respectively). In contrast, the fucosylation inhibitor *FUCA1* levels were lower in most iCCA than in non-neoplastic livers (119/186, 64%) (Figure 11A&B).

These results are consistent with the above findings of elevated fucose levels in iCCA tissues.

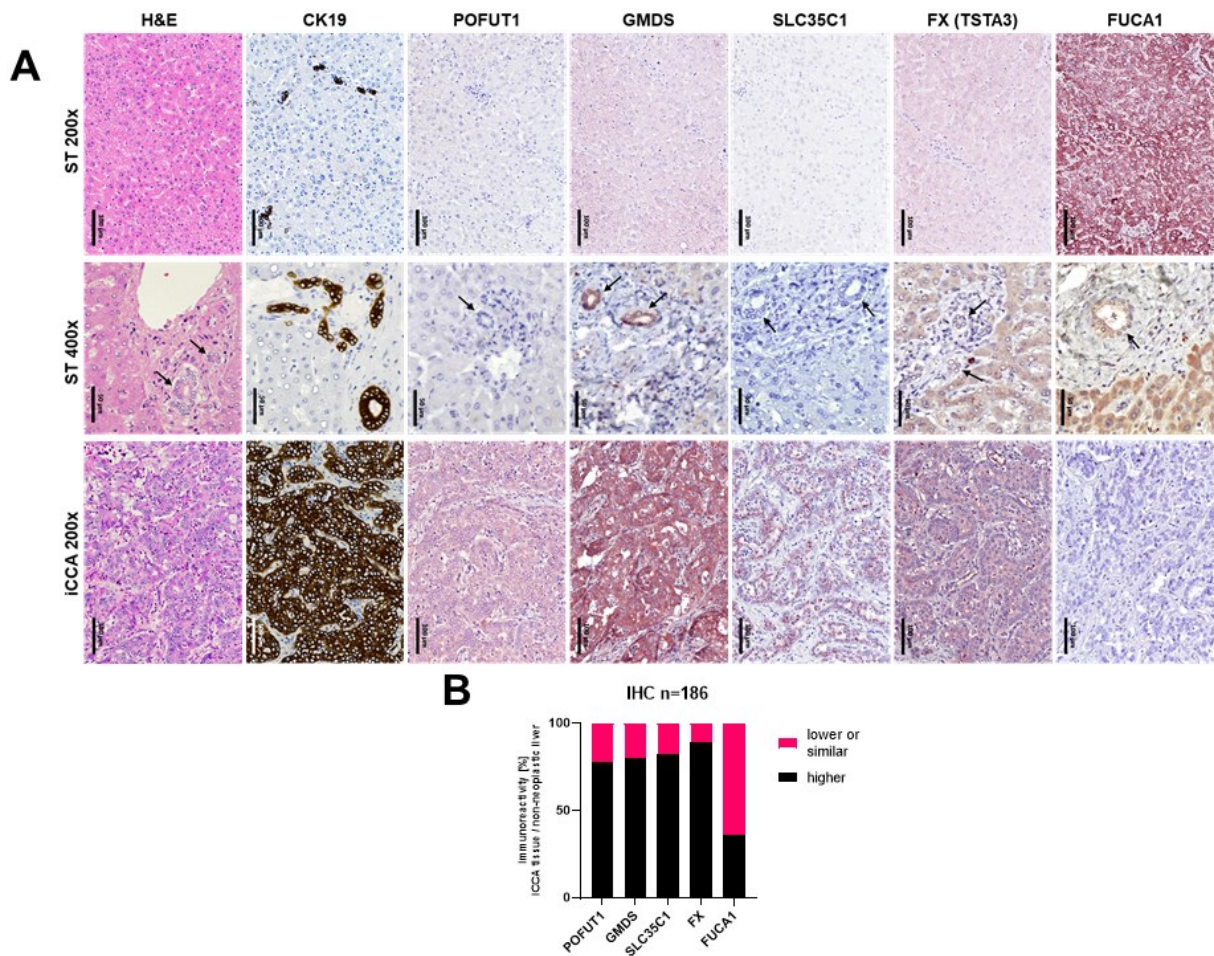


Figure 11. Representative immunohistochemical patterns of the major players of fucosylation in human intrahepatic cholangiocarcinoma (iCCA). **(A)** Immunohistochemical staining of POFUT1, GMDS, SLC35C1, FX, and FUCA1 in a non-tumorous surrounding tissue (ST) and one human iCCA specimen are shown. The ST is depicted at two magnifications. Note that the staining pattern for POFUT1, GMDS, SLC35C1, FX is significantly more pronounced in the tumor compartment when compared with ST and normal biliary cells (indicated by arrows). In contrast, the immunoreactivity for FUCA1 was stronger in ST than in the iCCA lesion. CK19 staining was used as a biliary marker. Magnification: 200x and 400x in ST; 200x in iCCA1 and iCCA2. Scale bar: 50 μ m in 400x; 100 μ m in 200x. **(B)** Higher immunoreactivity of POFUT1, GMDS, SLC35C1, and FX proteins in iCCA tissue compared to ST and biliary cells (BC) among 186 human iCCA samples (140/186, 77.4%; 149/186, 80.1%; 154/186, 82.8%; 165/186, 88.7%; respectively). FUCA1 levels were lower in most iCCA than in non-neoplastic livers (119/186, 64%). Higher = Higher than ST and BC; lower or similar = lower or similar than ST and BC. (Ament et al., 2023).

3.2.2 *SLC35C1* or *FX* Knockdown and 6AF Treatment Reduces Protein Fucosylation Levels, Notch Receptor Expression, and Notch Signal Transduction in Human iCCA Cell Lines

To assess the importance of fucose on iCCA growth and to unravel a possible new therapeutic approach for iCCA, I investigated the effect of targeting the major players of fucosylation on protein glycosylation and potential pathways regulated by fucosylation.

Besides the fucosyltransferases, the enzyme FX, catalyzing the formation of GDP-fucose, and the transporter SLC35C1 could be possible targets to interfere with protein fucosylation and, more specifically, Notch receptor fucosylation. Without EGF repeat fucosylation, the Notch receptor-ligand binding is prevented. Hence, the signal transduction and the subsequent expression of the Notch target genes will be reduced. To study the importance of 6AF and the mentioned two enzymes on the overall fucosylation and the Notch pathway, both genes were subject to knockdown via specific siRNA in KKKU213 and HUCCT1 cells. After the incubation of 48 hours with respective siRNAs, the gene expression levels for *SLC35C1* and *FX* were assessed, and the impact of all treatments on protein fucosylation and the Notch pathway was analyzed. The silencing worked well for both genes, as assessed by quantitative real-time RT-PCR (Figure 12A). Gene expression levels for *Notch1*, *Notch2*, *Sox9*, and *Hes1* decreased in both cell lines, especially after incubation with 6AF (Figure 12B).

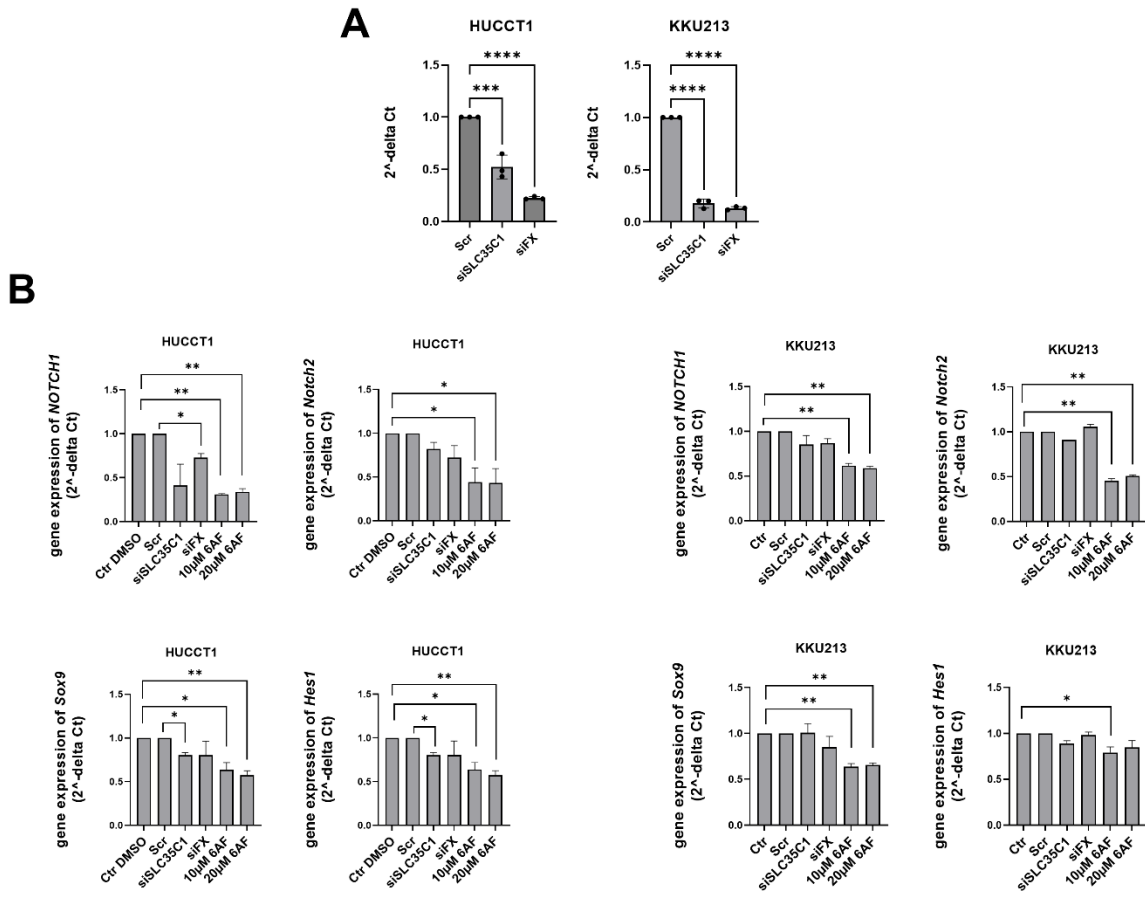


Figure 12. Fucosylation is a positive regulator of the NOTCH pathway in human intrahepatic cholangiocarcinoma (iCCA). **(A)** Silencing with small interfering RNA (siRNA) for both *SLC35C1* and *FX* genes showed a significant reduction of mRNA expression in HUCCT1 and KKU213 cells, as assessed by real-time quantitative PCR. Control (Ctrl), scrambled siRNA (Scr). One sample t-test: * $p < 0.01$, ** $p < 0.001$. **(B)** Gene expression levels in HUCCT1 and KKU-M213 were evaluated after silencing and drug incubation. Notch1 expression was significantly reduced by incubation with 20 μ M 6AF. The *Notch2*, *Sox9*, and *Hes1* expression levels were significantly reduced by 10 μ M 6AF. N=3, One-Way ANOVA: * $p < 0.1$, ** $p < 0.01$, *** $p < 0.001$, **** $p < 0.0001$

The subsequent test on protein levels with AAL, UEA-I, and LCA lectins revealed that protein fucosylation was reduced (Figure 13A). Especially the knockdown of *FX*

induced a strong effect in reducing overall fucosylation, although the most striking fucosylation reduction occurred in 6AF-treated cells in a dose-dependent manner. Thus, an alteration of GDP-fucose formation strongly affects protein fucosylation. Next, I evaluated the protein levels of the Notch 1 and Notch 2 receptors (NOTCH1, NOTCH2) and their target SOX9 in the same cells by immunoblotting (Figure 13B). In line with the reduced fucosylation levels detected after gene knockdown and 6AF treatment, NOTCH1 and SOX9 protein levels were decreased (Figure 13B). In the HUCCT1 cells, the NOTCH1 levels were only reduced by the incubation with 6AF. In the KKU213 cells, silencing of *FX* and treatment with 6AF negatively affected the NOTCH1 and SOX9 levels. NOTCH2 was only lowered due to fucosylation inhibition with 6AF in KKU213 cells but also by gene knockdown in HUCCT1 cells (Figure 13B). Again, incubation of the cells with 6AF, especially the highest 6AF dose, resulted in the three proteins' most potent and significant reduction.

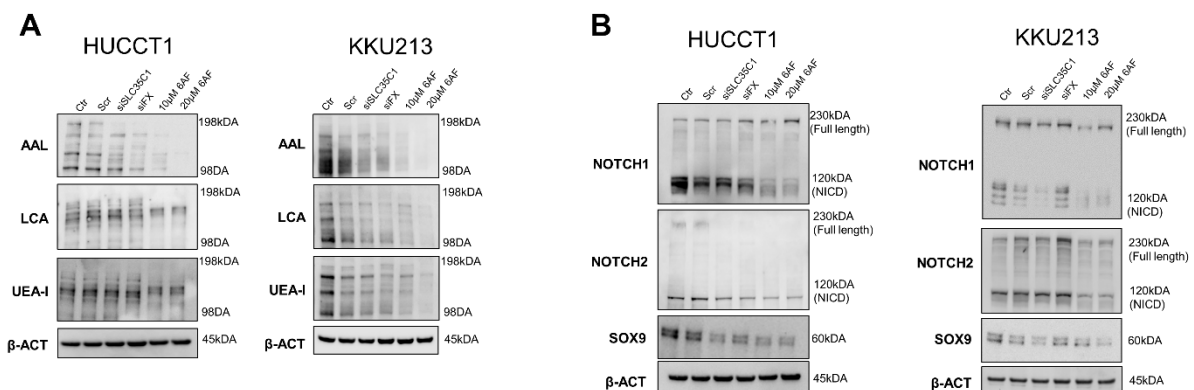


Figure 13. Fucosylation is a regulator of NOTCH signaling **(A)** Western blotting of AAL, UEA-I, and LCA lectins revealed reduced protein fucosylation levels after the knockdown of *SLC35C1* and *FX* genes and in response to treatment with 10μM and 20μM 6AF. Knockdown of *FX* showed the most pronounced effect. β-Actin (β-ACT) was used as a loading control. **(B)** NOTCH1 protein levels decreased after

silencing of *SLC35C1* and incubation with 6AF. NOTCH2 protein levels decreased after incubation with 6AF. SOX9 protein levels decreased after silencing of *SLC35C1* and incubation with 6AF. β -Actin (β -ACT) was used as a loading control.

Altogether, the data demonstrate that knockdown of either *SLC35C1* or *FX*, but especially of *FX*, and most strikingly, treatment with 20 μ M 6F results in reduced overall protein fucosylation levels, leading to a reduction in Notch receptors and Notch target levels.

One reason for the observed reduction of SOX9 levels could be a decreased Notch signal transduction. The Notch receptor is the only known receptor receiving its signal via cell-cell contact. Specifically, the Notch intracellular domain (NICD) translocates into the nucleus to induce target gene expression upon the binding of the Notch extracellular domain (NECD) to its ligands, such as Jagged1 (JAG1). Once in the nucleus, NICD forms a complex with the transcription factor CSL (CBF1/RBPJk/Suppressor of Hairless/Lag-1) and the coactivator Mastermind to finally induce target gene expression (D'Souza et al., 2008; Katsube and Sakamoto, 2005). To examine NOTCH-JAG1 interaction following fucosylation inhibition, HUCCT1 and K KU213 cells were treated with 6AF, either alone or combined with L-Fucose, and subsequently subjected to immunoprecipitation with an anti-JAG1 antibody and probed with an anti-NOTCH1 antibody. As expected, cells treated with 6AF alone showed reduced protein levels of NICD compared to the DMSO control (Figure 14A,B), implying a decrease in JAG1-NOTCH1 interaction and downstream pathway activation. On the other hand, adding L-Fucose eliminated the effects of 6AF, restoring the NICD levels as in DMSO-treated cells. Subsequently, I evaluated the fucosylation

effects on Notch activity using a dual luciferase assay. Again, iCCA cells were incubated with 6AF, either alone or in combination with L-Fucose. The Notch Inhibitor CB103 (Lopez Miranda et al. 2021) was a positive control for Notch signaling blockade. As hypothesized, inhibition of fucosylation by 6AF reduced NICD reporter activity, which was restored by adding L-Fucose (Figure 14C). Furthermore, treatment with the Notch transcriptional inhibitor CB103 was sufficient to block NICD activity completely.

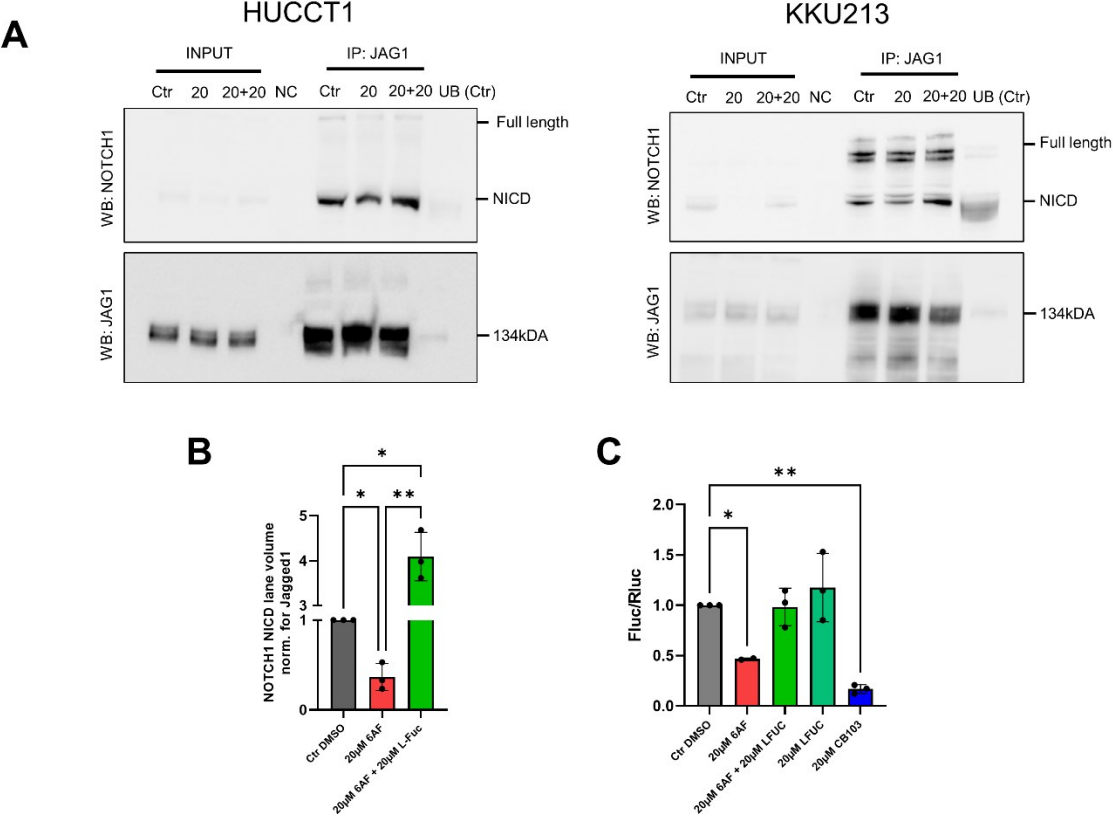


Figure 14. Reduced NOTCH signaling due to impaired ligand binding and receptor translocation **(A)** A total of 1,5mg protein lysate of HUCCT1 and KKU213 cells was used for co-immunoprecipitation (Co-IP). The cells were left untreated (Ctrl) or treated with 20µM 6AF, either alone or in combination with 20µM L-Fucose. Lysates were incubated with an anti-Jagged1 antibody bound to agarose beads for pull-down. After gel electrophoresis, the membranes were blotted with anti-NOTCH1 and anti-Jagged1 antibodies. **(B)** Lane volumes of the Co-IP experiments of the KKU213 cells in **(A)** were quantified with

the Image Lab™ Software. The NOTCH1 lane volumes were normalized against JAG1. NICD levels were significantly decreased upon incubation with 20μM 6AF. The addition of 20μM L-FUC significantly increased NICD protein levels. Similar data were obtained in HUCCT1 cells (not shown). One-Way ANOVA: * $p < 0.01$, ** $p < 0.001$. **(C)** The Notch receptor activity of KKU213 cells was analyzed with a luciferase assay and a Notch pathway reporter. The treatment with 20μM 6AF significantly reduced the Notch activity, whereas the addition of 20μM L-Fucose restored it. Administration of L-Fucose alone was able to increase the receptor activity drastically. Finally, the Notch transcriptional inhibitor CB103 blocked the receptor activity. Similar data were obtained in HUCCT1 cells (not shown). One-Way ANOVA: * $p < 0.01$, ** $p < 0.001$. Each experiment was at least performed with N=3.

3.3 Increased NOTCH Activation due to Aberrant FRINGE Levels in Human iCCA

Next, I evaluated the levels of members of the Fringe family, including LFNG, MFNG, and RFNG, which extend the O-fucose modification with sugar nucleotides and are responsible for NOTCH activation (Moloney et al. 2000), in our iCCA collection by immunohistochemistry. As observed for lectins and fucosylation enzymes, immunoreactivity for LFNG, MFNG, and RFNG proteins was weaker in normal biliary cells compared to iCCA (Figure 15A). Moreover, LFNG, MFNG, and RFNG levels were significantly higher in iCCA samples than in non-tumorous livers (129/186, 69.3%; 148/186, 79.6%; 162/186, 87.1%) (Figure 15B). According to the staining results, a significant upregulation of *LFNG*, *MFNG*, and *RFNG* mRNA characterized the iCCA specimens retrieved from the TCGA dataset (Figure 15C). These data support the existence of a robust fucosylation machinery that sustains the Notch pathway in human iCCA.

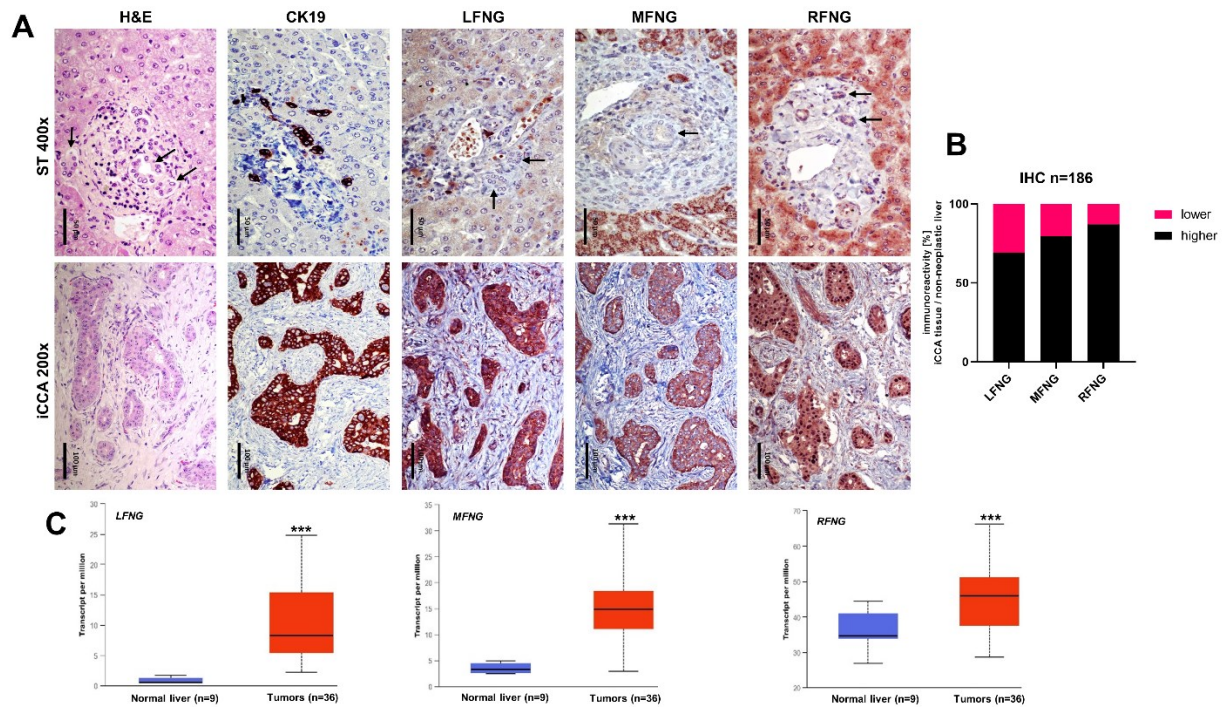


Figure 15. Fringe proteins responsible for NOTCH activation are upregulated in human intrahepatic cholangiocarcinoma (iCCA). **(A)** Representative immunohistochemical patterns of the main Fringe family proteins (LFNG, MFNG, and RFNG) in human intrahepatic cholangiocarcinoma (iCCA). Immunohistochemical staining of LFNG, MFNG, and RFNG in one non-tumorous surrounding tissue (ST) and human iCCA sample (iCCA) is shown. Note that the staining pattern for the three Fringe proteins is significantly more pronounced in the tumor compartment when compared with ST and normal biliary cells (indicated by arrows). CK19 was used as a biliary marker. Abbreviation: H&E, hematoxylin and eosin staining. Magnification: 400x in ST; 200x in iCCA. Scale bar: 50 μ m in 400x; 100 μ m in 200x. **(B)** Immunoreactivity of LFNG, MFNG, and RFNG on iCCA tissue compared to ST and biliary cells (BC) among 186 human iCCA samples (129/186, 69.3%; 148/186, 79.6%; 162/186, 87.1%). Higher = Higher than ST and BC; lower = lower than ST and BC. **(C)** mRNA data extracted from the UALCAN database (UALCAN, <http://ualcan.path.uab.edu>, last accessed September 28, 2022) for *LFNG*, *MFNG*, and *RFNG* genes are shown. Student's t-test: at least *** $p < 0.0001$. (Ament et al., 2023)

Overall, the present data indicate that fucosylation regulates the NOTCH pathway in this disease.

3.6 Fucosylation Influences the NF- κ B Pathway in Human iCCA Cells

Another relevant pathway in general hepatocarcinogenesis is the NF- κ B signaling cascade (Luedde and Schwabe, 2011; Czauderna et al., 2019). However, the role of NF- κ B in iCCA has not yet been investigated in greater detail. However, it is very likely that NF- κ B signaling, which has also been reported to be modulated by fucosylation (Doud et al., 2020), might also be a promising target in iCCA (Czauderna et al., 2019). To evaluate the effects of fucosylation on the NF- κ B pathway in iCCA, I treated the HUCCT1 and KKU213 cell lines with solvent alone and 6AF and assessed NF- κ B p65 transcriptional activity. To induce target gene expression, NF- κ B p65 has to translocate into the nucleus. In the cytoplasm, I κ B α binds to NF- κ B, inhibiting its nuclear localization and gene transcription. Upon stimulation by inflammatory cytokines, I κ B α is inactivated, and the NF- κ B complex can promote transcriptional activation (Yamamoto and Gaynor, 2004). To further study the importance of fucosylation on the NF- κ B pathway in human iCCA, I took advantage of the HUCCT1 and KKU213 iCCA cells subjected to the *FX* and *SLC35C1* knockdown and treated with 6AF (Figure 13A). Analysis of the blotted membranes revealed reduced NF- κ B p65 protein levels after silencing of *SLC35C1* and incubation with 6AF in both cell lines (Figure 16A,B). In addition, Bcl-xL, a canonical NF- κ B target, showed reduced protein levels after *SLC35C1* and *FX* gene knockdown and incubation with 6AF. It was significantly reduced after incubation with 6AF in both cell lines and after silencing of *FX* in KKU213 cells. The NF- κ B inhibitor alpha (I κ B α) inhibits the NF kappa B complex by binding and

sequestering it in the cytoplasm (Yamamoto and Gaynor, 2004). Treatments had no effect on the IκB protein levels in HUCCT1 cells (Figure 16A,B). In the KKU213 cell line, the levels of the IκBα decreased upon the silencing of *SLC35C1*, but increased after the knockdown of *FX* and fucosylation inhibition, leading to a decrease in the NF-κB p65/IκBα ratio in KKU213 cells (Figure 17A).

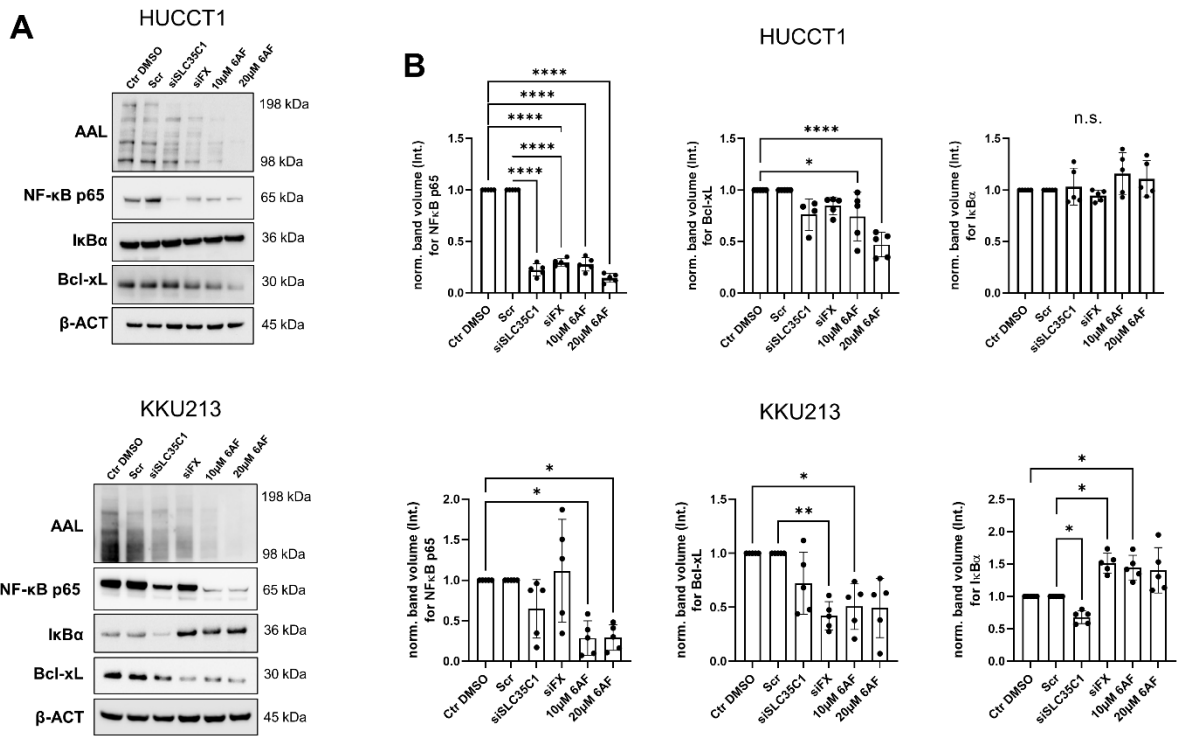


Figure 16. Fucosylation regulates the NF-κB pathway in intrahepatic cholangiocarcinoma (iCCA) cell lines. **(A&B)** NF-κB p65 significantly decreased after incubation with 6AF in both cell lines. Bcl-xL (an NF-κB canonical target) protein levels significantly decreased in HUCCT1 and KKU213 cells after inhibitor treatment. Only silencing of *FX* had a negative effect on the Bcl-xL protein levels in KKU213 cells. Specifically, IκBα protein levels significantly increased after *FX* gene silencing and after incubation with 6-AF in the KKU213 cells but showed no difference in HUCCT1 cells. In contrast, the silencing of

SLC35C1 reduced the protein levels of I κ B α in KKU213 cells. β -Actin (β -ACT) was used as a loading control. One-way ANOVA: * $p < 0.01$, ** $p < 0.001$

Notably, inhibition of cellular fucosylation by 6AF significantly reduced the NF- κ B p65 activity in the two cell lines (Figure 17B). Again, adding the L-Fucose to the medium annulled the suppressing effects on NF- κ B p65 activity by 6AF.

Thus, fucosylation sustains the NF- κ B pathway in iCCA by reactivating I κ B α and inhibiting NF- κ B p65.

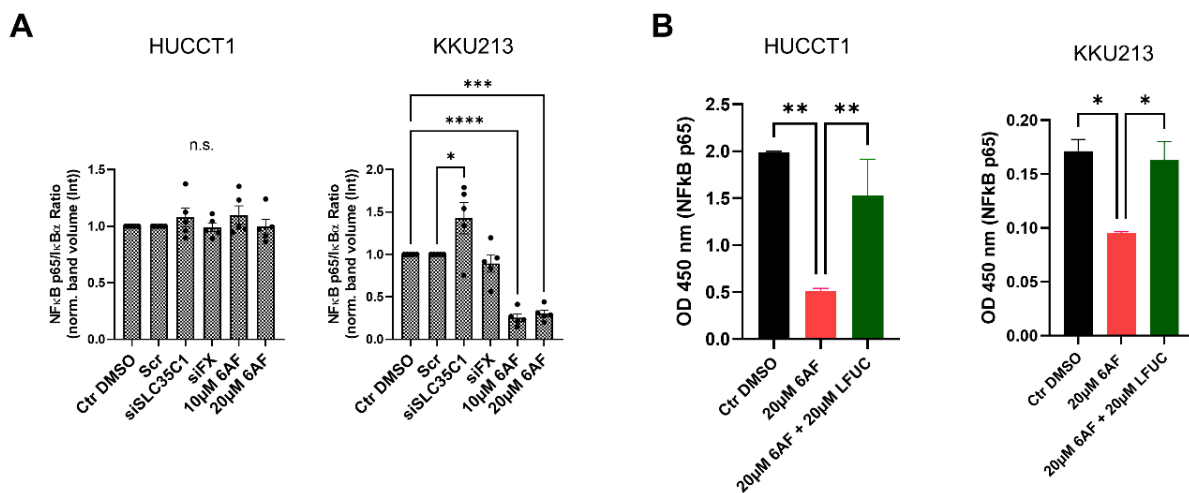


Figure 17. Reduced NF κ B translocation after fucosylation inhibition. **(A)** NF- κ B p65/I κ B α ratio increased after *SLC35C1* silencing and decreased after 6AF treatment in KKU213 cells. One-way ANOVA: * $p < 0.01$, **** $p < 0.00001$. **(B)** Nuclei extracts of cells incubated with and without 20 μ M 6AF and combined with 20 μ M L-FUC were used to assess NF- κ B p65 transcriptional activity. The degree of NF- κ B p65 activity was significantly reduced by the treatment with 20 μ M 6AF compared to the DMSO control in both cell lines. L-Fucose fully restored NF- κ B p65 transcriptional activity. One-way ANOVA: * $p < 0.01$.

3.7 EGFR as a Possible Link Between NF- κ B and Fucosylation in iCCA Cell Lines

Although in the course of this project I could clearly show that NF- κ B signaling depends on fucose, the reason remains unclear. In 1998 and 2000, two papers demonstrated that EGF induces NF- κ B activation by degradation of the inhibitory molecule I κ B α (Sun and Carpenter, 1998; Biswas et al., 2000). However, the exact mechanisms are still unknown. Nevertheless, it is already known that EGFR signaling depends on receptor fucosylation (Zhang et al. 2008). Therefore, it is likely that the crosstalk between EGFR and NF- κ B could be partly attributed to fucosylation. First, I wanted to exclude the possibility of a crosstalk between the NF- κ B and Notch pathways, which might lead to the influence on the NF- κ B signal pathway shown in Figures 16 and 17. For this purpose, *NOTCH1* was silenced with specific siRNA in iCCA cell lines (Figure 18). The knockdown of *NOTCH1* showed no effect on the protein levels of NF κ B related proteins (Figure 18A). Similar results were obtained on gene expression level (Figure 18B). Thus, regulation of the NF- κ B by Notch in iCCA seems unlikely.

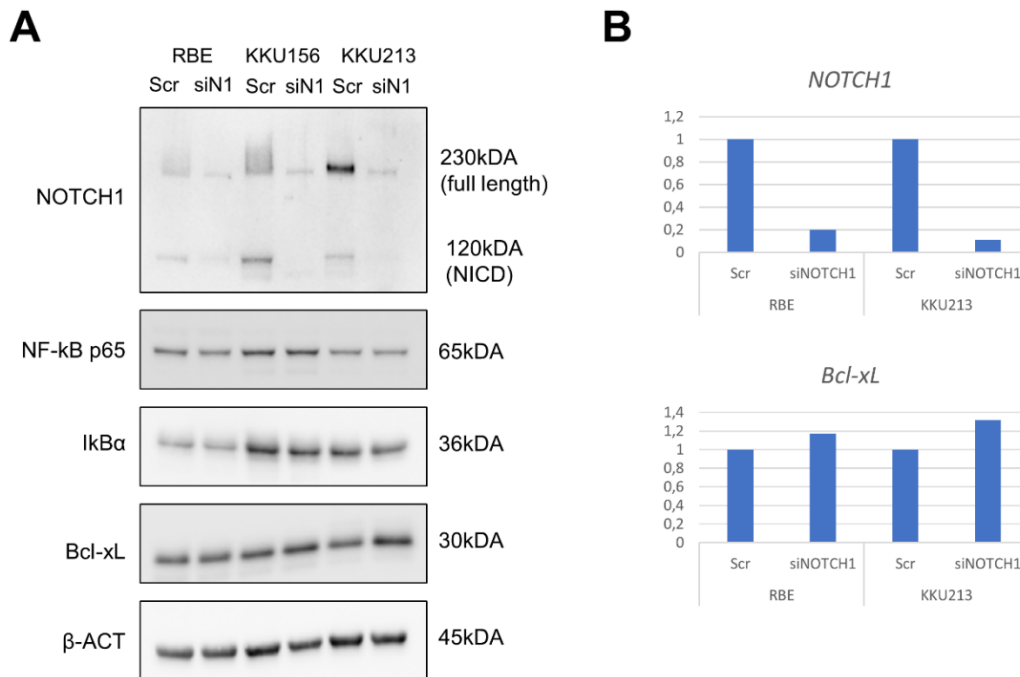


Figure 18. NOTCH does not influence the NK-kB pathway in human iCCA cell lines. **(A)** Silencing of *NOTCH1* gene via specific siRNA (siN1) does not lead to the downregulation of NF-kB p65, IκBα, and Bcl-xL proteins compared to scrambled siRNA (Scr) in RBE, KKU156, and KKU213 iCCA cell lines, as assessed by Western blot analysis. **(B)** Similar results were obtained when determining the mRNA levels of *Bcl-xL* in RBE and KKU213 cells depleted of *NOTCH1* using quantitative real-time RT-PCR. (Ament et al., 2023)

Next, I validated the influence of the fucosylation status on the EFR receptor (Figure 19). Knockdown of *EGFR* in HUCCT1 and KKU213 cells had no effect on NF-kB p65 protein levels but decreased Bcl-xL, a target gene of NF-kB p65. Moreover, the silencing of *EGFR* increased the IκBα levels in both cell lines, which is consistent with the underlying literature (Figure 19A) (Biswas et al. 2000). Furthermore, the knockdown of *SLC35C1* and *FX*, as well as the incubation with 6AF, led to a reduction

of EGFR protein levels (Figure 19B). These findings suggest that EGFR is one of the upstream regulators of the NF- κ B pathway in iCCA.

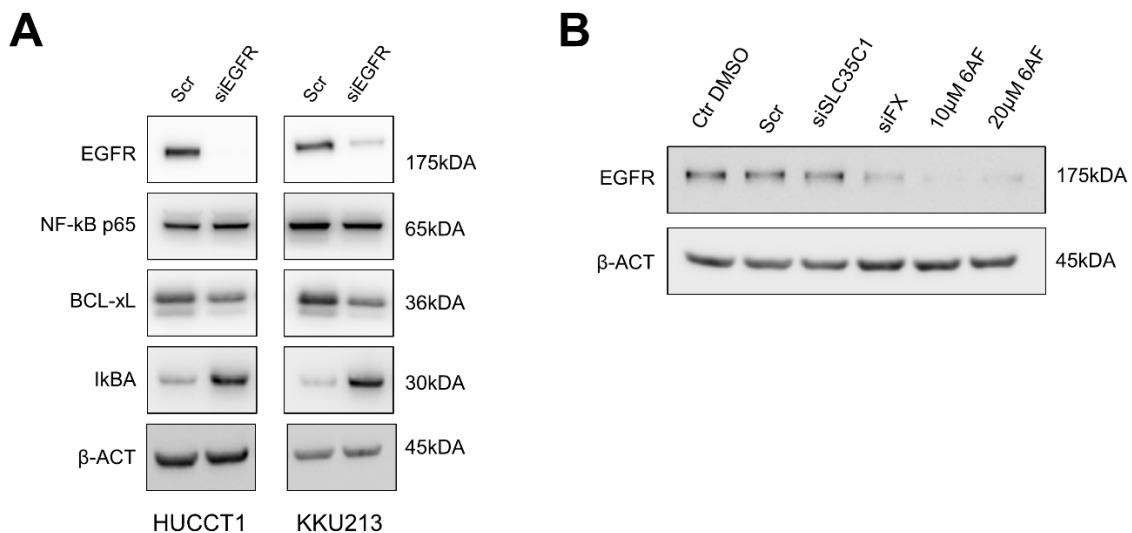


Figure 19. EGFR is an upstream inducer of the NF- κ B pathway and is modulated by fucosylation in iCCA cell lines. **(A)** Silencing of EGFR gene via specific siRNA (siEGFR) induces the upregulation of I κ B α and the downregulation of Bcl-xL protein compared to scrambled siRNA (Scr) in HUCCT1 and KKU213 iCCA cell lines, as assessed by Western blot analysis. EGFR knockdown had no effect on NF- κ B p65 levels. **(B)** Inhibition of the *FX* gene using specific siRNA (siFX) and treatment with two doses of the fucosylation inhibitor 6AF decreases the levels of EGFR protein in the KKU213 cell line. Similar results were obtained in the HUCCT1 cell line (not shown) (Ament et al., 2023).

3.8 6-Alkynylfucose Inhibits Cell Proliferation and Migration of iCCA Cell Lines

Since fucose is important for many cellular functions, it was reasonable to assume that 6AF also regulates the proliferation and migratory properties of iCCA cells. Furthermore, the ability to proliferate and migrate is among the hallmarks of cancer cells. To investigate the effect of 6AF on cell proliferation, human KKU213 and

HUCCT1 cells were incubated either alone or in combination with L-Fucose and measured with the xCELLigence Real-Time Cell Analysis (RTCA) instrument over a period of 35h - 70h. As expected, the degree of cellular fucosylation was reduced after treatment with 6AF, while the combination with L-Fucose restored the original levels (Figure 20A). Furthermore, L-Fucose addition to the medium accelerated the growth of the two iCCA cell lines in a dose-dependent manner (Figure 20B).

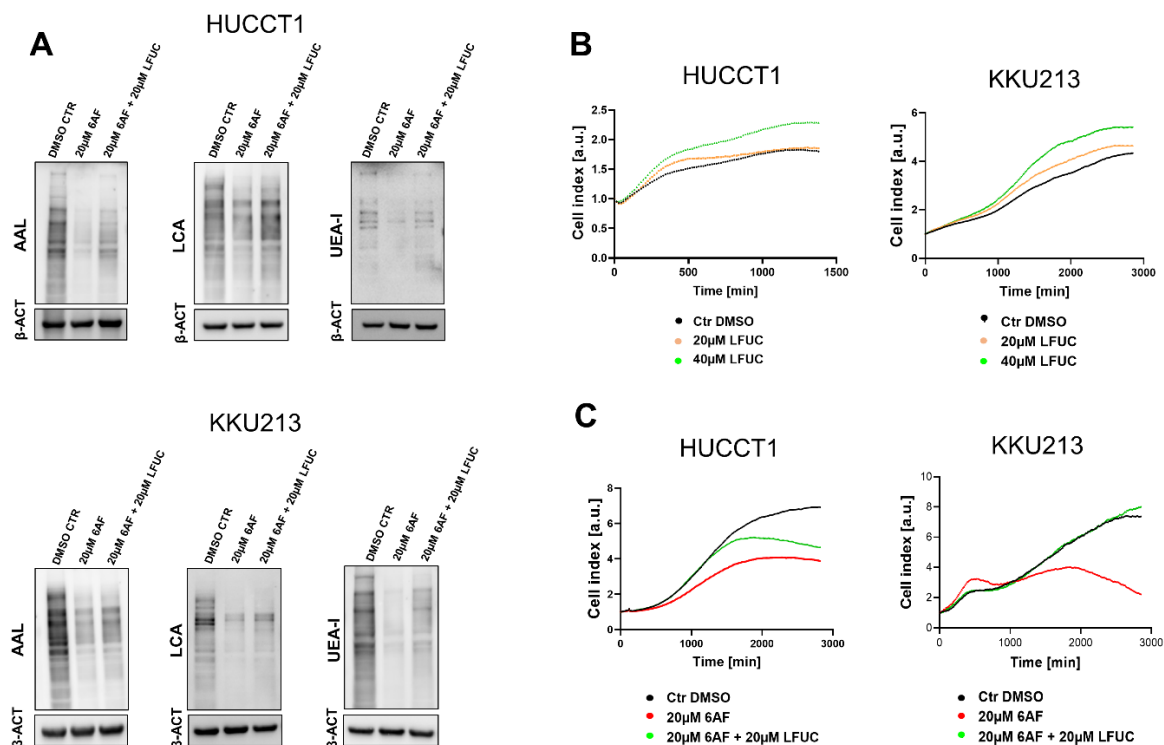


Figure 20 Effects of L-Fucose and 6AF on the proliferation and migration of human intrahepatic cholangiocarcinoma (iCCA) cell lines. **(A)** Treated with 20 µm 6AF alone reduced the fucosylation levels detected with AAL, LCA, and UEA-I. The addition of 20µM L-Fucose restored the fucose levels. **(B)** HUCCT1 and KKUM213 cells were cultured in DMEM containing 5% FBS, treated with 10, 20, and 40µM L-Fucose, and the *in vitro* growth was assessed using an xCELLigence® RTCA DP instrument. Proliferation per well was measured in triplicates. **(C)** HUCCT1 and KKU213 cells were treated with 6AF alone or in combination with 20µM L-Fucose, and their growth was evaluated as in **(A)**.

As shown in Figure 20C, cell proliferation was suppressed following treatment with 6AF in KKU213 and HUCCT1 cells, when compared with control cells. The addition of L-fucose restored the proliferation, indicating that the effect was truly due to the inhibition of fucosylation. No significant effects of 6AF on apoptosis were detected, even at 40 μ M concentration (Figure 21).

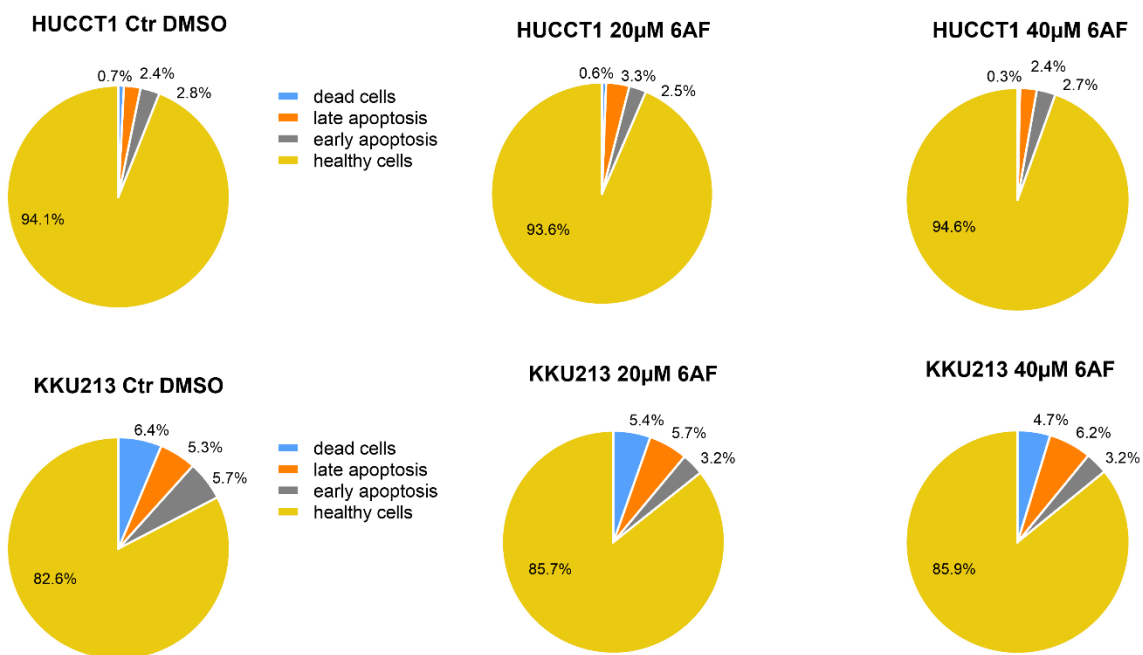


Figure 21. The fucosylation inhibitor 6AF does not affect apoptosis in HUCCT1 cells, as detected by FACS analysis.

As proliferation is affected, presumably also migration is influenced by 6AF. Therefore, I performed a scratch assay with cells cultured in media supplemented with 6AF alone or in combination with L-Fucose. After 48 hours of incubation, a scratch was made on the cell layer, and the exact spot was captured every two hours (Figure 22A,B).

Notably, the migration of the cells was significantly suppressed in cells treated with 20 μ M 6AF, effectively counteracted by L-Fucose supplementation.

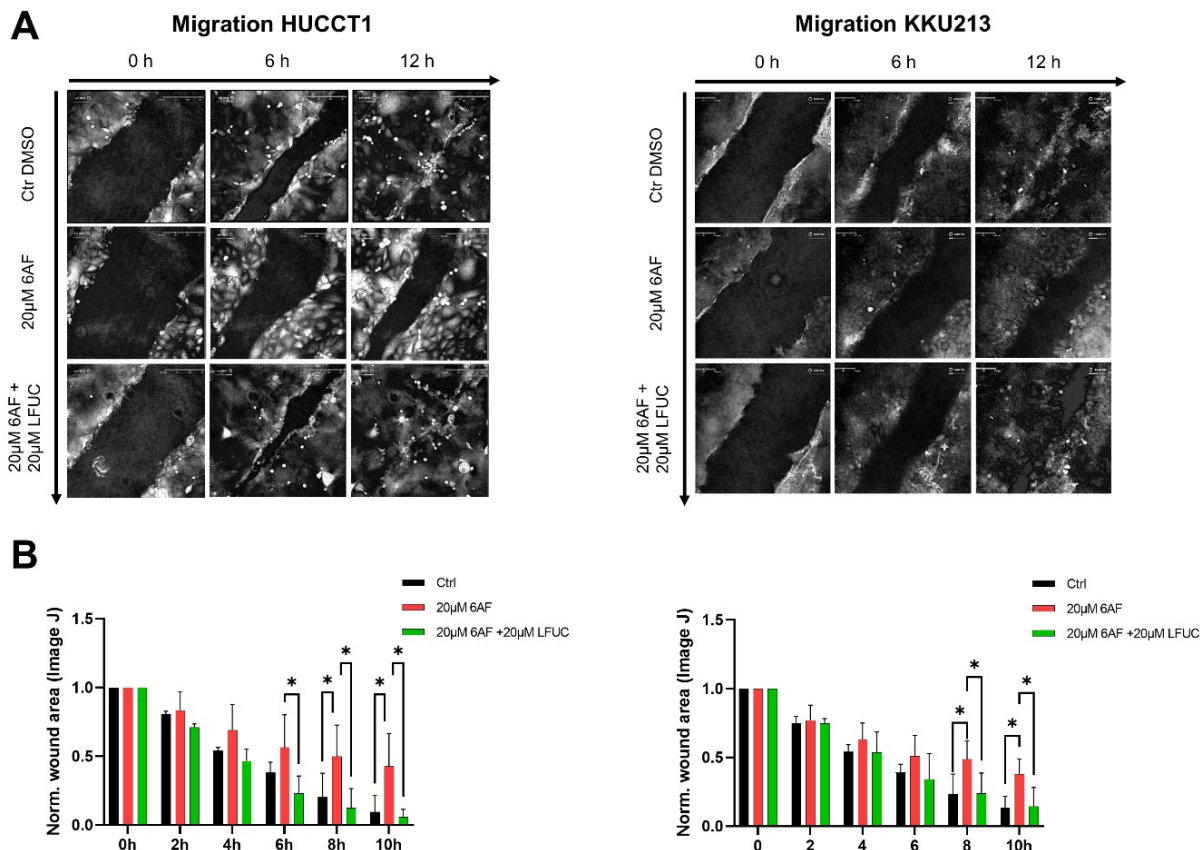


Figure 22. Fucosylation sustains the migration ability of human iCCA cells. **(A)** The migration properties of KKU-M213 cells decreased following the treatment of 6AF and increased after adding L-Fucose, as indicated by the scratch assay. **(B)** Quantitative values of the migration activity described in **(A)**; N=3; n.s (Two-way ANOVA).

3.9 Suppression of Fucosylation Reduces iCCA Growth *in Vivo*

Next, I evaluated the effect of interfering with overall fucosylation in an *in vivo* model of iCCA. For this purpose, I used the CAM assay; specifically, KKU-M213 cells were

pretreated with 6AF alone and combined with L-Fucose. Next, the cells were transplanted onto the chicken CAM and cultured *in ovo* for 5 days (Figure 23A). In accordance with *in vitro* data, the 6AF treated tumors displayed a decreased mean volume ($\sim 10\text{cm}^3$, *** $p < 0.001$) compared to the controls ($\sim 23\text{cm}^3$), whereas L-Fucose addition significantly reversed this effect (*** $p < 0.001$) and increased the volume (50cm^3 , *** $p < 0.001$) compared to the control (Figure 23B,C).

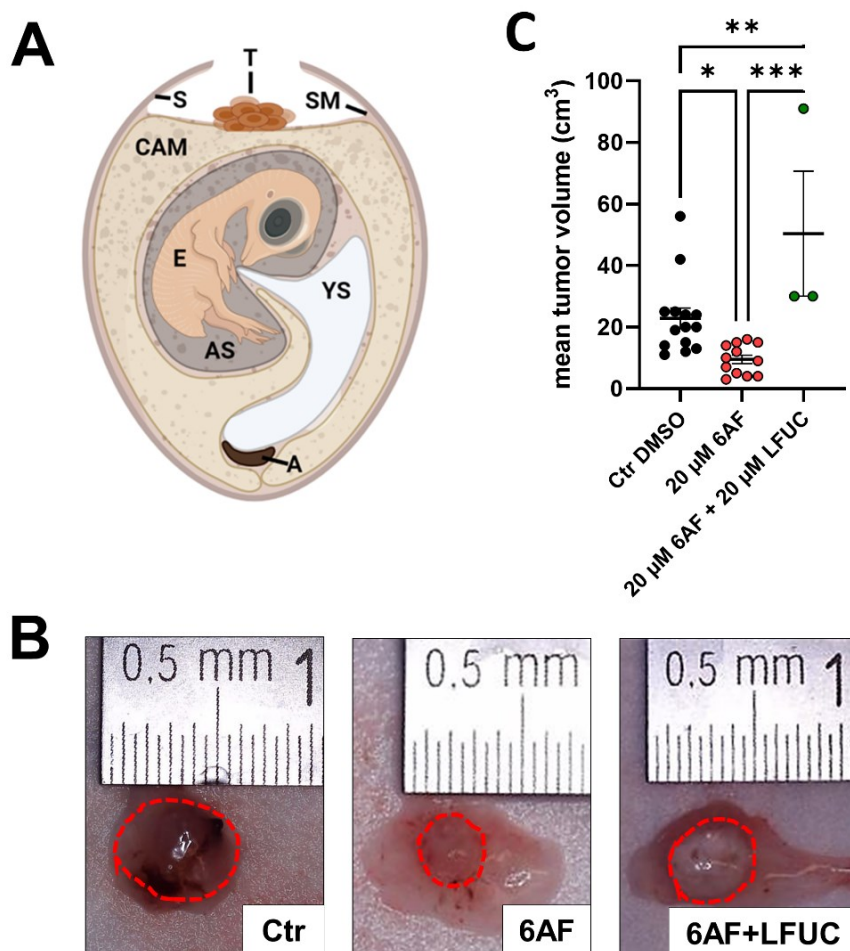


Figure 23. Fucosylation inhibition suppresses tumor growth of K KU-M213 cells in the chicken chorioallantoic membrane (CAM) *in vivo* model. **(A)** CAM assay scheme. A, albumen; AS, amniotic sac; CAM, chorioallantoic membrane; E, chick embryo; S, eggshell; SM, shell membrane; T, human tumor cells in Matrigel; YS, yolk sac. **(B)** Representative ex ovo images of xenograft tumors treated with or

without 20µM 6AF or a combination of 20µM 6AF and 20µM L-Fucose. Red dotted lines outline the tumor tissue. **(C)** Mean tumor volumes. Ctr DMSO (N=14), mean = 23cm³; 20µM 6AF (N=12), mean = 10 cm³; 20µM 6AF + 20µM L-Fucose (N=3), mean = 50 cm³. Treatment with 6AF significantly reduced, and the addition of L-Fucose significantly increased the mean tumor volume. One-way ANOVA: * p < 0.01, * p < 0.001, *** p < 0.0001. **(D)** Representative images of CK19 stained paraffin sections of CAM tumors (10x). (Figure modified from Ament et al., 2023)

In addition, CK19 staining showed a decreased number of malignant cholangiocytes in the tumors treated with 20µM 6AF (Figure 24). It can be due to decreased differentiation of cholangiocarcinoma cells or lowered proliferation in the already present cells, as well as increased apoptosis. The CK19 immunoreactivity was restored to the control levels in tumors treated with the combination of inhibitor and L-Fucose.

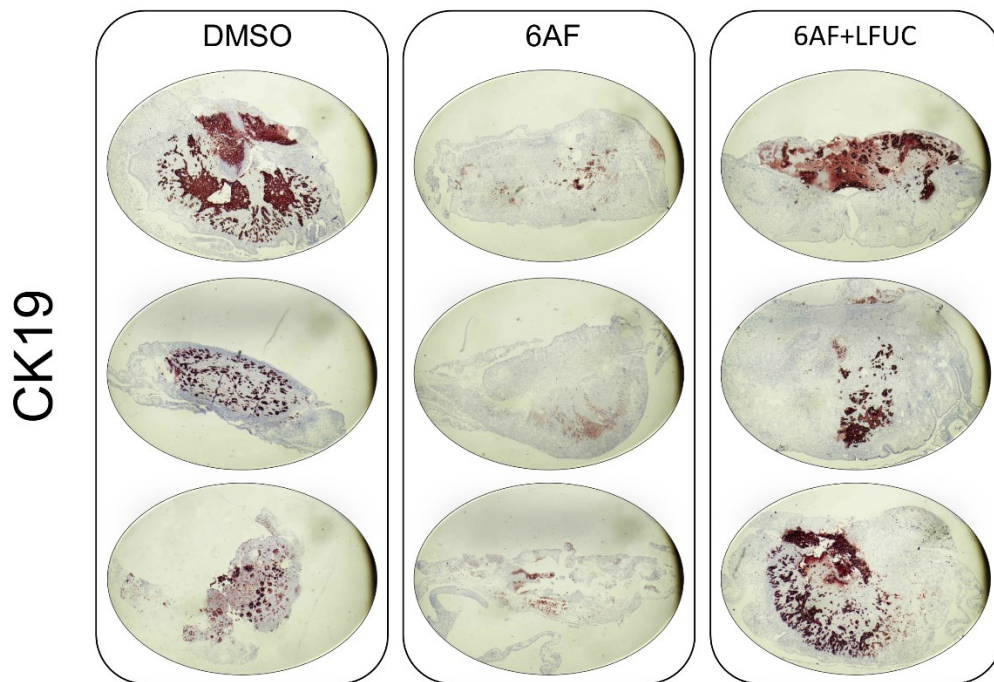


Figure 24. Representative images of CK19 stained paraffin sections of CAM tumors (10x). CK19 immunoreactivity was reduced in tumors treated with 6AF. The addition of LFUC annulled this effect.

At the cellular level, proliferation was lower in the 6AF-treated tumors compared to control (DMSO-treated) lesions. Adding L-Fucose increased proliferation compared with 6AF- and DMSO-treated tumors (Figure 25). In addition, apoptosis was highest in 6AF-treated cells, whereas similarly low levels of apoptosis were detected in DMSO-treated and 6AF+L-Fucose-treated cells (Figure 25). Besides a reduction of UEA-I and LCA (not shown), 6AF administration decreased NOTCH1 nuclear immunoreactivity in the lesions (Figure 25).

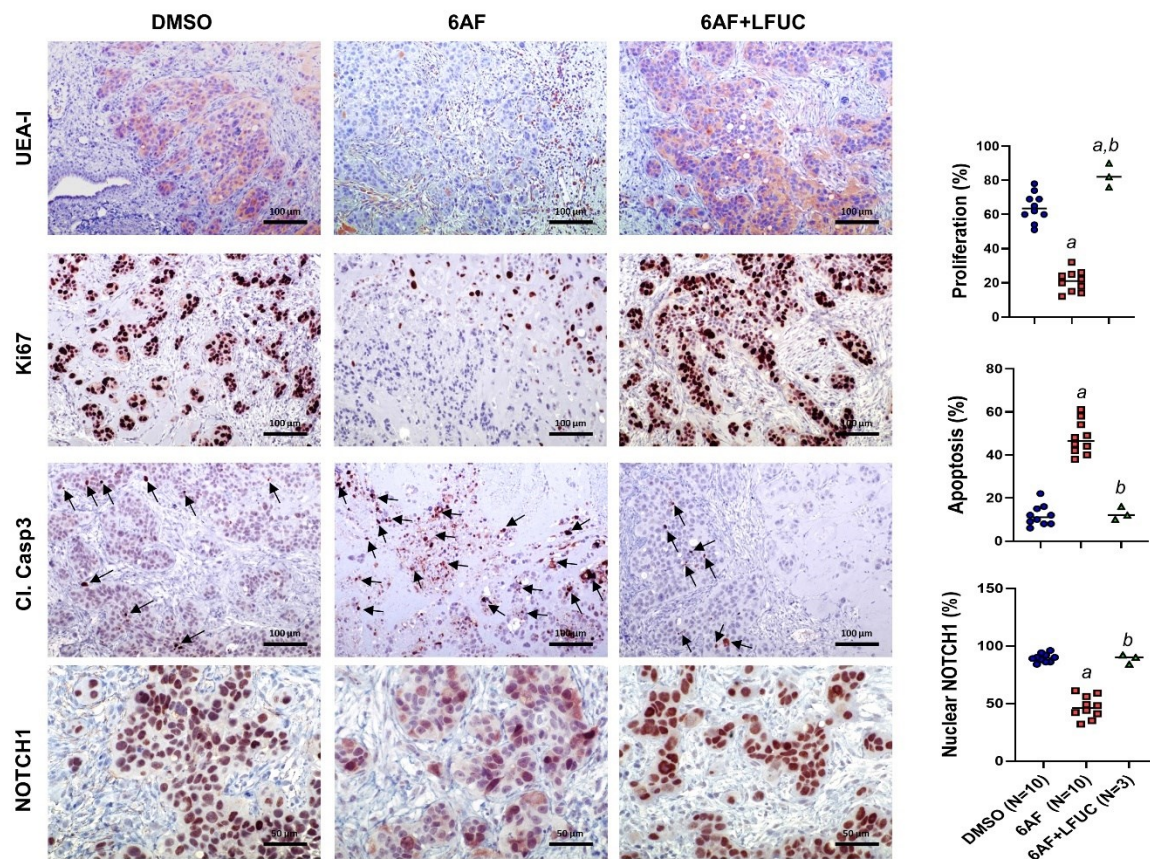


Figure 25. Effect of the fucosylation inhibitor 6AF on the growth of KKU-M213 intrahepatic cholangiocarcinoma (iCCA) cell line in the chick chorioallantoic membrane (CAM). Treatment with 6AF decreases proliferation and increases apoptosis in KKU-M213 cells compared with control (DMSO-treated) cells. Of note, the simultaneous administration of L-Fucose (L-FUC) annulled the anti-proliferative and apoptotic effects induced by 6AF. The arrows indicate the apoptotic bodies in the lesions. UEA-I staining is shown as proof of fucosylation inhibition. Mann-Whitney test: at least $p < 0.01$; a, vs. DMSO; b, vs. 6AF. Magnification: 200x. Scale bar: 100 μm in 200x. (Ament et al., 2023)

The present data indicate that fucosylation inhibition is detrimental to iCCA cell growth *in vivo*.

3.10 Aberrant Fucosylation in Mouse iCCA Lesions

Next, I determined whether altered fucosylation also occurs in intrahepatic cholangiocellular lesions developed in mouse models of iCCA. For this purpose, liver tissue lysates and liver tissue sections of wild-type female FVB/N mice subjected to hydrodynamic tail vein injection with 20µg of pT3-EF1α-TAZS89A or pT3-EF1α-YAPS127A combined with 20µg pT3-EF1α-HA-myr-AKT (AKT/TAZ and AKT/YAP mice) to induce iCCA formation were used to examine the fucosylation levels (provided by Dr. Xin Chen, University of California, San Francisco, USA). The immunohistochemical staining of the two iCCA models with fucose-binding lectins revealed a robust increase in fucose levels in the tumor lesions compared to the non-tumorous surrounding liver (Figure 26A,B).

Subsequently, I used frozen liver tissue for protein extraction to address whether the total protein fucosylation levels differ between wild-type livers (WT) and AKT/YAP or AKT/TAZ lesions. The subsequent Western blot analysis demonstrated that the fucose levels, as determined by the AAL, LCA, and UEA-I lectins, are significantly higher in liver tumor tissues from AKT/YAP and AKT/TAZ mice compared to WT livers (Figure 26C). These data indicate that increased fucosylation is strongly induced in the mouse models of iCCA. Thus, these models might be advantageous to understand better the contribution of aberrant fucosylation to cholangiocarcinogenesis and to test the effect in vivo of therapeutic strategies aimed at suppressing fucosylation in iCCA.

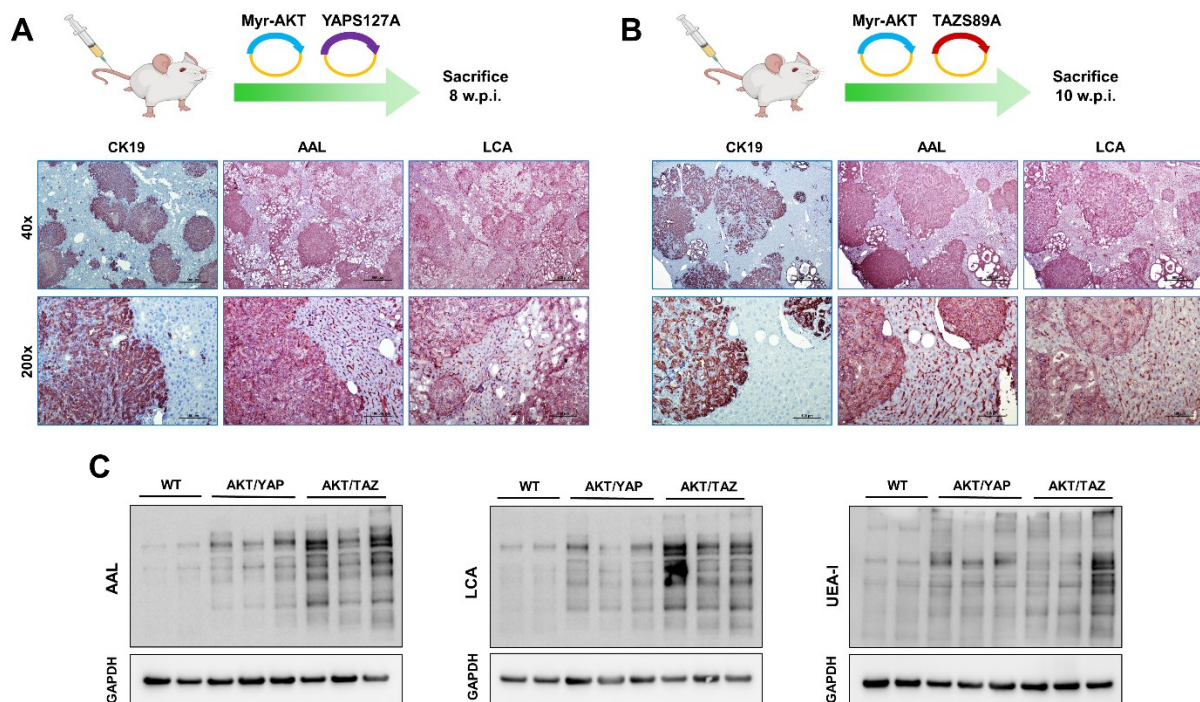


Figure 26. Aberrant fucosylation characterizes intrahepatic cholangiocarcinoma lesions developed in AKT/YAP and AKT/TAZ mouse models. AKT/YAP and AKT/TAZ mice were generated by hydrodynamic tail vein injection of an activated/myristoylated form of AKT (Myr-AKT) in association with activated YAP (YAPS127A) or TAZ (S89A) construct, as previously described (Cigliano et al., 2022; Zhang et al., 2017). Cholangiocellular lesions developed in AKT/YAP (**A**) and AKT/TAZ (**B**) mice displayed increased immunoreactivity for AAL and LCA lectins compared with non-tumorous surrounding livers. The positive immunoreactivity for the CK19 biliary marker confirms the cholangiocellular features of the lesions and helps demarcate them from the surrounding non-neoplastic parenchyma. At least six AKT/YAP and AKT/TAZ samples were analyzed by immunohistochemistry. Original magnification: 40x and 200x; scale bar: 500 μ m in 40x and 100 μ m in 200x. (**C**) Augmented fucosylation was further confirmed by Western blot analysis using the AAL, LCA, and UEA-I lectins and comparing wild-type livers injected with the empty vector (WT) with AKT/YAP and AKT/TAZ livers. At least three samples per mouse group were analyzed using Western blot analysis. Abbreviation: w.p.i., weeks post-injection. (Ament et al., 2023)

3.11 Impaired Colony Formation due to CRISPR Gene Knockout in Murine and Human iCCA Cells

The following experiments were conducted mainly by me during my three months stay in San Francisco, USA, in the lab of Dr. Xin Chen. I designed, constructed, and cloned the plasmids. I was trained by Dr. Tony Wang from the same lab.

To obtain a stronger and stable gene knockdown, iCCA cell lines were silenced using the CRISPR Cas9 method for *SLC35C1* and *FX*. Transfection of single guide (sg) RNA achieved a significant reduction in gene expression only for *FX*. Similar results were found at the protein level (Figure 27A). Nevertheless, fucosylation levels in HUCCT1 cells detected by *AAL*, *LCA*, and *UEA-1* were reduced after the knockout of both genes (Figure 27B). NF- κ B *p65* and *Bcl-xL* protein levels were reduced only after *FX* knockdown (Figure 27C). Moreover, the NOTCH1 (NICD) and HES1 protein levels were reduced after the knockout of *SLC35C1* and *FX*. For the colony-forming assay, murine HCC4 and human HUCCT1 cells transfected with corresponding lentivirus were plated in 6-well culture plates at a density 500 cells per well, respectively, in triplicate. Two weeks later, colonies were stained with crystal violet and captured (Figure 27D). Colony formation of both cell lines was impaired due to the knockout of *FX*. HUCCT1 cells also showed reduced colonies after the knockdown of *SLC35C1*.

These data show preliminary results for a stable knockdown of *SLC35C1* and *FX* in cell lines. The impact of the knockout of the two genes in iCCA cells *in vitro* and *in vivo* will be addressed in future experiments.

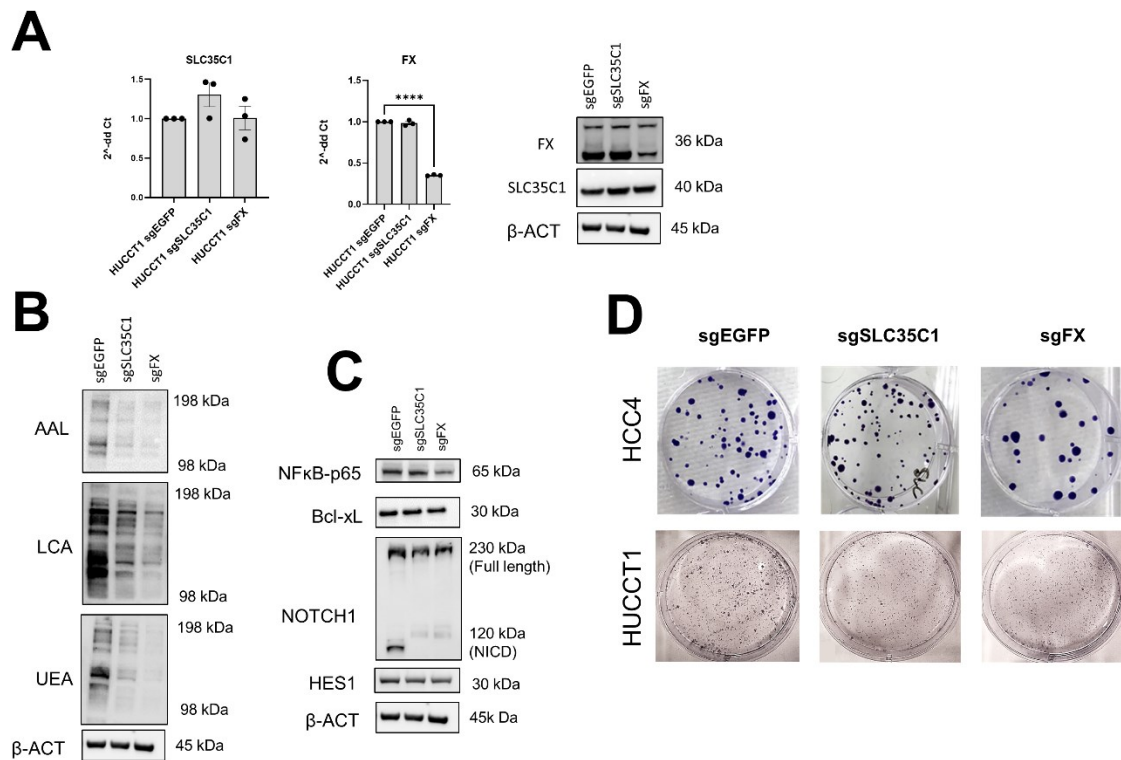


Figure 27. CRISPR knockout of *SLC35C1* and *FX* (**A**) CRISPR knockout resulted in the reduction of gene expression only for *sgFX* in HUCCT1 cells. Similar results were obtained on protein levels (**B**). Fucosylation levels in HUCCT1 cells detected by lectin blotting were reduced after knockout of both genes. (**C**) NF-κB p65 and Bcl-xL protein levels were reduced only after *FX* knockdown. NOTCH1 (NICD) and HES1 protein levels were reduced after knockdown of both genes. (**D**) Colony formation assay after knockdown of *SLC35C1* and *FX* in murine HCC4 and human HUCCT1 cells. Five-hundred cells per well were seeded in a 6-well plate. After 14 days, the colonies were stained with crystal violet. Both cell lines showed reduced colony number for *sgFX*. In the HUCCT1 cells also knockout of *SLC35C1* reduced the colony formation.

3.12 Increased Fucosylation in Cancer-Associated Fibroblasts (CAF)

To gain further insights into the role of fucosylation on the tumor microenvironment, I investigated the relevance of fucosylation on iCCA cancer-associated fibroblasts

(CAFs) (provided by Prof. G. Gannelli, Castellana Grotte, Italy; and Prof. Jesus Banales, San Sebastian, Spain). The LX-2 human normal hepatic stellate cell line was used as a control, since the origin of CAFs from human hepatic cells has been recently demonstrated (Affo et al. 2021). Notably, I found that fucosylation levels detected by AAL, LCA, and UEA-I lectins in CAFs were higher than in LX-2 cells (Figure 28A). In addition, CAF treatment with 6AF triggered a decrease in fucosylation, paralleled by a decline in the CAF activation marker osteopontin (Figure 28B) and CAF proliferation *in vitro* (Figure 28C). Although preliminary, these data indicate that fucosylation is pronounced in CAFs and affects their growth features in iCCA. Therefore, the present data suggest a possible function of fucosylation in the tumorous and non-tumorous compartments of iCCA.

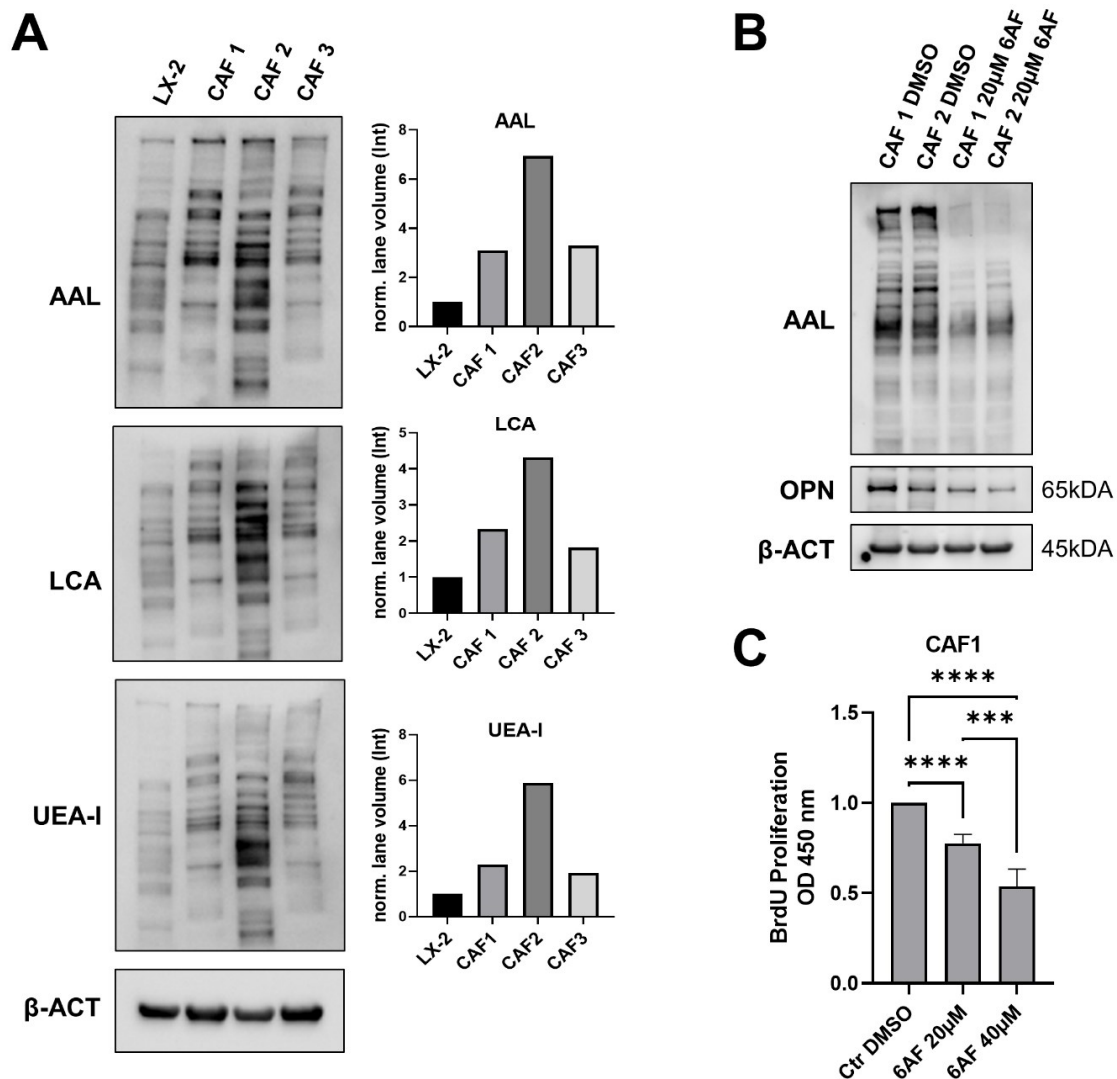


Figure 28. Overview of fucosylation relevance in cancer-associated fibroblasts (CAFs). **(A)** Three distinct CAF (CAF 1, 2, 3) and LX2 lysates were used for lectin blotting with AAL, LCA, and UEA-I. LX2 cells, derived from normal hepatic stellate cells, were used as a control. Protein fucosylation of all three CAF lysates was higher compared to LX2 cells. The left panels display the Western blot results, and right panels the quantification of signal intensity. **(B)** CAF 1 and CAF 2 cellular fucosylation was inhibited after incubation with 6AF for 48h compared to control cells (Ctr DMSO). Osteopontin (OPN) protein levels were also negatively influenced by 6AF treatment. β-Actin was used as a normalization control. **(C)** BrdU Cell Proliferation Assay. The proliferation of CAF1 decreased after incubation with 6AF for 48h in a dose-dependent manner. Experiments were performed three times in triplicate (N=9); One-Way ANOVA: *** $p < 0.001$, **** $p < 0.0001$. (Ament et al., 2023)

3.13 Fucosylation Regulates Pro-Inflammatory Signals in Human iCCA

Another interesting question was whether pro-inflammatory signals in iCCA are regulated by fucosylation. It was recently shown, indeed, that fucosylation inhibition attenuates oxidative stress and therefore reduces hepatotoxicity (Liu et al. 2022). Oxidative stress is a critical driver in acute liver failure, especially provoked by APAP-induced hepatotoxicity (Bunchorntavakul and Reddy, 2018). Incubation with 6AF decreased inducible nitric oxide synthase (iNOS) and NRF2 levels in HUCCT1 and KKU213 cell lines (Figure 29A). Also, 6AF administration reduced the levels of CD44 and CXCR4 stem cell markers in the same cell lines and CXCR4 in the CAM (29B,C), suggesting a pro-stemness action of fucosylation in iCCA.

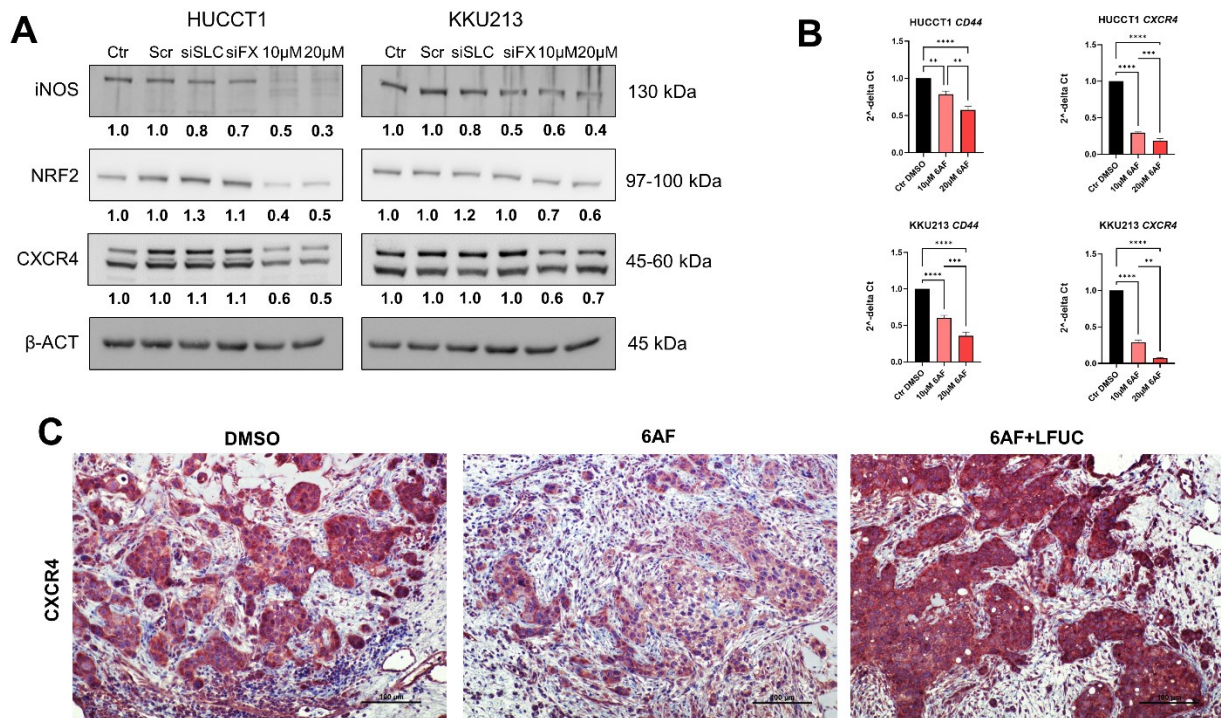


Figure 29. Fucosylation regulates pro-inflammatory signals in intrahepatic cholangiocarcinoma (iCCA). **(A)** Western blot analysis showing the downregulation of iNOS, NRF2, and CXCR4. While silencing of either *SLC35C1* (siSLC) or *FX* (siFX) did not affect the three proteins, the two indicated doses of 6AF decreased them to different extents in the two cell lines. **(B)** Gene expression levels of CD44 and CXCR4 in iCCA cells decreased after a 48h incubation with 10μM or 20μM 6AF. N=3, One-Way ANOVA: ** p<0,01, *** p<0.001, **** p < 0.0001. **(C)** Levels of CXCR4 were also downregulated in KKU213 cells implanted in the chick chorioallantoic membrane (CAM; Figure 8) after 6AF treatment, compared with DMSO treatment, as assessed by immunohistochemistry. L-Fucose supplementation to 6AF-treated cells (6AF + LFUC) restored CXCR4 expression in the implanted cells. Original magnification: 200x; scale bar: 100 μm. (Ament et al., 2023)

3.14 No Evidence of Further Signaling Pathways Affected by Fucose in Human iCCA

To determine whether other signaling pathways are affected by the inhibition of fucose, I treated two iCCA cell lines with 20 μ M 6AF or medium alone; subsequently, I used the cell lysates for Western blotting. Various oncogenic pathways, including the AKT/mTOR, Ras/MAPK, Hippo, etc., remained unaffected by 6AF administration in K KU213 and HUCCT1 cells (Figure 30A,B). High-throughput approaches will eventually uncover the additional targets of fucosylation in iCCA.

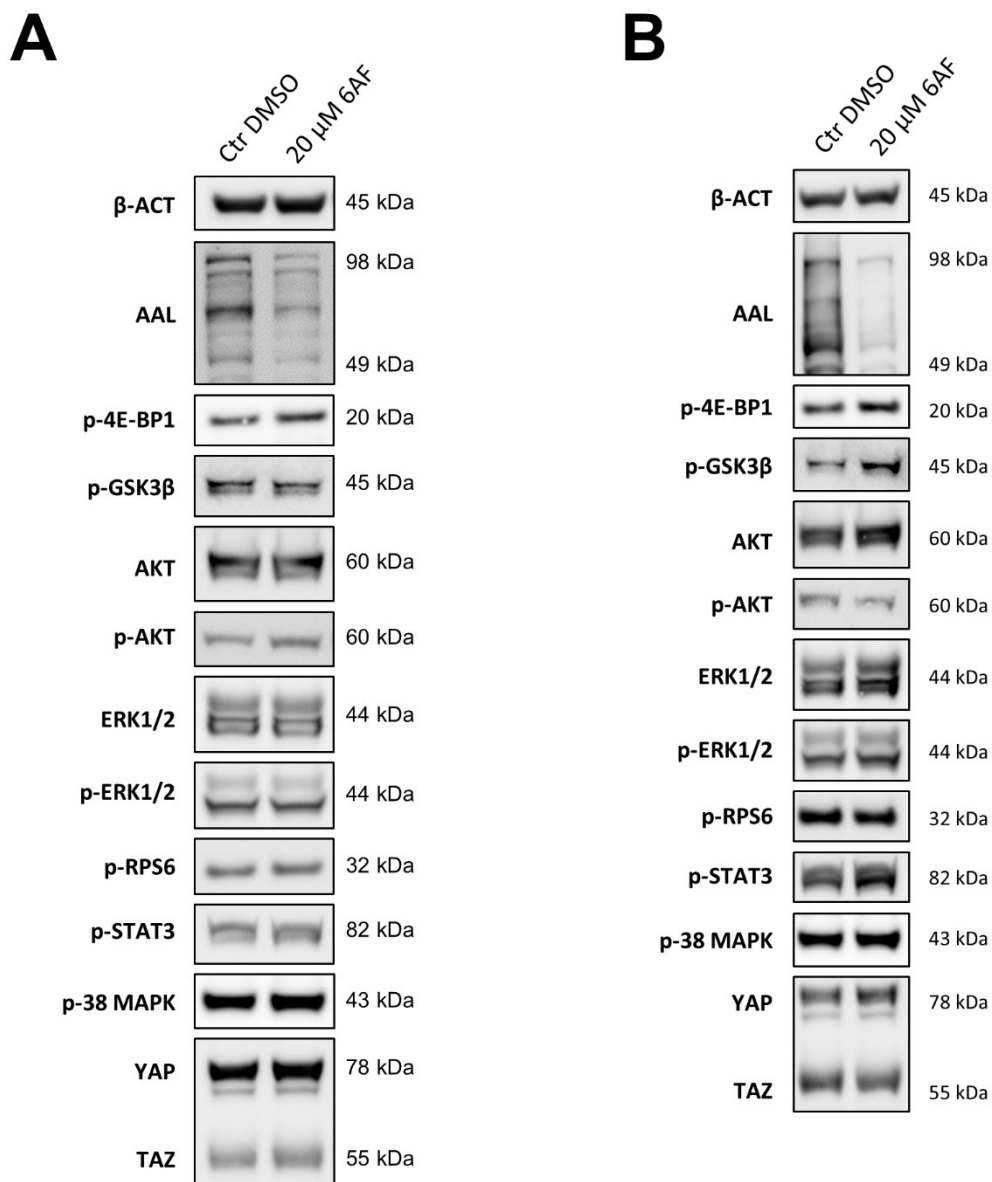


Figure 30. Inhibition of fucosylation does not affect AKT/mTOR, ERK/MAPK, p38MAPK, JAK/STAT3, and YAP/TAZ pathways in KKU213 and HUCCT1 human intrahepatic cholangiocarcinoma cell lines. Effects on the levels of the various pathways following the treatment with the fucosylation inhibitor 6AF in KKU213 (**A**) and HUCCT1 (**B**) cells are shown, as detected by Western blot analysis. β -Actin (β -Act) was used as a loading control. (Ament et al., 2023)

4. Discussion

Intrahepatic cholangiocarcinoma (iCCA) is a highly lethal tumor characterized by clinical aggressiveness and resistance to conventional treatments. (Banales et al., 2020; Braconi et al., 2019; Rizvi and Gores, 2013) Thus, novel and more effective therapeutic strategies are required to overcome this gloomy scenario and make this refractory cancer curable.

Here, I systematically analyzed the relevance of the fucosylation pathway in this aggressive disease. My data indicate that fucosylation is aberrantly upregulated in human iCCA. Furthermore, fucosylation levels were inversely correlated with the patient's prognosis, implying a function for augmented fucosylation both in iCCA development and progression. Elevated fucosylation was underlined by the robust and concomitant upregulation of all the pro-fucosylation proteins investigated, including POFUT1, GMDS, SLC35C1, FX, LFNG, MFNG, and RFNG, and the downregulation of FUCA1, the primary fucosylation inhibitor. The present findings support a wealth of evidence indicating a pathogenetic and prognostic role of fucosylation in various tumor entities, such as urological cancers, lung, colorectal, pancreas, prostate, breast, oral cavity, esophageal, and thyroid tumors. (Fujita et al., 2021; Liao et al., 2021) Thus, fucosylation might represent a previously underestimated oncogenic driver and a cancer hallmark.

At the cellular level, I found that fucosylation affects the growth of iCCA cells *in vitro* primarily by stimulating proliferation and migration. In contrast, fucosylation inhibition did not significantly affect apoptosis in KKU213 and HUCCT1 iCCA cell lines. Notably, potent apoptosis accompanied the administration of the 6AF inhibitor *in vivo/in ovo*, together with a reduction in proliferation. The reason for this discrepancy remains

unknown. However, the 3D growth of the KKU213 cells and the interaction with the chicken microenvironment presumably recapitulates the human disease more closely and suggest the effectiveness of fucosylation inhibition as a therapeutic strategy in this tumor type. Accordingly, in subsequent experiments, I demonstrated that 6AF also decreases the proliferation of CAFs derived from iCCA, suggesting that fucosylation inhibition might hamper the growth of this tumor type by affecting both the tumor and the microenvironment compartments. Future investigations in animal models of iCCA might help address this critical issue convincingly. In this regard, preliminary data from our laboratory show that fucosylation is consistently induced in cholangiocellular lesions from AKT/TAZ and AKT/YAP mouse models of iCCA. These findings suggest that aberrant fucosylation is a biochemical feature of cholangiocarcinogenesis in humans and mice, and these mouse models might represent a valuable tool for studying fucosylation in iCCA. In addition, these preclinical models will allow for determining the toxicity and the therapeutic window of fucosylation inhibitors in patients.

At the molecular level, I revealed that fucosylation sustains the activation of the NOTCH and NF- κ B signaling pathways in cholangiocarcinogenesis. Both molecular cascades have been previously shown to be modulated by fucosylation in other tumor types (Furukawa and Fukuda, 2016; Matsuura et al., 2008; Doud et al., 2020) and might be the critical oncogenic drivers targeted by fucosylation inhibitors in this deadly tumor. Moreover, 6AF decreased inducible nitric oxide synthase (iNOS) and NRF2 levels in HUCCT1 and KKU-M213 cell lines following previous evidence on the anti-inflammatory effects of fucosylation inhibition. (Liu et al., 2022) Also, 6AF administration reduced CD44 and CXCR4 stem cell markers in the same cell lines and

CXCR4 in the CAM, suggesting a pro-stemness action of fucosylation in iCCA. On the other hand, various oncogenic pathways, including the AKT/mTOR, Ras/MAPK, Hippo, etc., remained unaffected by 6AF administration in the same cells. Therefore, high-throughput approaches, such as proteomics and transcriptomics, should be applied to uncover the additional targets of fucosylation in iCCA.

Besides the pathogenetic importance of our data, the present findings might also have relevant translational implications. Since fucosylation inhibition significantly decreased iCCA growth *in vitro* and *in vivo*, therapeutic strategies aimed at suppressing fucosylation might be successful against several tumor entities, not limited to this cancer type. For this scope, more efficient fucosylation inhibitors should be developed and tested. In this regard, encouraging data showed recently that fluorinated rhamnosides efficiently block cellular fucosylation at a therapeutic dose. (Pijnenborg et al., 2021) On the other hand, due to the critical role of fucosylation in many physiological processes, (Kizuka et al., 2017) robust data from preclinical models in terms of *in vivo* toxicity should be generated before a clinical application of fucosylation inhibitors can be envisaged.

References

- Affo, Silvia; Nair, Ajay; Brundu, Francesco; Ravichandra, Aashreya; Bhattacharjee, Sonakshi; Matsuda, Michitaka et al. (2021): Promotion of cholangiocarcinoma growth by diverse cancer-associated fibroblast subpopulations. In: *Cancer cell* 39 (6), 866-882.e11. DOI: 10.1016/j.ccell.2021.03.012.
- Banales, Jesus M.; Cardinale, Vincenzo; Carpino, Guido; Marzioni, Marco; Andersen, Jesper B.; Invernizzi, Pietro et al. (2016): Expert consensus document: Cholangiocarcinoma: current knowledge and future perspectives consensus statement from the European Network for the Study of Cholangiocarcinoma (ENS-CCA). In: *Nature reviews. Gastroenterology & hepatology* 13 (5), S. 261–280. DOI: 10.1038/nrgastro.2016.51.
- Banales, Jesus M.; Marin, Jose J. G.; Lamarca, Angela; Rodrigues, Pedro M.; Khan, Shahid A.; Roberts, Lewis R. et al. (2020): Cholangiocarcinoma 2020: the next horizon in mechanisms and management. In: *Nature reviews. Gastroenterology & hepatology* 17 (9), S. 557–588. DOI: 10.1038/s41575-020-0310-z.
- Bartolini, Ilenia; Risaliti, Matteo; Fortuna, Laura; Agostini, Carlotta; Ringressi, Maria Novella; Taddei, Antonio; Muiesan, Paolo (2020): Current management of intrahepatic cholangiocarcinoma: from resection to palliative treatments. In: *Radiology and oncology* 54 (3), S. 263–271. DOI: 10.2478/raon-2020-0045.
- Benson, Al B. 3rd; Abrams, Thomas A.; Ben-Josef, Edgar; Bloomston, P. Mark; Botha, Jean F.; Clary, Bryan M. et al. (2009): NCCN clinical practice guidelines in oncology: hepatobiliary cancers. In: *Journal of the National Comprehensive Cancer Network : JNCCN* 7 (4), S. 350–391. DOI: 10.6004/jnccn.2009.0027.

- Biswas, D. K.; Cruz, A. P.; Gansberger, E.; Pardee, A. B. (2000): Epidermal growth factor-induced nuclear factor kappa B activation: A major pathway of cell-cycle progression in estrogen-receptor negative breast cancer cells. In: *Proceedings of the National Academy of Sciences of the United States of America* 97 (15), S. 8542–8547. DOI: 10.1073/pnas.97.15.8542.
- Braconi, Chiara; Roessler, Stephanie; Kruk, Beata; Lammert, Frank; Krawczyk, Marcin; Andersen, Jesper B. (2019): Molecular perturbations in cholangiocarcinoma: Is it time for precision medicine? In: *Liver international : official journal of the International Association for the Study of the Liver* 39 Suppl 1, S. 32–42. DOI: 10.1111/liv.14085.
- Bray, Sarah J. (2016): Notch signalling in context. In: *Nature Reviews Molecular Cell Biology* 17 (11), S. 722–735. DOI: 10.1038/nrm.2016.94.
- Bridgewater, John; Galle, Peter R.; Khan, Shahid A.; Llovet, Josep M.; Park, Joong Won; Patel, Tushar et al. (2014): Guidelines for the diagnosis and management of intrahepatic cholangiocarcinoma. In: *Journal of Hepatology* 60 (6), S. 1268–1289. DOI: 10.1016/j.jhep.2014.01.021.
- Bunchorntavakul, Chalermrat; Reddy, K. Rajender (2018): Acetaminophen (APAP or N-Acetyl-p-Aminophenol) and Acute Liver Failure. In: *Clinics in liver disease* 22 (2), S. 325–346. DOI: 10.1016/j.cld.2018.01.007.
- Cigliano, Antonio; Wang, Jingxiao; Chen, Xin; Calvisi, Diego F. (2017): Role of the Notch signaling in cholangiocarcinoma. In: *Expert Opinion on Therapeutic Targets* 21 (5), S. 471–483. DOI: 10.1080/14728222.2017.1310842.

- Cigliano, Antonio; Zhang, Shanshan; Ribback, Silvia; Steinmann, Sara; Sini, Marcella; Ament, Cindy E. et al. (2022): The Hippo pathway effector TAZ induces intrahepatic cholangiocarcinoma in mice and is ubiquitously activated in the human disease. In: *Journal of experimental & clinical cancer research* : CR 41 (1), S. 192. DOI: 10.1186/s13046-022-02394-2.
- Czauderna, Carolin; Castven, Darko; Mahn, Friederike L.; Marquardt, Jens U. (2019): Context-Dependent Role of NF- κ B Signaling in Primary Liver Cancer-from Tumor Development to Therapeutic Implications. In: *Cancers (Basel)* 11 (8). DOI: 10.3390/cancers11081053.
- D'Souza, B.; Miyamoto, A.; Weinmaster, G. (2008): The many facets of Notch ligands. In: *Oncogene* 27 (38), S. 5148–5167. DOI: 10.1038/onc.2008.229.
- Dodson, Rebecca M.; Weiss, Matthew J.; Cosgrove, David; Herman, Joseph M.; Kamel, Ihab; Anders, Robert et al. (2013): Intrahepatic cholangiocarcinoma: management options and emerging therapies. In: *Journal of the American College of Surgeons* 217 (4), 736-750.e4. DOI: 10.1016/j.jamcollsurg.2013.05.021.
- Doud, Emma H.; Shetty, Trupti; Abt, Melissa; Mosley, Amber L.; Corson, Timothy W.; Mehta, Anand; Yeh, Elizabeth S. (2020): NF- κ B Signaling Is Regulated by Fucosylation in Metastatic Breast Cancer Cells. In: *Biomedicines* 8 (12). DOI: 10.3390/biomedicines8120600.
- EASL Clinical Practice Guidelines: management of cholestatic liver diseases (2009). In: *Journal of Hepatology* 51 (2), S. 237–267.
- El-Serag, Hashem B.; Engels, Eric A.; Landgren, Ola; Chiao, Elizabeth; Henderson, Louise; Amaratunge, Harshinie C.; Giordano, Thomas P. (2009): Risk of

hepatobiliary and pancreatic cancers after hepatitis C virus infection: A population-based study of U.S. veterans. In: *Hepatology (Baltimore, Md.)* 49 (1), S. 116–123. DOI: 10.1002/hep.22606.

Forner, Alejandro; Vidili, Gianpaolo; Rengo, Marco; Bujanda, Luis; Ponz-Sarvisé, Mariano; Lamarca, Angela (2019): Clinical presentation, diagnosis and staging of cholangiocarcinoma. In: *Liver International* 39 Suppl 1 (S1), S. 98–107. DOI: 10.1111/liv.14086.

Fujita, Kazutoshi; Hatano, Koji; Hashimoto, Mamoru; Tomiyama, Eisuke; Miyoshi, Eiji; Nonomura, Norio; Uemura, Hirotsugu (2021): Fucosylation in Urological Cancers. In: *International journal of molecular sciences* 22 (24). DOI: 10.3390/ijms222413333.

Furukawa, Koichi; Fukuda, Minoru (2016): Glycosignals in cancer: Mechanisms of malignant phenotypes.

Geisler, Fabian; Strazzabosco, Mario (2015): Emerging roles of Notch signaling in liver disease. In: *Hepatology (Baltimore, Md.)* 61 (1), S. 382–392. DOI: 10.1002/hep.27268.

Hayden, Matthew S.; Ghosh, Sankar (2008): Shared principles in NF-kappaB signaling. In: *Cell* 132 (3), S. 344–362. DOI: 10.1016/j.cell.2008.01.020.

Katsube, Ken Ichi; Sakamoto, Kei (2005): Notch in vertebrates - Molecular aspects of the signal. In: *International Journal of Developmental Biology* 49 (2-3 SPEC. ISS), S. 369–374. DOI: 10.1387/ijdb.041950kk.

- Khan, Shahid A.; Tavolari, Simona; Brandi, Giovanni (2019): Cholangiocarcinoma: Epidemiology and risk factors. In: *Liver international : official journal of the International Association for the Study of the Liver* 39 (S1), S. 19–31. DOI: 10.1111/liv.14095.
- Kim, Preston; Littau, Michael; Baker, Talia B.; Abdelsattar, Zaid; Tonelli, Celsa; Bunn, Corinne et al. (2022): Intrahepatic cholangiocarcinoma: Is there a role for liver transplantation? In: *Surgery* 171 (3), S. 741–746. DOI: 10.1016/j.surg.2021.09.034.
- Kizuka, Yasuhiko; Nakano, Miyako; Yamaguchi, Yoshiki; Nakajima, Kazuki; Oka, Ritsuko; Sato, Keiko et al. (2017): An Alkynyl-Fucose Halts Hepatoma Cell Migration and Invasion by Inhibiting GDP-Fucose-Synthesizing Enzyme FX, TSTA3. In: *Cell Chemical Biology* 24 (12), 1467-1478.e5. DOI: 10.1016/j.chembiol.2017.08.023.
- Krenzien, Felix; Nevermann, Nora; Krombholz, Alina; Benzing, Christian; Haber, Philipp; Fehrenbach, Uli et al. (2022): Treatment of Intrahepatic Cholangiocarcinoma-A Multidisciplinary Approach. In: *Cancers (Basel)* 14 (2). DOI: 10.3390/cancers14020362.
- Kumagai, Shinji; Kurumatani, Norio; Arimoto, Akira; Ichihara, Gaku (2013): Cholangiocarcinoma among offset colour proof-printing workers exposed to 1,2-dichloropropane and/or dichloromethane. In: *Occupational and environmental medicine* 70 (7), S. 508–510. DOI: 10.1136/oemed-2012-101246.
- Lau, Sean K.; Prakash, Sonam; Geller, Stephen A.; Alsabeh, Randa (2002): Comparative immunohistochemical profile of hepatocellular carcinoma,

- cholangiocarcinoma, and metastatic adenocarcinoma. In: *Human pathology* 33 (12), S. 1175–1181. DOI: 10.1053/hupa.2002.130104.
- Lee, Tae Y.; Lee, Sang S.; Jung, Seok W.; Jeon, Seong H.; Yun, Sung-Cheol; Oh, Hyoung-Chul et al. (2008): Hepatitis B virus infection and intrahepatic cholangiocarcinoma in Korea: a case-control study. In: *The American journal of gastroenterology* 103 (7), S. 1716–1720. DOI: 10.1111/j.1572-0241.2008.01796.x.
- Lewis, Jason (2017): Pathological patterns of biliary disease. In: *Clinical liver disease* 10 (5), S. 107–110. DOI: 10.1002/cld.667.
- Li, L.; Krantz, I. D.; Deng, Y.; Genin, A.; Banta, A. B.; Collins, C. C. et al. (1997): Alagille syndrome is caused by mutations in human Jagged1, which encodes a ligand for Notch1. In: *Nature genetics* 16 (3), S. 243–251. DOI: 10.1038/ng0797-243.
- Liao, Chengcheng; An, Jiaying; Yi, Suqin; Tan, Zhangxue; Wang, Hui; Li, Hao et al. (2021): FUT8 and Protein Core Fucosylation in Tumours: From Diagnosis to Treatment. In: *Journal of Cancer* 12 (13), S. 4109–4120. DOI: 10.7150/jca.58268.
- Liu, Ting; Zhang, Lingyun; Joo, Donghyun; Sun, Shao-Cong (2017): NF- κ B signaling in inflammation. In: *Signal Transduction and Targeted Therapy* 2, 17023-. DOI: 10.1038/sigtrans.2017.23.
- Liu, Zhaoguo; Tu, Mengjue; Shi, Jianan; Zhou, Hong; Meng, Guoliang; Gu, Jianguo; Wang, Yuqin (2022): Inhibition of fucosylation by 2-fluorofucose attenuated acetaminophen-induced liver injury via its anti-inflammation and anti-oxidative stress effects. In: *Frontiers in pharmacology* 13, S. 939317. DOI: 10.3389/fphar.2022.939317.

- Lopez Miranda, Elena; Stathis, Anastasios; Hess, Dagmar; Racca, Fabricio; Quon, Doris; Rodon, Jordi et al. (2021): Phase 1 study of CB-103, a novel first-in-class inhibitor of the CSL-NICD gene transcription factor complex in human cancers. In: *JCO* 39 (15_suppl), S. 3020. DOI: 10.1200/JCO.2021.39.15_suppl.3020.
- Luedde, Tom; Schwabe, Robert F. (2011): NF- κ B in the liver--linking injury, fibrosis and hepatocellular carcinoma. In: *Nature reviews. Gastroenterology & hepatology* 8 (2), S. 108–118. DOI: 10.1038/nrgastro.2010.213.
- Mancarella, Serena; Gigante, Isabella; Serino, Grazia; Pizzuto, Elena; Dituri, Francesco; Valentini, Maria F. et al. (2022): Crenigacestat blocking notch pathway reduces liver fibrosis in the surrounding ecosystem of intrahepatic CCA via TGF- β inhibition. In: *Journal of experimental & clinical cancer research : CR* 41 (1), S. 331. DOI: 10.1186/s13046-022-02536-6.
- Matsuura, Aiko; Ito, Makiko; Sakaidani, Yuta; Kondo, Tatsuhiko; Murakami, Kosuke; Furukawa, Koichi et al. (2008): O-linked N-acetylglucosamine is present on the extracellular domain of notch receptors. In: *Journal of Biological Chemistry* 283 (51), S. 35486–35495. DOI: 10.1074/jbc.M806202200.
- Moloney, Daniel J.; Shair, Louisa H.; Lu, Frederick M.; Xia, Jie; Locke, Robert; Matta, Khushi L.; Haltiwanger, Robert S. (2000): Mammalian Notch1 is modified with two unusual forms of O-linked glycosylation found on epidermal growth factor-like modules. In: *Journal of Biological Chemistry* 275 (13), S. 9604–9611. DOI: 10.1074/jbc.275.13.9604.
- Navaneethan, Udayakumar; Njei, Basile; Lourdusamy, Vennisvasanth; Konjeti, Rajesh; Vargo, John J.; Parsi, Mansour A. (2015): Comparative effectiveness of

biliary brush cytology and intraductal biopsy for detection of malignant biliary strictures: a systematic review and meta-analysis. In: *Gastrointestinal endoscopy* 81 (1), S. 168–176. DOI: 10.1016/j.gie.2014.09.017.

Nuzzo, Gennaro; Giuliani, Felice; Ardito, Francesco; Giovannini, Ivo; Aldrighetti, Luca; Belli, Giulio et al. (2012): Improvement in perioperative and long-term outcome after surgical treatment of hilar cholangiocarcinoma: results of an Italian multicenter analysis of 440 patients. In: *Archives of surgery (Chicago, Ill. : 1960)* 147 (1), S. 26–34. DOI: 10.1001/archsurg.2011.771.

Pijnenborg, Johan F. A.; Rossing, Emiel; Merx, Jona; Noga, Marek J.; Titulaer, Willem H. C.; Eerden, Nienke et al. (2021): Fluorinated rhamnosides inhibit cellular fucosylation. In: *Nature communications* 12 (1), S. 7024. DOI: 10.1038/s41467-021-27355-9.

Razumilava, Nataliya; Gores, Gregory J. (2014): Cholangiocarcinoma. In: *Lancet (London, England)* 383 (9935), S. 2168–2179. DOI: 10.1016/S0140-6736(13)61903-0.

Rizvi, Sumera; Gores, Gregory J. (2013): Pathogenesis, diagnosis, and management of cholangiocarcinoma. In: *Gastroenterology* 145 (6), S. 1215–1229. DOI: 10.1053/j.gastro.2013.10.013.

Rullier, A.; Le Bail, B.; Fawaz, R.; Blanc, J. F.; Saric, J.; Bioulac-Sage, P. (2000): Cytokeratin 7 and 20 expression in cholangiocarcinomas varies along the biliary tract but still differs from that in colorectal carcinoma metastasis. In: *The American journal of surgical pathology* 24 (6), S. 870–876. DOI: 10.1097/00000478-200006000-00014.

- Sapisochin, G.; Facciuto, M.; Rubbia-Brandt, L.; Marti, J.; Mehta, N.; Yao, F. Y. et al. (2016): Liver transplantation for "very early" intrahepatic cholangiocarcinoma: International retrospective study supporting a prospective assessment. In: *Hepatology (Baltimore, Md.)* 64 (4), S. 1178–1188. DOI: 10.1002/hep.28744.
- Shaib, Yasser H.; El-Serag, Hashem B.; Davila, Jessica A.; Morgan, Robert; McGlynn, Katherine A. (2005): Risk factors of intrahepatic cholangiocarcinoma in the United States: a case-control study. In: *Gastroenterology* 128 (3), S. 620–626. DOI: 10.1053/j.gastro.2004.12.048.
- Shimada, Kazuaki; Sano, Tsuyoshi; Sakamoto, Yoshihiro; Esaki, Minoru; Kosuge, Tomoo; Ojima, Hidenori (2007): Surgical outcomes of the mass-forming plus periductal infiltrating types of intrahepatic cholangiocarcinoma: a comparative study with the typical mass-forming type of intrahepatic cholangiocarcinoma. In: *World journal of surgery* 31 (10), S. 2016–2022. DOI: 10.1007/s00268-007-9194-0.
- Vecchio, Giancarlo; Parascandolo, Alessia; Allocca, Chiara; Ugolini, Clara; Basolo, Fulvio; Moracci, Marco et al. (2017): Human α -L-fucosidase-1 attenuates the invasive properties of thyroid cancer. In: *Oncotarget* 8 (16), S. 27075–27092. DOI: 10.18632/oncotarget.15635.
- Xue, Tong-Chun; Zhang, Bo-Heng; Ye, Sheng-Long; Ren, Zheng-Gang (2015): Differentially expressed gene profiles of intrahepatic cholangiocarcinoma, hepatocellular carcinoma, and combined hepatocellular-cholangiocarcinoma by integrated microarray analysis. In: *Tumour biology : the journal of the International*

Society for Oncodevelopmental Biology and Medicine 36 (8), S. 5891–5899. DOI: 10.1007/s13277-015-3261-1.

Yamamoto, Yumi; Gaynor, Richard B. (2004): I κ B kinases: key regulators of the NF- κ B pathway. In: *Trends in Biochemical Sciences* 29 (2), S. 72–79. DOI: 10.1016/j.tibs.2003.12.003.

Zhang, Shanshan; Song, Xinhua; Cao, Dan; Xu, Zhong; Fan, Biao; Che, Li et al. (2017): Pan-mTOR inhibitor MLN0128 is effective against intrahepatic cholangiocarcinoma in mice. In: *Journal of Hepatology* 67 (6), S. 1194–1203. DOI: 10.1016/j.jhep.2017.07.006.

Zhang, Zhenbo; Sun, Ping; Liu, Jiwei; Fu, Li; Yan, Jie; Liu, Yuejian et al. (2008): Suppression of FUT1/FUT4 expression by siRNA inhibits tumor growth. In: *Biochimica et biophysica acta* 1783 (2), S. 287–296. DOI: 10.1016/j.bbamcr.2007.10.007.

Zong, Yiwei; Panikkar, Archana; Xu, Jie; Antoniou, Aline; Raynaud, Peggy; Lemaigre, Frederic; Stanger, Ben Z. (2009): Notch signaling controls liver development by regulating biliary differentiation. In: *Development* 136 (10), S. 1727–1739. DOI: 10.1242/dev.029140.

List of Abbreviations

AAL	<i>Aleuria aurantia lectin</i>
Bcl-xL	B-cell lymphoma extra-large
CAF	cancer-associated fibroblast
CAM	chick chorioallantoic membrane
CSL	CBF1/RBPJk/Suppressor of Hairless/Lag-1
dCCA	distal cholangiocarcinoma
EGFR	epidermal growth factor receptor
EGF	epidermal growth factor
ER	endoplasmic reticulum
FGFR	fibroblast growth factor receptor
FPGT	fucose-1-phosphate guanylyl transferase
FUCA1	α -L-fucosidase-1
FUK	L-fucose kinase
FUTs	Fucosyltransferases
FX	GDP-L fucose synthetase
Golgi	Golgi apparatus
GMDS	GDP-mannose 4,6-dehydratase
HCC	hepatocellular carcinoma
HES1	hairy and enhancer of split-1
HPC	hepatic progenitor cells
iCCA	intrahepatic cholangiocarcinoma

IDH	isocitrate dehydrogenase
JAG1	Jagged1
KKU213	KKU-M213
LCA	<i>Lens culinaris agglutinin</i>
LFNG	lunatic fringe
MAML	mastermind-like
MFNG	manic fringe
NECD	NOTCH extracellular domain
NF-κB	Nuclear factor kappa-light-chain-enhancer of activated B cells
NHC	normal human cholangiocytes
NICD	NOTCH receptor intracellular domain
OS	overall survival
pCCA	perihilar cholangiocarcinoma
POFUT1	GDP-fucose protein O-fucosyltransferase 1
RFNG	radical fringe
RBPJ	immunoglobulin kappa J region
SLC35C1	GDP-fucose transmembrane transporter
SOX9	SRY-Box Transcription Factor 9; Hes1: hairy and enhancer of split-1
UEA-I	<i>Ulex europeus agglutinin type I</i>
6AF	6-alkynylfucose

List of Figures

Figure 1. Intrahepatic cholangiocarcinoma classification.....	7
Figure 2. Risk factors for intrahepatic cholangiocarcinoma.....	9
Figure 3. Overview of the Fucosylation Pathway.....	13
Figure 4. The Notch pathway.....	17
Figure 5. The NF- κ B pathway.....	19
Figure 6. The interplay between Fucose and human iCCA relevant pathways and its possible targets to interfere in this relationship.....	21
Figure 7. Representative immunohistochemical patterns of AAL, UEA-I, and LCA lectins in human intrahepatic cholangiocarcinoma (iCCA).....	54
Figure 8. Levels of global fucosylation in human intrahepatic cholangiocarcinoma (iCCA) and normal cholangiocyte (NC) cell lines, as assessed by Western blot analysis.....	55
Figure 9. Levels of global fucosylation in human intrahepatic cholangiocarcinoma (iCCA) specimens.....	57
Figure 10. Levels of the main fucosylation positive regulators and the fucosylation inhibitor FUCA1 in human intrahepatic cholangiocarcinoma (iCCA) specimens.....	58
Figure 11. Representative immunohistochemical patterns of the major players of fucosylation in human intrahepatic cholangiocarcinoma (iCCA).....	60

Figure 12. Fucosylation is a positive regulator of the NOTCH pathway in human intrahepatic cholangiocarcinoma (iCCA).	62
Figure 13. Fucosylation is a regulator of NOTCH signaling	63
Figure 14. Reduced NOTCH signaling due to impaired ligand binding and receptor translocation	65
Figure 15. Fringe proteins responsible for NOTCH activation are upregulated in human intrahepatic cholangiocarcinoma (iCCA).	67
Figure 16. Fucosylation regulates the NF- κ B pathway in intrahepatic cholangiocarcinoma (iCCA) cell lines.	69
Figure 17. Reduced NF κ B translocation after fucosylation inhibition.	70
Figure 18. NOTCH does not influence the NF- κ B pathway in human iCCA cell lines.	72
Figure 19. EGFR is an upstream inducer of the NF- κ B pathway and is modulated by fucosylation in iCCA cell lines.....	73
Figure 20. Effects of L-Fucose and 6AF on proliferation and migration of human intrahepatic cholangiocarcinoma (iCCA) cell lines.....	74
Figure 21. No effects on apoptosis were induced by 6AF in the same cell lines, as detected by FACS analysis.....	75
Figure 22. Fucosylation sustains the migration ability of iCCA cells Fucosylation. ...	76
Figure 23. Fucosylation inhibition suppresses tumor growth of KKU-M213 cells in the chicken chorioallantoic membrane (CAM) in vivo model.	75

Figure 24. Representative images of CK19 stained paraffin sections of CAM tumors (10x).....	79
Figure 25. Effect of the fucosylation inhibitor 6AF on the growth of KKU-M213 intrahepatic cholangiocarcinoma (iCCA) cell line in the chick chorioallantoic membrane (CAM).....	80
Figure 26. Aberrant fucosylation characterizes intrahepatic cholangiocarcinoma lesions developed in AKT/YAP and AKT/TAZ mouse models.	82
Figure 27. Hydrodynamic tail injection in six FVB/N mice per group.....	84
Figure 28. Overview of fucosylation relevance in cancer-associated fibroblasts (CAFs).....	86
Figure 29. Fucosylation regulates pro-inflammatory signals in intrahepatic cholangiocarcinoma (iCCA).....	88
Figure 30. Inhibition of fucosylation does not affect AKT/mTOR, ERK/MAPK, p38MAPK, JAK/STAT3, and YAP/TAZ pathways in KKU213 and HUCCT1 human intrahepatic cholangiocarcinoma cell lines.....	90

List of tables

Table 1. Consumables.....	22
Table 2. Media, Buffers, and Reagents.....	24
Table 3. Kits Used During this Project.....	27
Table 4. Antibodies for Immunohistochemistry and Western Blotting.....	28
Table 5. TaqMan Gene Expression Probes.....	31
Table 6. Clinicopathological Features of iCCA Patients.....	32
Table 7. Software for Data Analysis and Illustration.....	33
Table 8. Three Steps for Membrane Blotting.....	40
Table 9. Lectins for Lectin Blotting and their Target Structure.....	41
Table 10. Protocol for Reverse Transcription.....	42

Supplementary Material

DETAILED STATISTICAL ANALYSES

The analysis included data from 37 patients with human intrahepatic cholangiocarcinoma (27 male and 10 female, all with survival data). The variables have been analyzed using the Statistical Package for Social Science (SPSS, version 22.0, Chicago, IL, USA).

Descriptive statistics

Sex	Number (%)	Mean survival (SD)
Male	27 (73.0)	30.78 (16.75)
Female	10 (27.0)	23.80 (14.16)
Total	37	28.89 (16.20)

Mean survival is 28.89 months (SD 16.20)

(differences between males and females are not statistically significant)

AAL in human intrahepatic cholangiocarcinoma

Low and high *AAL protein* values were recoded into binary variables (0/1) using the median values (*AAL protein* = 67564241) as the cut-off. The whole dataset was then divided into 18 subjects with values of *AAL* below the median and 19 subjects above the median. Statistical comparison between the two groups was performed using the **log-rank test**:

Marker	Number of subjects (%)	Mean survival in months (SD)	Log-rank test
<i>AAL protein</i> < 67564241	18 (48.6)	33.94 (17.19)	–
<i>AAL protein</i> ≥ 67564241	19 (51.4)	24.10 (14.01)	0.076
Total	37	28.89 (16.20)	

Conclusion 1: *patients with AAL protein values above the median 67564241 did not survive, on average, significantly shorter than patients with AAL protein below 67564241 (see Kaplan-Meier curve).*

However, since the **p-value** is close to the significance threshold, a cut-off corresponding to the third percentile (134982894) was also tested. In this case, the difference was statistically significant (**log-rank test, 0.005**) (see Kaplan-Meier curve).

LCA in human intrahepatic cholangiocarcinoma

Low and high *LCA protein* values were recoded into binary variables (0/1) using the median values (*LCA protein* = 28581903) as the cut-off. The whole dataset was then divided into 18 subjects with values of *LCA* below the median and 19 subjects above the median. Statistical comparison between the two groups was performed using the **log-rank test**:

Marker	Number of subjects (%)	Mean survival in months (SD)	Log-rank test
<i>LCA protein</i> < 28581903	18 (48.6)	30.44 (15.23)	–
<i>LCA protein</i> ≥ 28581903	19 (51.4)	27.42 (17.36)	0.900
Total	37	28.89 (16.20)	

Conclusion 2: *patients with LCA protein values above the median 28581903 did not survive, on average, significantly shorter than patients with LCA protein below 28581903 (see Kaplan-Meier curve).*

UEA-I in human intrahepatic cholangiocarcinoma

Low and high *UEA-I protein* values were recoded into binary variables (0/1) using the median values (*UEA protein = 52270175*) as the cut-off. The whole dataset was then divided into 18 subjects with values of *UEA* below the median and 19 subjects above the median. Statistical comparison between the two groups was performed using the **log-rank test**:

Marker	Number of subjects (%)	Mean survival in months (SD)	Log-rank test
UEA-I protein < 52270175	18 (48.6)	38.94 (14.28)	–
UEA-I protein ≥ 52270175	19 (51.4)	19.37 (11.65)	<0.0001
Total	37	28.89 (16.20)	

Conclusion 2: *patients with UEA protein values above the median 52270175 survive, on average, significantly shorter than patients with UEA protein below 52270175 (see Kaplan-Meier curve).*

Differences in the dependent variables (*AAL*, *LCA*, and *UEA-I*) were evaluated with the Mann-Whitney U test for dichotomous variables or the Kruskal-Wallis test for variables with three or more values.

Correlation analysis was performed by calculating Spearman's coefficient

Variable	No. cases	AAL	p-value
<i>Age (years)</i>			
< 65	21	70223691.952 ± 55295124.4828	0.123
≥ 65	16	107982963.313 ± 73013507.5501	
<i>Sex</i>			
Male	27	85613925.481 ± 66492995.6699	0.880
Female	10	89084895.600 ± 65845669.8742	
<i>Survival</i>			
< 28 mo.	18	119156069.000 ± 67873363.2922	0.002
≥ 28 mo.	19	55663984.316 ± 46239593.8182	
<i>Cirrhosis</i>			
No	26	91034853.500 ± 67221132.7488	0.756
Yes	11	75956250.273 ± 62720478.3443	
<i>Etiology</i>			
HBV	9	46848009.778 ± 39377145.2239	0.013[#]
HCV	6	98416347.000 ± 69005519.2435	
Hepatolithiasis	5	159279312.800 ± 54829077.8507	
Not available	17	81994012.353 ± 63242164.6445	
<i>Diameter</i>			

< 5 cm	28	87965878.500 ± 70581172.4357	0.958
≥ 5 cm	9	82153371.778 ± 49151563.3424	
<i>Lymph Node Metastasis</i>			
No	24	78634933.708 ± 59175482.9445	0.321
Yes	13	101168195.000 ± 75961364.6848	
<i>Lung Metastasis</i>			
No	30	82555160.867 ± 60278705.4416	0.458
Yes	7	103681445.429 ± 87709512.1012	
<i>Differentiation</i>			
Well	19	76443743.105 ± 61969534.9676	0.873 [#]
Moderately	9	88672277.111 ± 51417055.2185	
Poorly	9	105771481.222 ± 85500746.8908	
<i>Tumor number</i>			
Single	29	89284157.069 ± 66420893.1419	0.786
Multiple	8	76648048.625 ± 64954162.4607	

[#]Kruskal-Wallis test

Significant differences in fucosylation levels detected by AAL were found for survival and etiology.

Variable	No. cases	LCA	p-value
<i>Age (years)</i>			
< 65	21	98102106.661 ± 245643252.7195	0.617
≥ 65	16	59498646.306 ± 91171253.6143	
<i>Sex</i>			
Male	27	98356934.674 ± 224031993.4199	0.180
Female	10	35648534.460 ± 35564999.5790	
<i>Survival</i>			
< 28 mo.	18	128380488.661 ±	0.134
≥ 28 mo.	19	271342084.7404	
		36909146.574 ± 29850325.0013	
<i>Cirrhosis</i>			
No	26	100394693.865 ±	0.316
Yes	11	228475382.8155	
		36532776.390 ± 29117818.3125	
<i>Etiology</i>			
HBV	9	29068683.877 ± 18977817.2806	0.046[#]
HCV	6	62087503.650 ± 50719000.5130	
Hepatitis	5	327720025.960 ± 487846322.5884	
Not available	17	43492898.482 ± 37606245.1418	
<i>Diameter</i>			

< 5 cm ≥ 5 cm	28 9	57437997.689 ± 74296336.8415 155984293.944 ± 375806987.3819	0.821
<i>Lymph Node Metastasis</i> No Yes	24 13	40521968.825 ± 33295725.2612 156891948.384 ± 316930368.3433	0.540
<i>Lung Metastasis</i> No Yes	30 7	80097567.143 ± 206509797.7649 87027938.071 ± 134172019.2250	0.865
<i>Differentiation</i> Well Moderately Poorly	19 9 9	40425892,757 ± 32158280,4126 174633214,433 ± 371260354,7715 74703520,944 ± 118956423,1481	0.738 [#]
<i>Tumor number</i> Single Multiple	29 8	88823166.772 ± 217043642.0883 54531343.049 ± 51592084.4975	0.928

[#]Kruskal-Wallis test

A borderline significant difference in fucosylation levels detected by LCA was found for etiology.

Variable	No. cases	UEA-I	p-value
<i>Age (years)</i> < 65 ≥ 65	21 16	72217749.429 ± 60535793.7542 89991021.063 ± 87620859.0812	0.639
<i>Sex</i> Male Female	27 10	81248087.704 ± 73474015.2805 76273070.700 ± 75115960.8264	0.801
<i>Survival</i> < 28 mo. ≥ 28 mo.	18 19	116718421.889 ± 89401833.8223 45026183.211 ± 20999447.1180	<0.0001
<i>Cirrhosis</i> No Yes	26 11	86854478.308 ± 84490673.3100 63473876.273 ± 29375436.3541	0.961
<i>Etiology</i> HBV HCV Hepatolithiasis Not available	9 6 5 17	51022734.111 ± 28450462.9083 71160358.333 ± 29802170.2571 141273694.000 ± 123111086.6969 80229049.882 ± 76231965.7705	0.123 [#]
<i>Diameter</i> < 5 cm	28	86423733.893 ± 80361493.4808	0.412

≥ 5 cm	9	59618280.667 ± 38830590.6420	
<i>Lymph Node Metastasis</i>			
No	24	52010951.083 ± 25428763.9460	0.002
Yes	13	131397403.769 ± 101368234.9584	
<i>Lung Metastasis</i>			
No	30	67735035.533 ± 52977243.1362	0.160
Yes	7	132054001.286 ± 120035103.3828	
<i>Differentiation</i>			
Well	19	70116230.789 ± 57639016.9347	0.834 [#]
Moderately	9	65039799.667 ± 41059690.4137	
Poorly	9	115429165.889 ± 113394578.1402	
<i>Tumor number</i>			
Single	29	74773916.552 ± 71506500.7407	0.194
Multiple	8	98498186.875 ± 79842067.8999	

[#]Kruskal-Wallis test

Significant differences in fucosylation levels detected by UEA-I were found for survival and lymph node metastasis.

Correlation (Spearman)

Variable	AAL	p-value	LCA	p-value	UEA-I	p-value
<i>Age</i>	0.125	0.460	-0.134	0.430	-0.070	0.681
<i>Sex</i>	0.028	0.867	-0.228	0.175	-0.046	0.789
<i>Survival</i>	-0.443	0.006	-0.206	0.222	-0.752	<0.0001
<i>Cirrhosis</i>	-0.055	0.745	-0.172	0.310	-0.011	0.948
<i>Etiology</i>	0.134	0.428	0.089	0.600	0.101	0.552
<i>Diameter</i>	0.012	0.945	0.041	0.808	-0.142	0.403
<i>Lymph Node Metastasis</i>	0.170	0.315	0.106	0.532	0.498	0.002
<i>Lung Metastasis</i>	0.129	0.446	-0.032	0.849	0.239	0.154
<i>Differentiation</i>	-0.078	0.646	-0.044	0.796	-0.080	0.640
<i>Tumor number</i>	-0.049	0.772	-0.018	0.914	0.221	0.188

Conclusion: AAL shows a significant negative correlation with patient survival; UEA-I shows a significant negative correlation with survival and a significant positive correlation with lymph node metastasis.

Acknowledgements

I would like to thank Prof. Dr. Matthias Evert for the opportunity to write my doctoral thesis at the Institute of Pathology.

I would like to thank my supervisor Prof. Dr. Diego F. Calvisi. Thank you for the tremendous support, the positive encouragement and for the many great opportunities that have opened up for me in the last 3 years. I really appreciate all you have done for me. You truly had great impact on my future career.

Thank you, Prof. Dr. Marina Kreutz for mentoring my PhD project, for taking over the position of the second examiner of my thesis and for accompanying me for so many years.

Thank you, Prof. Dr. Tobias Pukrop, for mentoring my PhD project and for many helpful and interesting suggestions.

Also special thanks to Dr. Xin Chen for the great opportunity to work in the USA for 3 months during my PhD program and for mentoring my PhD project.

Thank you, Ingrid Winkel and Manfred Meyer, for your patience, your help and all the fun we had. And thank you for the fact that I have not once felt uncomfortable at work in the last few years. I was always happy to meet you in the lab, which makes it really difficult for me to leave.

And of course, thank you Dr. Sara Steinmann for your support and the great teamwork.

I would also like to thank my family, friends and Jan for all their comfort and support.

Selbstständigkeitserklärung

“Ich, Ament Cindy, geboren am 30.01.1992 in Weiden i.d.Opf., erkläre hiermit, dass ich die vorliegende Arbeit ohne unzulässige Hilfe Dritter und ohne Benutzung anderer als der angegebenen Hilfsmittel angefertigt habe.

Die aus anderen Quellen direkt oder indirekt übernommenen Daten und Konzepte sind unter Angabe der Quelle gekennzeichnet. Insbesondere habe ich nicht die entgeltliche Hilfe von Vermittlungs- bzw. Beratungsdiensten (Promotionsberater*innen oder andere Personen) in Anspruch genommen.

Die Arbeit wurde bisher weder im In- noch im Ausland in gleicher oder ähnlicher Form einer anderen Prüfungsbehörde vorgelegt.“

Regensburg, 23.01.2023

Ort, Datum

eigenhändige Unterschrift

des/r Promovenden*in